Phenomenology of natural supersymmetry with non-universal gaugino masses

February 2017

Junichiro KAWAMURA

川村 淳一郎

Phenomenology of natural supersymmetry with non-universal gaugino masses

February 2017

Waseda University

Graduate School of Advanced Science and Engineering

Department of Pure and Applied Physics

Research on theoretical particle physics

Junichiro KAWAMURA

川村 淳一郎

Contents

1 Introduction **3**

2 Review of non-universal gaugino mass scenario **7**
2.1 Brief review of MSSM 7
2.1.1 Action and matter contents 7
2.1.2 Higgs sector 9
2.1.3 Renormalization group running 11
2.2 Non-universal gaugino masses 12
2.3 Fine-tuning and the Higgs boson mass 13
2.4 Summary 17

3 The Higgs boson mass in deflected mirage mediation **18**
3.1 Mediations of supersymmetry breaking 18
3.2 Theoretical backgrounds of deflected mirage mediation 21
3.3 Mass spectrum of deflected mirage mediation 24
3.3.1 Parameter assumptions and overview of analysis 24
3.3.2 Mass spectrum of mirage mediation 25
3.3.3 Mass spectrum of deflected mirage mediation 29
3.3.4 Mirage mediation without tachyonic masses 33
3.4 Summary 34

4 LHC phenomenology with non-universal gaugino masses **37**
4.1 General features of LHC 37
4.2 Masses and Decays 37
4.2.1 Boundary conditions 37
4.2.2 Higgs bosons 40
4.2.3 Neutralino and chargino 41
4.2.4 Colored sparticles 42
4.3 Exclusion limits on non-universal gaugino mass scenario 44
4.3.1 Top squark search 44
4.3.2 Gluino search 52
4.4 Summary 54

5 Dark matter phenomenology with non-universal gaugino masses 56
5.1 Dark matter scenarios . . . 56
5.2 Mass spectrum with light bino . . . 57
5.3 Dark matter observations . . . 58
5.3.1 Parameter settings . . . 58
5.3.2 Constraints from dark matter observations . . . 59
5.4 Collider signals . . . 60
5.5 Summary . . . 61

6 Conclusion 63

A The SM-like Higgs boson mass in the MSSM 65
A.1 Higgs boson and third-generation squark sector . . . 65
A.2 Higgs boson mass for $m_{\rm SUSY} \gtrsim m_A$ . . . 66
A.2.1 Tree-level relations . . . 66
A.2.2 Threshold correction . . . 67
A.2.3 Renormalization group . . . 69
A.3 Higgs boson mass for $m_A < m_{\rm SUSY}$ . . . 72
A.3.1 Threshold corrections . . . 72
A.3.2 Renormalization group . . . 74

B Renormalization group equations 76

C Muon anomalous magnetic moment with non-universal gaugino masses 79

D Soft parameters of moduli and anomaly mediations 81
D.1 General formulae . . . 81
D.2 Anomalous dimensions and their derivatives in the MSSM . . . 83

Chapter 1

Introduction

The Standard Model (SM) of particle physics is known as the theory describing our world below the electroweak (EW) scale. The SM can explain most results of experiments and observations so far. In particular, the discovery of the Higgs boson [1, 2] means that all of the particles in the SM are confirmed, and then the SM is now established.

Although there is no room to doubt it, the SM can not explain all the observations so far altogether and there are too many free parameters left in the SM to consider it as the final theory. Furthermore, these parameters sometimes have hierarchical structures or are required to be fine-tuned to explain observations. For instance, there is no suitable candidate for dark matters which are necessary to explain cosmological observations. The hierarchical structure of the Yukawa matrices is one of the unsolved issues of the SM.

The Higgs sector of the SM contains many puzzles. The shape of the Higgs potential is crucial to trigger the spontaneous EW symmetry breaking, but it is merely put by hand. Hence, we can not explain how the EW symmetry breaking occurs and we can not predict the Higgs boson mass at all. Furthermore, there is an instability of the Higgs boson mass under radiative corrections. The radiative correction for the Higgs boson mass diverges quadratically, then its value depends on a cutoff scale quadratically. Hence, the required accuracy for the cancellation between the bare mass and the counter term is extremely high if the SM describes the nature up to some scale such as the Planck scale $\sim 10^{18}$ GeV far from the EW scale. This fine-tuning problem is often called the gauge hierarchy problem. For these reasons, it is natural that the SM is considered as a low energy effective theory of some new physics which appears not far from the EW scale.

Supersymmetry is known as the well-motivated physics beyond the SM. A benefit to introduce the supersymmetry is that it provides an elegant solution for the gauge hierarchy problem. The supersymmetry requires the pairwise existence of a boson and a fermion, and quadratic divergences are canceled among loop corrections mediated by bosons and fermions. Thus the Higgs boson mass can be stabilized under radiative corrections.

The Minimal Supersymmetric Standard Model (MSSM) [3, 4] has been studied intensively because of the following reasons. The values of gauge coupling constants are unified at a high scale when they are extrapolated by renormalization group (RG). This fact accommodates the MSSM to unified theories like Grand Unification Theories (GUT) or superstring theory.

Parameters of the Higgs potential in the SM are put by hand, hence we can not predict the Higgs boson mass and how the spontaneous EW symmetry breaking occurs. In the MSSM, quartic couplings in the Higgs potential are related to the gauge couplings, and the Higgs boson mass is better controlled than the SM one. Besides, it is known that the mass squared of the Higgs boson goes to negative through the RG evolution in a wide parameter space even if its value is positive at the unification scale $\sim 10^{16}$ GeV, where the three gauge coupling constants are unified. The so-called R-parity is assumed in the MSSM to prohibit too rapid proton decay induced by the baryon and lepton number violating operators which can not be prohibited by the gauge symmetries. The lightest supersymmetric particle (LSP) becomes stable as a consequence of the R-parity, accordingly the LSP can be a good candidate for dark matters.

The Large Hadron Collider (LHC) experiment started and its results severely constrain the parameter space of the MSSM. The LHC experiment discovered the SM Higgs boson and its mass is measured at 125 GeV [5]. The tree-level Higgs boson mass in the MSSM can not be greater than the Z-boson mass, 91.2 GeV. Hence, large radiative corrections are necessary. The top squarks, which are superpartners of the top quarks, give the largest radiative correction. They have to be heavier than $\mathcal{O}$(TeV) in order to lift up the SM-like Higgs boson mass in the MSSM. Furthermore, experimental lower bounds for sparticle masses have been tightened, since no signals expected from sparticles have been found so far.

The LHC results seem to suggest heavy sparticles, but they are not favored from the naturalness point of view. One of the important guidelines to consider new physics is naturalness, that is, all observables are given without fine-tunings of model parameters. One strong motivation to introduce supersymmetry was that it protects scalar masses from the instability due to quadratic divergences, and thus the Higgs boson mass can be realized without fine-tunings. Even in the MSSM, there exists a potential fine-tuning problem to realize the EW scale, the so-called little hierarchy problem. The value of Z-boson mass m_Z, or equivalently vacuum expectation value (VEV) of Higgs boson, relates to the parameters of the MSSM as,

$$m_Z^2 = \frac{|m_{H_d}^2 - m_{H_u}^2|}{\sqrt{1-\sin^2 2\beta}} - m_{H_u}^2 - m_{H_d}^2 - 2|\mu|^2. \tag{1.1}$$

Here, $\tan\beta \equiv v_u/v_d$, where $v_u,\ v_d$ are VEVs of up-type and down-type Higgs bosons, respectively. The parameters $m_{H_u},\ m_{H_d}$ are soft scalar masses for up- and down-type Higgs bosons, and μ is the so-called μ-parameter corresponding to a higgsino mass. This relation shows how the EW scale is obtained from the parameters of the MSSM. A fine-tuning is required, if a typical scale of the MSSM is far above the EW scale as the LHC results seem to suggest. For example, if the top squark mass is larger than sub-TeV, the required degree of tuning is $\mathcal{O}(0.01\%)$. This fine-tuning problem, called the little hierarchy problem, is caused by a hierarchy between the EW scale and the scale of the MSSM.

One way to accommodate the LHC result, especially the 125 GeV Higgs boson mass, to the naturalness argument is to consider non-universal gaugino masses (NUGM) [6, 7]. Once a certain ratio among gaugino masses are realized, the Higgs boson mass is enhanced while keeping the degree of tuning being relaxed. Some other solutions have been proposed since the Higgs boson discovery, but they requires a certain relation among soft scalar masses. The soft scalar masses are less controllable than gaugino masses, since values of gaugino masses at

low scale is determined by gaugino masses itself at 1-loop level, while the soft scalar masses depend on all the other supersymmetry breaking parameters even at 1-loop level. Besides, the gauge kinetic functions and superpotentials tend to be protected by holomorphy, while the Kähler potential does not, which indicates that the soft scalar masses that are often produced through the Kähler potential is presumably unstable under radiative corrections. Also from a phenomenological point of view, the NUGM scenario even enhances the Higgs boson mass instead of merely reducing the fine-tuning.

The supersymmetry must be broken in realistic supersymmetric models, because supersymmetry forces a boson and a fermion in the same supermultiplet to have the same mass. However it is clearly incompatible with the observations. The supersymmetry must not be broken explicitly to prevent quadratic divergences but it should be broken spontaneously. Besides, the supertrace theorem tells us that any MSSM particle cannot break supersymmetry so large that sparticles masses are consistent with the past as well as recent experimental results. Therefore, the supersymmetry is considered to be broken outside the MSSM, and it is mediated to the MSSM by some mechanisms.

The mediation mechanism of supersymmetry breaking is an important ingredient of supersymmetric models both from phenomenological and theoretical aspects. Phenomenologically, it fixes relative values of all the dimensionful parameters in the MSSM except the μ-parameter. Once we identify the supersymmetry breaking mediation mechanism, we may obtain information about how the MSSM fields are embedded into underlying theories. In superstring models, mediation mechanism is often related to physics of moduli fields originated from higher-dimensional tensor or vector fields. Thus it carries information about geometry of extra-dimensions.

The mixture of moduli [8, 9] and anomaly mediations [10, 11], the so-called mirage mediation [12–16], is an interesting scenario to theoretically control the gaugino mass ratio. Such a situation looks like non-trivial, because the moduli mediation occurs at the tree-level, while the anomaly mediation comes from quantum corrections, and its contributions are suppressed by a loop factor. It is known that the KKLT-type moduli stabilization scenario would rather predict such a situation [17, 18]. A more general situation than the mirage mediation is the mixture of moduli, anomaly and gauge mediated supersymmetry breaking, the so-called deflected mirage mediation [19, 20].

The LHC started to search for an evidence of new physics including supersymmetry. The run-I of the LHC with the center of mass energy $\sqrt{s} = 7$ and 8 TeV finished in 2014, and the run-II with $\sqrt{s} = 13$ and 14 TeV is now running and this will last until the end of 2019. The High Luminosity (HL)-LHC is also planned at the same center of mass energy as the run-II one, but with the instantaneous luminosity higher than that of the run-II. This is planned to start in 2023 and last until 2039. The LHC phenomenology will be one of the most important areas of particle physics in the next decades.

Dark matter physics is also intensively surveyed by both collider experiments and cosmological observations utilizing satellites and underground detectors. There are many indirect evidences for dark matter, but we have not detected it directly. These direct detection experiments for the dark matter give constraints on its properties. Since the neutralino LSP in the MSSM is a good candidate for the dark matter, these results can be translated into constraints

on the MSSM parameter space [21].

In this thesis, we study detailed phenomenology of the non-universal gaugino mass (NUGM) scenario anticipating how it is realized by the supersymmetry breaking mediation mechanism. In Chapter 2, we review the NUGM scenario, how it enhances the Higgs boson mass, while evading the fine-tuning and keeping relevant sparticles light. Chapter 3 is devoted to an investigation of the deflected mirage mediation based on the recent experimental data. We show a sparticle mass spectrum when the Higgs boson mass is 125 GeV and the μ-parameter is small. A collider phenomenology of the NUGM scenario is studied in Chapter 4. We discuss how to test the NUGM scenario at the LHC. In Chapter 5, we focus on dark matter physics in the NUGM scenario. Finally, we conclude this thesis in Chapter 6. In addition, four appendices are included in this thesis. The Higgs boson mass formulae, those are used in the analysis of Chapters 2 and 3, are shown in Appendix A. The 1-loop renormalization group equations for the MSSM parameters are listed in Appendix B. Appendix C discusses the muon g-2 anomaly in the NUGM scenario. The formulae for the soft parameters in generic moduli couplings to matter fields are shown in Appendix D.

Chapter 2

Review of non-universal gaugino mass scenario

2.1 Brief review of MSSM

2.1.1 Action and matter contents

In this chapter, we review the non-universal gaugino mass (NUGM) scenario [7, 22]. First, we briefly review the MSSM, see also for a review [3, 4]. The most general supersymmetric Lagrangian can be written in the superfield formalism as,

$$\mathcal{L} = \int d^4\theta \; K(\overline{\Phi}^I, \Phi_I) + \left(\int d^2\theta \Big[W(\Phi_I) + f_a(\Phi_I) \mathcal{W}_a^2 \Big] + \text{h.c.} \right), \tag{2.1}$$

where θ is a 4D Weyl spinor corresponding to Grassmannian coordinates of the superspace. The real function K and holomorphic functions f_a, W of chiral supermultiplets Φ_I are called the Kähler potential, gauge kinetic function and superpotential, respectively. The index I runs over all chiral supermultiplets in the model. If the model has a gauge symmetry G_a and Φ_I is charged under G_a, Φ_I in the Kähler potential has to be replaced by $e^V \Phi_I \equiv e^{2g_a T^a V^a} \Phi_I$, where g_a, T_a is a gauge coupling constant, the representation matrix for the chiral multiplet Φ_I, respectively. V_a is a vector supermultiplet containing the gauge field. $\mathcal{W}_a$ is a field-strength chiral superfield. The subscript a runs over gauge symmetry of the model. Customary, we call terms coming from $\int d^4\theta$ integral as D-terms and those from $\int d^2\theta$ as F-terms. Once we focus on renormalizable terms, the Kähler potential must have the form,

$$K(\overline{\Phi}^I, \; e^V \Phi_I) = \sum_I \overline{\Phi}^I e^V \Phi_I, \tag{2.2}$$

the gauge kinetic function has to be constant and the superpotential has to be a polynomial up to cubic order.

For the MSSM, the superpotential is given by

$$W_{\text{MSSM}} = \bar{u}^n (y_u)^m_n Q_m H_u + \bar{d}^n (y_d)^m_n Q_m H_d + \bar{e}^n (y_e)^m_n L_m H_d + \mu H_u \epsilon H_d, \tag{2.3}$$

chiral supermultiplet Φ_I		spin 0	spin 1/2	$SU(3)_C$	$SU(2)_L$	$U(1)_Y$
squark, quark ($\times$3 gens.)	Q	$(\tilde{u}_L\ \tilde{d}_L)$	$(u_L\ d_L)$	3	2	1/6
	$\bar{u}$	$\tilde{u}_R^*$	$u_R^\dagger$	$\bar{3}$	1	-2/3
	$\bar{d}$	$\tilde{d}_R^*$	$d_R^\dagger$	$\bar{3}$	1	1/3
slepton, lepton ($\times$3 gens.)	L	$(\tilde{\nu}_L\ \tilde{e}_L)$	$(\nu_L\ e_L)$	1	2	-1/2
	$\bar{e}$	$\tilde{e}_R^*$	$e_R^\dagger$	1	1	1
Higgs, higgsino	H_u	$(H_u^+\ H_u^0)$	$(\tilde{H}_u^+\ \tilde{H}_u^0)$	1	2	1/2
	H_d	$(H_d^0\ H_d^-)$	$(\tilde{H}_d^0\ \tilde{H}_d^-)$	1	2	-1/2

Table 2.1: Matter contents of chiral supermultiplets in the MSSM.

gauge supermultiplet V_a	spin 1/2	spin 1	$SU(3)_C$	$SU(2)_L$	$U(1)_Y$
gluino, gluon	$\tilde{g}$	g	8	1	0
wino, W boson	$\tilde{W}^\pm\ \tilde{W}^0$	$W^\pm\ W^0$	1	3	0
bino, B boson	$\tilde{B}^0$	B^0	1	1	0

Table 2.2: Matter contents of gauge supermultiplets in the MSSM.

where μ is a μ-parameter corresponding to the higgsino mass and $y_{u,d,e}$ are the Yukawa matrices for up-type quarks, down-type quarks and leptons, respectively. The indices $m,\ n = 1, 2, 3$ runs over flavors of the quarks and the leptons. Note that the R-parity is imposed in the MSSM, and baryon and lepton number violating terms are prohibited.

The matter contents of the MSSM are listed in Table 2.1 and Table 2.2. A chiral supermultiplet Φ_I contains a scalar (spin-0) and a Weyl fermion (spin-1/2) denoted by ϕ_i and ψ_i, respectively. A vector supermultiplet V_a contains a gauge field of a gauge group G_a and a Majorana fermion λ_a which is usually called as gaugino. Although L and H_d have the same quantum numbers under the SM gauge group, they are distinguished by the R-parity. Hence, all the chiral supermultiplets in the MSSM have the diagonalized form of Kähler potential Eq. (2.2) and there is no mixing among them. Note that there are two Higgs supermultiplets in order to construct Yukawa couplings to both up and down quarks without conflicting with holomorphy of superpotentials and to cancel the contributions to $U(1)_Y$ anomaly between these two higgsinos. We have obtained the supersymmetric part of the MSSM.

As mentioned in Introduction, supersymmetry must be spontaneously broken, or often called, softly broken. A general form of Lagrangian that causes soft breaking of supersymmetry reads as,

$$-\mathcal{L}_{\rm soft} = \phi^{*i} {m^2}_i^j \phi_j + \left[\frac{1}{2} M_a \lambda^a \lambda^a \ + a^{ijk}\phi_i\phi_j\phi_k + b^{ij}\phi_i\phi_j + \text{h.c.}\right], \tag{2.4}$$

where $\phi_i,\ \lambda_a$ are the scalar field contained in the chiral supermultiplet Φ_I and gaugino for gauge group G_a. This Lagrangian contains soft supersymmetry breaking parameters, ${m^2}_i^j,\ M_a,\ a^{ijk},\ b^{ij}$

called soft masses, gaugino masses, A-terms and B-terms, respectively.

In the MSSM, the scalar field ϕ_i runs over all scalar fields, namely the squarks $\tilde{Q} = (\tilde{u}_L,\ \tilde{d}_L),\ \tilde{u}_R,\ \tilde{d}_R$, the sleptons $\tilde{L} = (\tilde{\nu}_L,\ \tilde{e}_L),\ \tilde{e}_R$ and the Higgs bosons $H_u = (H_u^+,\ H_u^0),\ H_d = (H_d^0,\ H_d^-)$. The gaugino λ_a runs over the gluino $\tilde{g}$, wino $\tilde{W}^{0,\pm}$ and bino $\tilde{B}$, which are superpartners of the gluon, the W- and the Z-boson and the photon, respectively. The soft supersymmetry breaking part of the MSSM Lagrangian is expressed in terms of matter fields explicitly, as

$$\begin{aligned}
-\mathcal{L}_{\rm soft}^{\rm MSSM} &= \tilde{Q}^{\dagger m}(m_Q^2)_m{}^n\tilde{Q}_n + \tilde{L}^{\dagger m}(m_L^2)_m{}^n\tilde{L}_n + \tilde{u}_R^{*m}(m_u^2)_m{}^n\tilde{u}_{Rn} + \tilde{d}_R^{*m}(m_d^2)_m{}^n\tilde{d}_{Rn} + \tilde{e}_R^{*m}(m_e^2)_m{}^n\tilde{e}_{Rn} \\
&\quad + m_{H_u}^2 H_u^\dagger H_u + m_{H_d}^2 H_d^\dagger H_d \\
&\quad + \Big[\ \frac{1}{2}M_3\tilde{g}\tilde{g} + \frac{1}{2}M_2\tilde{W}\tilde{W} + \frac{1}{2}M_1\tilde{B}\tilde{B} \\
&\quad + \tilde{u}_{Rm}(a_u)^{mn}\tilde{Q}_n H_u + \tilde{d}_{Rm}(a_d)^{mn}\tilde{Q}_n H_d + \tilde{e}_{Rm}(a_e)^{mn}\tilde{L}_n H_d + bH_u\epsilon H_d + \text{h.c.}\ \Big], \qquad (2.5)
\end{aligned}$$

where $n,\ m = 1, 2, 3$ run over flavor indices. Now we have the full Lagrangian of the MSSM.

2.1.2 Higgs sector

The Higgs potential is,

$$\begin{aligned}
V &= (|\mu|^2 + m_{H_u}^2)(|H_u^0|^2 + |H_u^+|^2) + (|\mu|^2 + m_{H_d}^2)(|H_d^0|^2 + |H_d^-|^2) \\
&\quad + [b(H_u^+ H_d^- - H_u^0 H_d^0) + \text{h.c.}] \\
&\quad + \frac{1}{8}(\frac{3}{5}g_1^2 + g_2^2)(|H_u^0|^2 + |H_u^+|^2 - |H_d^0|^2 - |H_d^-|^2)^2 + \frac{1}{2}g_2^2|H_u^+ H_d^{0*} + H_u^0 H_d^{-*}|^2, \quad (2.6)
\end{aligned}$$

where the terms with gauge coupling constants $g_1,\ g_2$ are D-terms and all the other terms are soft terms except the terms containing the μ-parameter.

We can use a gauge degree of freedom of $SU(2)_L$ to make the VEV of H_u^+ equal to zero without loss of generality, and the VEV of H_d^- is also vanishing at this vacuum. Under this condition, we finally obtain minimization conditions for the Higgs potential,

$$\begin{aligned}
\sin(2\beta) &= \frac{2b}{m_{H_u}^2 + m_{H_d}^2 + 2|\mu|^2}, \qquad (2.7) \\
m_Z^2 &= \frac{|m_{H_d}^2 - m_{H_u}^2|}{\sqrt{1 - \sin^2(2\beta)}} - m_{H_u}^2 - m_{H_d}^2 - 2|\mu|^2, \qquad (2.8)
\end{aligned}$$

where $\tan\beta \equiv v_u/v_d$ is defined as the ratio of the two Higgs VEVs $v_u \equiv \langle H_u^0 \rangle$ and $v_d \equiv \langle H_d^0 \rangle$. The VEV of the SM-like Higgs boson v is related to these VEVs as $v_u^2 + v_d^2 \equiv v^2 \sim (174\text{GeV})^2$. The potential must satisfy the following conditions,

$$\begin{aligned}
2b &< 2|\mu|^2 + m_{H_u}^2 + m_{H_d}^2, \qquad (2.9) \\
b^2 &> (|\mu|^2 + m_{H_u}^2)(|\mu|^2 + m_{H_d}^2). \qquad (2.10)
\end{aligned}$$

The former condition is for the potential to be bounded from below, and the latter condition is to make the symmetric point $H_u = H_d = 0$ unstable.

The minimization condition Eq. (2.8) is modified by radiative corrections, in particular, contributions from the top squarks can be sizable. When we denote radiative corrections to the Higgs potential as $\Delta V_{\rm eff}(H_u, H_d)$, contributions to the minimization condition can be expressed by shifts of the soft masses,

$$m_{H_u}^2 \;\to\; m_{H_u}^2 + \frac{1}{2v_u}\frac{\partial}{\partial H_u}\Delta V_{\rm eff}(H_u, v_d)\Big|_{H_u \to v_u}, \tag{2.11}$$

$$m_{H_d}^2 \;\to\; m_{H_d}^2 + \frac{1}{2v_d}\frac{\partial}{\partial H_d}\Delta V_{\rm eff}(v_u, H_d)\Big|_{H_d \to v_d}. \tag{2.12}$$

The radiative corrections for the Higgs potential $\Delta V_{\rm eff}(H_u, H_d)$ is nothing but the well-known Coleman-Weinberg potential. Its explicit form at 1-loop level is shown in Eq. (A.21) of Appendix A. We included the contributions from the third-generation quarks, squarks and the neutralinos, charginos, although the latter effects are negligibly small.

Equation (2.8) shows how the EW symmetry breaking scale is generated in the MSSM. If the values of m_{H_u}, m_{H_d}, μ are greatly larger than the EW scale, fine-tuning is required among these parameters. Two of those parameters m_{H_u}, m_{H_d} and all the other mass parameters are relevant to soft supersymmetry breaking, but the μ-parameter is a supersymmetric parameter. Hence, there is no reason why it has a relation to the supersymmetry breaking parameters. Thus at least the value of the μ-parameter and the sum of all the other terms consisting of soft parameters should not have significantly large values compared with the EW scale in order to avoid fine-tunings. This fine-tuning problem to realize the EW scale is called the little hierarchy problem.

The lightest CP-even Higgs boson corresponds to the SM Higgs boson, the mass of which is measured about 125 GeV. The SM-like Higgs boson mass is calculable in the MSSM, since the quartic couplings of the Higgs bosons are related to the gauge couplings. It is well known that quantum corrections give significant contribution to the SM-like Higgs boson mass, especially contributions from top squarks are important owing to the large top Yukawa coupling constant. The SM-like Higgs boson mass with the dominant radiative corrections is given by [23]

$$m_h^2 \;\simeq\; m_Z^2 \cos^2(2\beta) + \frac{3}{8\pi^2}\frac{m_t^4}{v^2}\left[\log\frac{M_{\rm st}^2}{m_t^2} + \frac{2A_t^2}{M_{\rm st}^2}\left(1 - \frac{A_t^2}{12M_{\rm st}^2}\right)\right], \tag{2.13}$$

where m_t, $M_{\rm st} \equiv \sqrt{m_Q m_u}$ and A_t represent the top quark mass, top squark mass scale and A-term for the top squark, respectively. More precise expression is shown in Appendix A. The observed Higgs boson mass is 125 GeV, while the tree-level mass is always smaller than the Z-boson mass $m_Z = 91.2$ GeV, hence the large radiative correction is required. The top squark mass scale must be larger than sub-TeV to explain the observed value of 125 GeV unless the last term of Eq. (2.13) gives significant contribution. The last term depends on the ratio A_t/M_{st} and it is maximized when this ratio is $\sqrt{6}$. Since A_t corresponds to the mixing between left- and right-handed top squarks, the situation with $A_t/M_{st} \simeq \sqrt{6}$ is called the "maximal mixing".

2.1.3 Renormalization group running

The top squark parameters are important not only for the Higgs boson mass, but also for the EW symmetry breaking. The minimization condition Eq. (2.8) is a relation for values of $m_{H_u},\ m_{H_d},\ \mu$ around the EW scale, while their values would be given at the unification scale where values of the gauge coupling constants unify and some underlying theory appears. This indicates that the values of $m_{H_u},\ m_{H_d},\ \mu$ in Eq.(2.8) involve other parameters, including top squark parameters, through the RG evolution.

In the large $\tan\beta$ limit, Eq. (2.8) can approximately be written as

$$m_Z^2 \simeq -2|\mu|^2 - 2m_{H_u}^2. \tag{2.14}$$

Note that the value of $m_{H_u}^2$ should be negative in order to bring the EW symmetry breaking. This relation indicates that small $|m_{H_u}^2|$ is necessary to avoid the fine-tuning problem of the μ-parameter, which is a part of the little hierarchy problem.

One attractive feature of the MSSM is that $m_{H_u}^2$ tends to be negative at low energies even if it is positive at the unification scale. The 1-loop RG equation for m_{H_u} is

$$\begin{aligned}\frac{d}{dt}m_{H_u}^2 &= \frac{1}{16\pi^2}\Big(6\mathrm{Tr}\left[(m_{H_u}^2 + m_Q^2)y_u^\dagger y_u + y_u^\dagger m_u^2 y_u + a_u^\dagger a_u\right] \\ &\quad -6g_2^2|M_2|^2 - \frac{6}{5}g_1^2|M_1|^2 + \frac{3}{5}g_1^2 S\Big),\end{aligned} \tag{2.15}$$

where

$$S \equiv m_{H_u}^2 - m_{H_d}^2 + \mathrm{Tr}(m_Q^2 - m_L^2 - 2m_u^2 + m_d^2 + m_e^2). \tag{2.16}$$

The logarithm of renormalization scale Q is defined as $t = \ln Q/\Lambda$. In our analysis, the cutoff scale Λ is assigned to the gauge coupling unification scale. The unification scale is defined as a scale where $\sum_{a<b}|g_a(t) - g_b(t)|,\ (a,b=1,2,3)$ is minimized. It is typically $\sim 2.0\times 10^{16}$ GeV and slightly depends on the typical sparticle mass m_{SUSY} where sparticles decouple from the theory. All RG equations of the MSSM parameters [24–26] are listed in Appendix B and the full 2-loop RG equations of the MSSM are derived in Ref. [27]. The top Yukawa coupling constant is much larger than other Yukawa coupling constants, so that dominant contributions come from the terms proportional to $y_t \simeq (y_u)_{33}$ and the gauge coupling constants. The term proportional to the top Yukawa coupling constant forces $m_{H_u}^2$ to be negative at low energies even when its value is positive at a high scale. This fact indicates that value of $m_{H_u}^2$ appearing in Eq. (2.8) depends on the top squark parameters

The MSSM RG equations can be solved numerically. In this chapter, we assume that the Yukawa couplings can be neglected except those for the third-generation and solve 1-loop RG equations listed in Appendix B. We also assume that the soft masses and the A-terms have universal values m_0 and A_0 at the unification scale, respectively, but the the gaugino masses do not have the same value. When we take $\tan\beta = 15$, the value of $m_{H_u}^2$ at a typical scale of sparticles, which is assumed to be $m_{\mathrm{SUSY}} = 1$ TeV, is found to depend on the boundary conditions at the unification scale as

$$\begin{aligned}m_{H_u}^2(m_{\mathrm{SUSY}}) &\simeq 0.005M_1^2 - 0.005M_1M_2 + 0.202M_2^2 - 0.021M_1M_3 - 0.134M_2M_3 \\ &\quad -1.56M_3^2 - A_0(0.011M_1 + 0.064M_2 + 0.238M_3 + 0.097A_0) - 0.069m_0^2.\end{aligned} \tag{2.17}$$

The value of $m_{H_u}^2$ gets a large negative value when the top squark parameters $m_Q,\ m_u,\ A_t$ and the gluino mass term M_3 have large values. The required degree of tuning in Eq. (2.8) becomes severer as the top squark is heavy to explain the Higgs boson mass, or lower bounds on gluino mass is tightened by experiments.

Similarly, the top squark parameters $m_Q,\ m_u,\ A_t$ at $m_{\rm SUSY} = 1$ TeV are related to the boundary conditions as

$$\begin{aligned} m_Q^2(m_{\rm SUSY}) &\simeq -0.007M_1^2 - 0.002M_1M_2 + 0.349M_2^2 - 0.008M_1M_3 - 0.056M_2M_3 + 3.21M_3^2 \\ &\quad -(0.004M_1 + 0.029M_2 + 0.107M_3 + 0.044A_0)A_0 + 0.600m_0^2, \qquad (2.18) \\ m_u^2(m_{\rm SUSY}) &\simeq 0.044M_1^2 - 0.003M_1M_2 - 0.157M_2^2 - 0.014M_1M_3 - 0.089M_2M_3 + 2.77M_3^2 \\ &\quad -(0.007M_1 + 0.043M_2 + 0.159M_3 + 0.065A_0)A_0 + 0.287m_0^2, \qquad (2.19) \\ A_t(m_{\rm SUSY}) &\simeq 0.032M_1 + 0.236M_2 + 1.42M_3 + 0.273A_0. \qquad (2.20) \end{aligned}$$

We can see that the gluino mass M_3 gives the most significant contributions to these parameters. If the terms proportional to M_3^2 dominate the RG evolution, the ratio $A_t/M_{\rm st}$ is always smaller than unity. The top squark mass has to be heavier than $\mathcal{O}$(TeV) to explain the 125 GeV Higgs boson mass, and then the required degree of tuning is $\mathcal{O}(0.01\%)$ as will be discussed later. The fine-tuning is required to explain 125 GeV Higgs boson unless the value of A_t is greatly larger than M_3 to enhance the Higgs boson mass, and/or $m_{H_u}^2$ is much larger than M_3 to reduce the value of $m_{H_u}^2$ at the EW scale. However such situations would be difficult to be realized by mediation mechanisms of supersymmetry breaking. Therefore it is challenging to realize the Higgs boson mass without a fine-tuning when the gluino mass term M_3 dominates the RG evolution.

2.2 Non-universal gaugino masses

In this section, we consider non-universal gaugino masses at the unification scale to solve the little hierarchy problem induced by the Higgs boson mass.

The ratio $A_t/M_{\rm st} \simeq \sqrt{6}$ is necessary to realize the observed Higgs boson mass while keeping the top squark mass less than sub TeV. This ratio can be increased efficiently by taking large values of wino mass M_2 compared with the gluino mass M_3. For the right-handed top squark soft mass m_u, the coefficient for the M_2^2 term is negative and opposite to that for M_3^2 term. As a result, the value of m_u reduces as M_2 increases. Besides, the value of $|A_t|$ increases at the same time.

Thus the ratio $A_t/M_{\rm st}$ increases as the wino mass parameter M_2 increases. Note that top squark becomes tachyonic if M_2 is too large compared with M_3, and then there is an upper bound on the ratio $M_2/M_3 \lesssim 4$ - 5 for $m_u^2 > 0$, or more precisely, the eigenvalues of the mass squared matrix for the top squark should be positive.

It is interesting that the degree of tuning is also relaxed when the wino mass parameter is increased. In particular, the contributions from the gluino mass term can be canceled by the M_2^2 term if the wino-to-gluino mass ratio $M_2/M_3 \simeq 3.1$. Thus $m_{H_u}^2(m_{\rm SUSY})$ can be close to the EW scale when the wino-to-gluino mass ratio $M_2/M_3 \gtrsim 3$. Note that the EW symmetry

breaking can not occur, or equivalently Eq. (2.8) does not have a solution if $m_{H_u}^2 \gtrsim -m_Z^2/2$. This gives an upper bound on $M_2/M_3 \lesssim 3.5$, depending on values of the other parameters. Therefore we find that the wino-to-gluino mass ratio $3 \lesssim M_2/M_3 \lesssim 4$ is favored not only to increase the Higgs boson mass owing to the sizable ratio of $A_t/M_{\rm st}$, but also to reduce the value of μ-parameter.

2.3 Fine-tuning and the Higgs boson mass

The LHC experiment gives stringent constraints on the parameter space of the MSSM. In particular, the gluino mass has to be heavier than at least 1.5 TeV although precise limit is shown in the subsequent chapters. Since $M_3(m_{\rm SUSY}) \simeq 2.3\ M_3$, the current LHC result requires $M_3 \gtrsim 650$ GeV. The gluino mass pushes up masses of the squarks above TeV, so that the typical scale of sparticles is larger than the EW scale and there remain potentially fine-tuning problems.

We employ a measure for degrees of parameter tuning as [28],

$$\Delta \equiv \max_a |\Delta_a| = \max_a \left| \frac{\partial \ln m_Z^2}{\partial \ln a^2} \right|, \tag{2.21}$$

where a runs over all fundamental parameters of the MSSM. Since we do not know what is fundamental parameters for the MSSM, we consider several patterns of fundamental parameters. In all cases we discuss here, the value of μ-parameter at the unification scale is treated as a fundamental parameter because it is a unique supersymmetry preserving parameter. On the oater hand, we consider several ways to identify fundamental parameters among soft breaking parameters. As will be discussed in next chapter, the fundamental parameters would be identified when we specify mediation mechanisms of supersymmetry breaking.

The first choice is

$$\Delta_1 \equiv \max_{a \in \{\mu,\ M_1,\ M_2,\ M_3,\ A_0,\ m_0\}} |\Delta_a|, \tag{2.22}$$

where all gaugino masses and the universal A-term and soft mass are considered to be independent parameters to each other.

The second one is

$$\Delta_2 \equiv \max_{a \in \{\mu,\ M_{\rm gaugino},\ m_{\rm scalar}\}} |\Delta_a|, \tag{2.23}$$

where $M_{\rm gaugino} \equiv M_3 \equiv M_1/r_1 \equiv M_2/r_2$ and $m_{\rm scalar} \equiv m_0 \equiv A_0/r_A$. The gaugino mass ratios $r_{1,2}$ and the ratio of A-term to soft mass r_A are fixed by some mechanism and their scales are treated as fundamental parameters.

The last choice is

$$\Delta_3 \equiv \max_{a \in \{\mu,\ M_{\rm all}\}} |\Delta_a|, \tag{2.24}$$

where $M_{\rm all} \equiv M_3 \equiv M_1/r_1 \equiv M_2/r_2 \equiv m_0/r_m \equiv A_0/r'_A$, so that all of the ratios among soft terms are fixed and the overall scale is considered to be fundamental. Conventionally, the overall scale is represented by the gluino mass M_3, but this does not matter because of the definition of the degree of tuning with e.g. $\log M_3^2$. Note that the minimization condition of the Higgs potential Eq. (2.8) implies

$$\sum_a \Delta_a = 1 \tag{2.25}$$

at tree-level, because values of soft masses at low energies can be written by their values at the unification scale quadratically as in Eq. (2.17). This relation is broken by the radiative corrections Eq. (2.12). This means that $\Delta_3 \simeq |\Delta_\mu| \simeq |\Delta_{M_3}|$.

At 1-loop level, The RG-effects to the μ-parameter can be factorized, then

$$\Delta_\mu \equiv \frac{\partial\, \ln m_Z^2}{\partial\, \ln \mu_0^2} \simeq \frac{\partial\, \ln m_Z^2}{\partial\, \ln \mu_{\rm SUSY}^2} = \frac{2\mu_{\rm SUSY}^2}{m_Z^2}, \tag{2.26}$$

where μ_0 and $\mu_{\rm SUSY}$ are values of μ-parameter at the unification scale and the supersymmetry scale, respectively. Thus the value of μ-parameter has to be smaller than about 200 GeV (650 GeV) for $\Delta_3 \lesssim 10$ (100).

Note that there are dependences on fundamental parameters through $\tan\beta$, because VEVs of the Higgs bosons are determined by their mass terms, including m_{H_u}, m_{H_d}. However, such contributions will be suppressed by $\tan^3\beta \gtrsim \mathcal{O}(1000)$ due to the fact that $\tan\beta$ dependence of m_Z^2 is only through $1/(1-\tan^2\beta)$, as can be read from Eq.(2.8).

Figure 2.1 shows values of each tuning parameter with the assumption $M_3 = m_0 = A_0 = 1$ TeV at the unification scale. These are obtained by solving the 1-loop SM RG equations for the Yukawa and gauge coupling constants below the supersymmetry scale defined as $m_{\rm SUSY} = \sqrt{m_Q m_u}$, and the 1-loop MSSM RG equations for the Yukawa coupling constants, the gauge coupling constants and the soft parameters above $m_{\rm SUSY}$. Note that we neglect Yukawa couplings except for the third-generation fermions. Values of Δ_a are calculated at $m_{\rm SUSY}$. There is no suitable values of μ-parameter and b-term that satisfy Eq. (2.8) in the gray region and the top squark becomes tachyonic in the brown region.

We can see that the tuning of the μ-parameter is relaxed as r_2 increases. The tuning of the A-term and the scalar mass are not so sensitive to the gaugino mass ratio and are not so severe in this case. Note that the tuning of A-term can become severer if it becomes larger and cannot be relaxed efficiently by changing the gaugino mass ratios.

The middle row of Fig. 2.1 shows the tunings of gaugino mass parameters. Since Δ_{M_3} is always larger than about 400, their degrees of tunings are severer than $\Delta_1 \gtrsim 370$, which means that required tuning is tighter than $\sim 0.25\%$, if their values are determined independently and there is no correlation among them. In particular, the degree of tuning the wino mass parameter becomes severer for larger values of wino mass where the tuning of μ-parameter is favorably relaxed. Incidentally, Δ_μ becomes larger than any other Δ_a in small M_2 region, including the universal gaugino mass case.

It is reasonable that the gaugino mass ratios are fixed by supersymmetry breaking mediation mechanism, and gaugino masses have some relations among them. For instance, gaugino masses

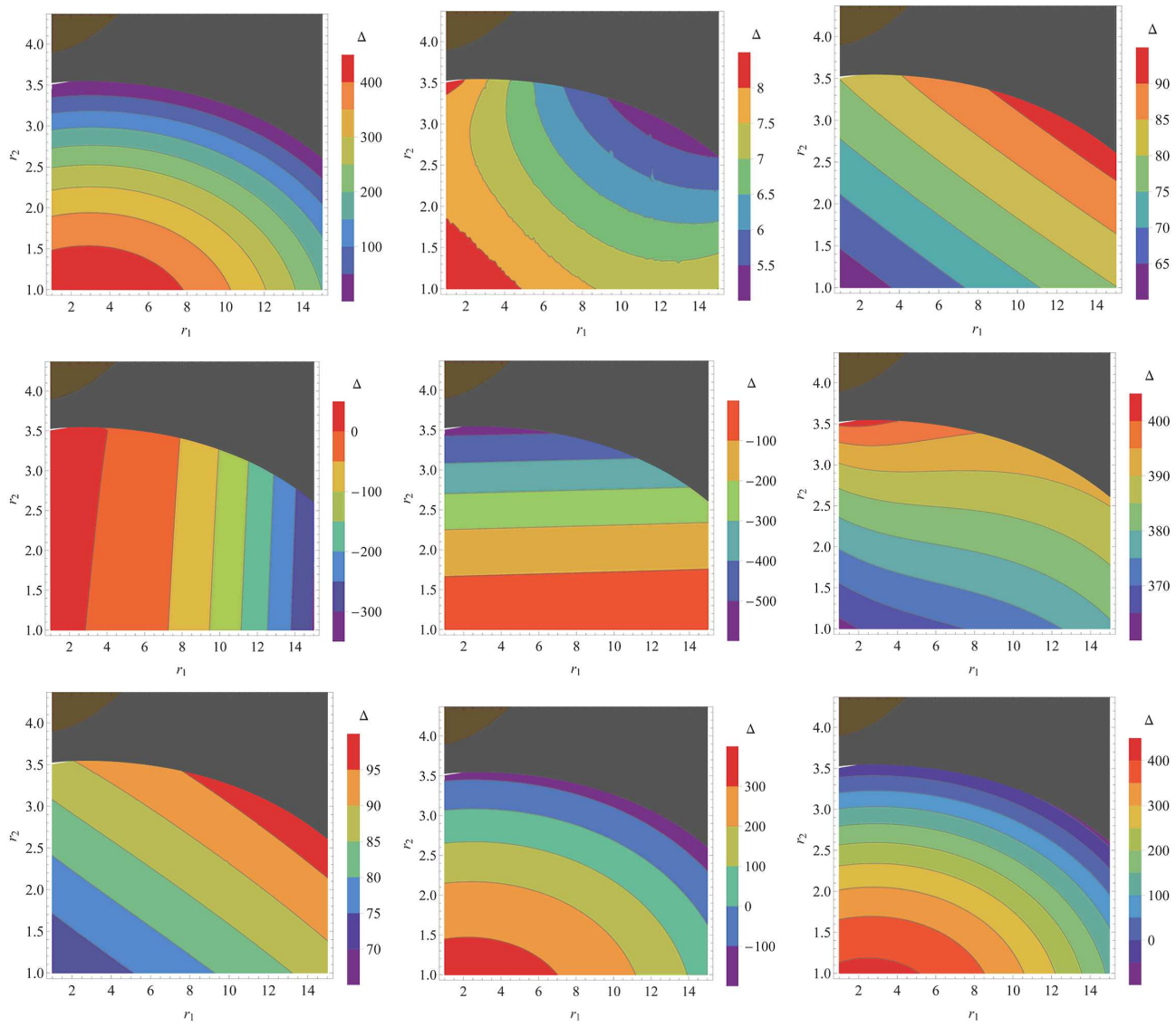

Figure 2.1: Values of tuning parameters in the parameter space (r_1, r_2) with a boundary condition $M_3 = A_0 = m_0 = 1.0$ TeV. $\Delta_a = \Delta_\mu$ (top left), Δ_{m_0} (top center), Δ_{A_0} (top right), Δ_{M_1} (middle left), Δ_{M_2} (middle center), Δ_{M_3} (middle right), $\Delta_{M_{\rm scalar}}$ (bottom left), $\Delta_{m_{\rm gaugino}}$ (bottom center), $\Delta_{\rm all}$ (bottom right), respectively.

are determined by the beta function coefficients, which are determined by discrete parameters such as the Casimir invariants and the number of representations in the anomaly mediation. Therefore, the definition of the tuning measure Δ_1, defined as Eq. (2.22), is always larger than about 350, but this may be meaningless.

The fine-tuning measure Δ_2 might be more reasonable. The left and center in the bottom row of Fig. 2.1 show the degree of tuning of the overall scalar parameters $m_{\rm scalar}$ and gaugino masses $M_{\rm gaugino}$, respectively. We can see $\Delta_{\rm scalar} < 100$ because Δ_{A_0} and Δ_{m_0} are already small.

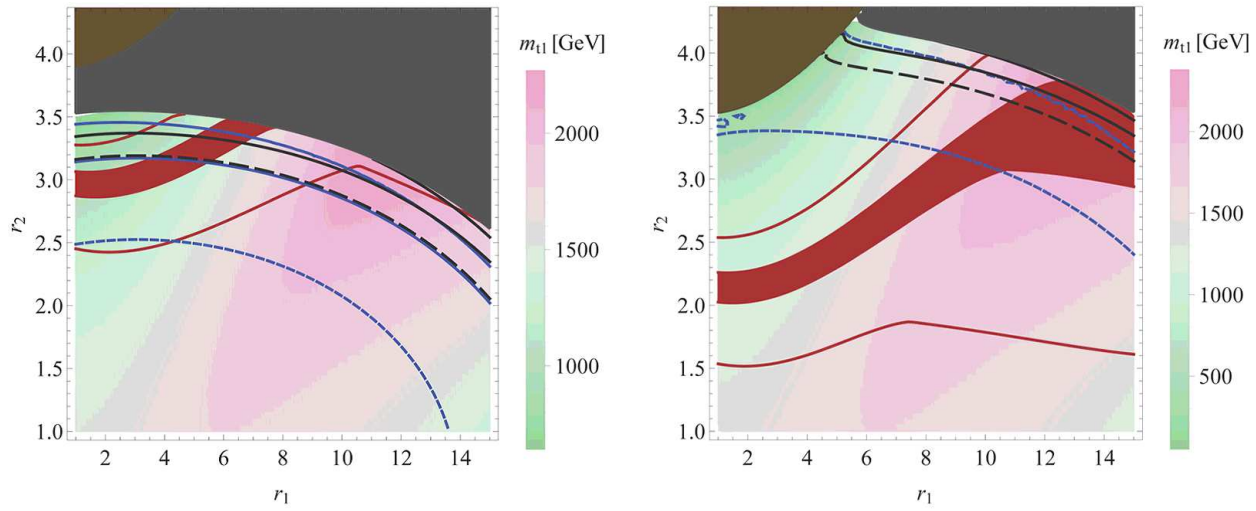

Figure 2.2: The Higgs boson mass, the top squark mass and the degree of tunings on the gaugino mass ratio plane with $M_3 = m_0 = 1.0$ TeV and $A_0 = 1.0$ (2.0) TeV in the left (right) panel. The blue solid (dashed) lines represent $\Delta_2 = 100$ (250) and the black solid (dashed) lines represent $\Delta_3 = 50$ (100). The Higgs boson mass is 125.09 ± 0.24 GeV in the red band, and lower (upper) red solid line corresponds to 124 (126) GeV. The background color indicates the lightest top squark mass and there is no suitable value of μ-parameter to explain the EW symmetry breaking in the gray region.

On the other hand, the tuning for gaugino mass parameter is significantly relaxed, especially $\Delta_{M_{\rm gaugino}}$ can be completely vanishing. This is because the signs of Δ_{M_1} and Δ_{M_2} are opposite to that of Δ_{M_3}, then the degree of tuning is also canceled by the gaugino mass ratio, in addition to the cancellation for the tuning of μ-parameter. Therefore Δ_2 can be less than 100, which means that the required tuning is better than 1%-level.

The right panel of the bottom row in Fig. 2.1 shows the degree of tuning when all of the soft parameters are determined by one parameter. As we expected from Eq. (2.25), its value is almost the same as Δ_μ, but a small difference comes from radiative corrections. Thus Δ_3 can be smaller than 100, and the required tuning is relaxed above a few %-level.

Let us turn our attention to the Higgs boson mass. Figure 2.2 shows the Higgs boson mass, the top squark mass and values of tuning measures Δ_2, Δ_3. The boundary condition is $M_3 = m_0 = 1.0$ TeV and $A_0 = 1.0$ and 2.0 TeV in the left and right panels, respectively. The Higgs boson mass is in a range 125.09 ± 0.24 GeV in the red band, and the lower (upper) red line corresponds to 124 (126) GeV. We calculate the Higgs boson mass by the renormalization group method paying attention to light right-handed top squark. Details of the calculation are shown in Appendix A. The lower lines are bended when the left-handed top squark mass becomes lighter than that of right-handed one in large r_1 region.

The Higgs boson mass can reach the observed value easily for $A_0 = 2.0$ TeV. It reaches to the observed value only when the right-handed top squark is relatively light and the ratio $A_t/M_{\rm st}$ is enhanced for $A_0 = 1.0$ TeV.

There is no suitable values of the μ-parameter to bring the realistic EW symmetry breaking in the gray region and the top squark becomes tachyonic in the brown region. The background indicates the lightest top squark mass. We can see that the top squark tends to be light for $A_0 = 2.0$ TeV due to a large mixing in the top squark mass matrix and then it can be lighter than 1.0 TeV.

The blue dashed and solid lines correspond to $\Delta_2 = 250$ and 100, respectively. Δ_2 can be smaller than 100 between the two solid lines in the case of $A_0 = 1.0$ TeV, but it is always larger than 200 because of the severe tuning induced by the A-term if $A_0 = 2.0$ TeV. Thus $A_0 = 1.0$ TeV is obviously favored from the naturalness based on the tuning parameter Δ_2. On the other hand, Δ_3 can be smaller than 50 in both cases. Therefore both of them are favored if we adopt the definition of the degree of tuning Eq.(2.24) as long as gaugino masses are fixed with suitable ratios.

2.4 Summary

In this chapter, we reviewed the Non-Universal Gaugino Mass (NUGM) scenario that can accommodate the observed Higgs boson mass to the naturalness argument. The most important ingredient of this scenario is a suitable ratio of wino-to-gluino mass parameter M_2/M_3 at the unification scale. Larger values of M_2 not only reduce the values of $|m^2_{H_u}|$ around the EW scale, but also increase the ratio $A_t/M_{\rm st}$ which gives significant enhancement for the Higgs boson mass as a consequence of the RG evolution. We showed that the Higgs boson mass can reach about 125 GeV while keeping the degree of tuning relaxed above %-level if we adopt the definitions Eq. (2.23) or Eq. (2.24).

This scenario is also interesting from a phenomenological viewpoint, because some particles tend to be light and can be tested by experiments or observations in near future. The exclusion limits of this scenario at the LHC experiment is presented in Chapter 4 and those at dark matter experiments are in Chapter 5. An expected contribution to the muon magnetic moment from sparticle contributions is shown in Appendix C.

It is known that there exists several ways to realize such a relatively large wino mass parameter at the unification scale. One possibility is to rely on the mirage mediation [15, 16], a mixture of the moduli and the anomaly mediations. We study this possibility and its generalization in the next chapter. Another explanation of a suitably large wino mass is given by moduli-mixing gauge kinetic functions [29]. It is quite dependent on superstring models how the moduli fields appear in gauge kinetic functions, and their VEVs of the scalar components and the F-term are fixed. We need to know how the MSSM is embedded into D-brane configurations, such as winding numbers, intersections and magnetic fluxes, and so on. This is quite interesting but is beyond the scope of this thesis, so we focus on the first possibility, that is, the mirage mediation and its generalization.

Chapter 3

The Higgs boson mass in deflected mirage mediation

In this chapter, we study supersymmetry breaking mediation mechanism that realizes the NUGM scenario [30]. Here we consider a general class of mediation mechanism, the so-called deflected mirage mediation (DMM), where three well-motivated supersymmetry breaking mediations co-exist. We identify the parameter space of the DMM and discuss compatibility of the naturalness with the recent observations. We first review the mediation mechanisms of supersymmetry breaking in Section 3.1. We also review theoretical backgrounds of the DMM, especially how it is realized by moduli stabilization mechanism in Section 3.2. Section 3.3 is devoted to phenomenological discussions of the DMM. We summarize this chapter in Section 3.4.

3.1 Mediations of supersymmetry breaking

Supersymmetry must be broken in order to make masses different between a boson and a fermion in the same supermultiplet, but it should be broken spontaneously to avoid quadratic divergences for scalar masses. We can derive the following mass sum rule at tree-level, the so-called supertrace theorem, from the most general non-anomalous renormalizable supersymmetric Lagrangian,

$$\mathrm{Tr}(\mathbf{m}_S^2) - 2\mathrm{Tr}(\mathbf{m}_F^\dagger \mathbf{m}_F) + 3\mathrm{Tr}(\mathrm{m}_V^2) = 0, \tag{3.1}$$

where $\mathbf{m}_S,\ \mathbf{m}_F,\ \mathbf{m}_V$ are mass matrices for scalars, fermions and vectors in the model, respectively. The mass terms come from both the superpotential and the Kähler potential after some scalar fields obtain nonzero VEVs. If some of these supermultiplets are block-diagonal and do not mix with other sectors, the same relation holds for those supermultiplets. Then if it is true for the electron supermultiplet, there is a sum rule,

$$m_{\tilde{e}_1}^2 + m_{\tilde{e}_2}^2 = 2m_e^2, \tag{3.2}$$

where $m_{\tilde{e}_1}$, $m_{\tilde{e}_2}$ are the mass eigenvalues of mass matrix for the two selectrons. It is clearly inconsistent with the observation, since a selectron lighter than about 100 GeV has been excluded. Moreover mixing of the electron with other fermions are severely constrained by lepton flavor violation experiments, thus the MSSM fields cannot break supersymmetry sufficiently large. Similar argument can apply for other MSSM particles. Furthermore, fields responsible for large supersymmetry breaking may not couple to the MSSM particles directly. It is quite difficult that the breaking field couples to the MSSM particles, respecting all constraints from flavor violation searches. Therefore supersymmetry breaking should occur separately from the MSSM, and such a sector separated from the MSSM is called the hidden sector.

Loopholes for the supertrace sum rule are found by considering non-renormalizable interactions or radiatively induced interactions. The former is often called the gravity mediation [8, 9, 31–34]. In the gravity mediation models, supersymmetry breaking fields couple to MSSM fields through higher dimensional couplings. A cutoff scale for these couplings is usually considered at the Planck scale as naturally expected from the supergravity which is a localized supersymmetry. The supersymmetry breaking field is usually considered as a singlet for the SM gauge group, because it is difficult to make its potential to break the supersymmetry if the field is charged under the SM gauge symmetries. The supersymmetry breaking field should couple to the MSSM sfermions in a universal way, or with respect to flavor structure of the Yukawa interactions in some sense, otherwise it easily induces unwanted flavor violations. Universal couplings are often assumed in gravity mediation models, but there are models without such an assumption. For example, if the supersymmetry breaking field strongly couples to the first- and the second-generations but weakly for the third-generation, the flavor violating processes are suppressed due to decoupling of two of three generations. The gravity mediation is less predictable and highly depends on the underlying theory.

There are two well-motivated mediation mechanisms induced by radiative corrections. One is the gauge mediation [35, 36], where supersymmetry breaking effects are mediated by gauge interaction. Since gauge interactions are basically independent of flavors of sfermions, it is free from flavor violations. Some exotic matter fields charged under the SM gauge group, the so-called messenger fields, are mandatory to mediate supersymmetry breaking by the gauge interactions. These messenger fields must have large masses to evade experimental bounds and they must not produce $U(1)_Y$ anomaly. Then these messenger fields are usually considered as vector-like, and they consist of some representations of GUT gauge groups to hold an attractive feature of the MSSM, i.e. the gauge coupling unification. Thus the minimal setup for the gauge mediation is to introduce vector-like fields that can be completely embedded into 5 and $\bar{5}$ representations of $SU(5)$.

Another radiatively mediated scenario is called the anomaly mediation [10,11]. The anomaly mediation always exists in the MSSM, although its effect could be quite small compared with contributions from the other mediation mechanisms. In anomaly mediation, supersymmetry breaking is mediated by the super-Weyl anomaly, which can be understood as that mediated by a compensator field in conformal supergravity context. The anomaly mediated contributions are completely determined by the anomalous dimensions of MSSM fields and then they are insensitive to the UV physics. Since anomalous dimensions are dependent on gauge coupling constants and Yukawa matrices, these contributions are flavor universal or respect the flavor

structure of the Yukawa matrices. Thus the anomaly mediation is attractive because of its predictability and is safe from flavor violation. However, it should be noted that the anomaly mediation predicts tachyonic sleptons at low energies and some additional contribution is necessary to avoid such a problem.

The relatively large wino mass cannot be realized in the simplest case of the above three mediation mechanisms. If a supersymmetry breaking field appears in the gauge kinetic function universally to each gauge supermultiplet, the gaugino masses are also universal. Since the gaugino masses are proportional to the gauge coupling constants both in gauge and in anomaly mediations, the gluino mass is always heavier than the wino mass parameter at the GUT scale.

The mirage mediation [12–14], which is mixture of moduli and anomaly mediations, would be the most promising possibility to realize the large wino mass. Here, the moduli mediation is classified in the gravity mediation where the mediator field is moduli fields. Moduli fields always appear, in compactified extra-dimensional models, like superstring models, as massless-modes originating from extra-dimensional component of higher dimensional tensor or vector fields. Once we assume that one modulus field couples to each SM supermultiplet universally and contributions from modulus and anomaly mediations are comparable, suitably large wino-to-gluino mass ratio can be obtained. It seems non-trivial that the loop-induced anomaly mediated contributions are comparable with tree-level contributions from the moduli mediation, but we have an underlying scenario that realizes such a situation known as the KKLT moduli stabilization mechanism [17,18]. Phenomenology of the mirage mediation is studied in Refs. [37–40]

The mirage mediation has been studied as a model favored from the naturalness due to its mirage unification feature [15, 16]. If the special relation for the modulus mediation is achieved, values of soft parameters are unified at some low energy scale. This scale is called the mirage unification scale. The mirage unification scale is determined by the ratio of the contributions from modulus and anomaly mediations. This feature allows us to control values of soft parameters including m_{H_u} at low energies and then we can realize a natural sparticle spectrum. However, the mirage unification condition forces A-term to be less than $\sqrt{2}$ times the soft top squark masses at the mirage unification scale, then the heavy top squark mass is required to explain the 125 GeV Higgs boson mass.

A small μ-parameter has been understood as a result of the mirage unification, but we also know that the gaugino mass is actually crucial to keep the μ-parameter small. Hence the mirage unification will not absolutely necessary, and the gaugino mass ratio would be the most important. Thus we consider the mirage mediation framework with and without the mirage unification condition. Furthermore, a model is proposed, the so-called deflected mirage mediation [19, 20], where the gauge mediation contributes comparably as the other two contributions. The phenomenology of the deflected mirage mediation was discussed in Refs. [41–43] before the discovery of Higgs boson.

In this chapter, we investigate this general class of supersymmetry breaking scenario, and identify the parameter space where the observed Higgs boson mass can be explained while keeping the degree of tuning still relaxed.

3.2 Theoretical backgrounds of deflected mirage mediation

Following Ref. [19], a starting point is the four-dimensional $\mathcal{N} = 1$ effective supergravity Lagrangian of the KKLT-type. We assume that a modulus field, denoted as T, remains in the effective theory. The Kähler potential has a following form at the leading order of matter fields,

$$K = -3\log(T+\overline{T}) + \frac{X\overline{X}}{(T+\overline{T})^{n_X}} + \frac{Q_I\overline{Q}^I}{(T+\overline{T})^{n_I}}, \tag{3.3}$$

where Q_I denotes the MSSM field with I runs over the MSSM matters. A SM gauge singlet field X is a source of supersymmetry breaking for the gauge mediation and $n_X,\ n_I$ are modular weights of the singlet X and the MSSM field Q_I. Values of modular weights have rational numbers and they are determined by, e.g., properties of D-branes where the matter fields live. We assume that values of the modular weights are flavor independent for the quark and lepton supermultiplets to avoid unwanted flavor violations. Note that we employ unit that the Planck scale $M_p \simeq 2.4 \times 10^{18}$ GeV is unity in this section. The superpotential W is expressed as

$$W = W_0(T) + W_1(X) + X\Psi\overline{\Psi} + W_{\rm MSSM}, \tag{3.4}$$

where $W_0(T),\ W_1(X)$ are superpotentials that stabilize T and X, respectively. Ψ and $\overline{\Psi}$ are the vector-like pairs of messenger fields, which consist of 5 and $\bar{5}$ representations of $SU(5)$. There are $N_{\rm mess}$ pairs of the vector-like messengers although they are not shown explicitly. $W_{\rm MSSM}$ is the usual MSSM superpotential that contains the Yukawa interactions and the μ-term as defined in Eq. (2.3). We assume that the gauge kinetic function is given by

$$f_a = T, \tag{3.5}$$

where $a = 1, 2, 3$ corresponds respectively to $U(1)_Y,\ SU(2)_L,\ SU(3)_C$ of SM gauge groups. The VEV of the scalar component of T determines the values of three gauge coupling constants at the unification scale $\sim 10^{16}$ GeV, and they have definitely the same value because of the gauge coupling unification in the MSSM.

Once we assume that the modulus T, the compensator C^* and the singlet X have non-zero VEVs, we can calculate the soft parameters in this setup [44]. Since the gauge mediated contributions are given at the so-called messenger scale $M_{\rm mess} = \langle X \rangle$, which is usually taken at the intermediate scale, the soft parameters at the unification scale are given by the modulus and the anomaly mediations, namely the pure mirage mediations. The soft parameters at the

*Compensator field is used in the conformal supergravity formulation and it plays a role of messenger for the anomaly mediation.

unification scale are given by

$$M_a(M_{\rm GUT}) = \frac{F^T}{T+\overline{T}} + \frac{g_0^2}{16\pi^2} b'_a \frac{F^C}{C}, \tag{3.6}$$

$$A^{ijk}(M_{\rm GUT}) = (3-n_i-n_j-n_k)\frac{F^T}{T+\overline{T}} + \left[y^{ljk}\gamma_l{}^i + (i\leftrightarrow j) + (i\leftrightarrow k)\right]\frac{F^C}{C}, \tag{3.7}$$

$$m^2{}_i{}^j(M_{\rm GUT}) = (1-n_i)\left|\frac{F^T}{T+\overline{T}}\right|^2 \delta_i{}^j - \theta_i{}^j\left(\frac{F^T}{T+\overline{T}}\frac{F^{\overline{C}}}{\overline{C}} + \text{c.c.}\right) + \frac{1}{2}\dot{\gamma}_i^j\left|\frac{F^C}{C}\right|^2, \tag{3.8}$$

where F^T, F^C are the VEVs of F-terms for the modulus T and the compensator C. T, C in the denominators are understood as their VEVs. These values will be fixed by moduli stabilization mechanisms. g_0 is the universal value for the unified gauge couplings. $b'_a \equiv b_a + N_{\rm mess}$, $(a = 1,2,3)$ are beta function coefficients for the gauge coupling constants above the messenger scale and $b_a = (-3,\ 1,\ 33/5)$ are those of the MSSM. γ is the anomalous dimension matrix and $\theta, \dot{\gamma}$ are defined by derivatives of the anomalous dimensions γ with respect to the modulus T and the renormalization scale $\ln Q$, respectively. They can be written as

$$16\pi^2\gamma_i{}^j = \frac{1}{2}\sum_{l,m} y_{ilm}y^{jlm} - \sum_a 2c_a(Q_i)g_a^2\delta_i{}^j, \tag{3.9}$$

$$-16\pi^2\theta_i{}^j = \frac{1}{2}\sum_{l,m}(3-n_i-n_l-n_m)y_{ilm}y^{jlm} - \sum_a 2c_a(Q_i)g_a^2\delta_i{}^j, \tag{3.10}$$

$$16\pi^2\dot{\gamma}_i^j = \frac{1}{2}\sum_{l,m}\left(b_{y_{ilm}}y^{jlm} + y_{ilm}b_y{}^{jlm}\right) - \sum_a 4c_a(Q_i)b'_a g_a^4\delta_i{}^j \tag{3.11}$$

where $c_a(Q_i)$ is the quadratic Casimir for matter field Q_i under gauge group G_a. b_y^{ijk} is the beta function for the Yukawa coupling constant y^{ijk} and $y_{ijk} = (y^{ijk})^*$. Their explicit formulae for the MSSM are listed in Appendix D.

At the messenger scale, the messenger fields decouple from the theory and this gives threshold corrections to gaugino mases and soft masses but for A-terms in the typical gauge mediation models. These corrections read as

$$\Delta M_a(M_{\rm mess}) = -N_{\rm mess}\frac{g_a^2(M_{\rm mess})}{16\pi^2}\left(\frac{F^C}{C} + \frac{F^X}{X}\right), \tag{3.12}$$

$$\Delta m^2{}_i{}^j(M_{\rm mess}) = \sum_a 2c_a(Q_i)N_{\rm mess}\frac{g_a^4(M_{\rm mess})}{(16\pi^2)^2}\left|\frac{F^C}{C} + \frac{F^X}{X}\right|^2\delta_i{}^j. \tag{3.13}$$

It is convenient to introduce ratios of contributions from the anomaly and the gauge mediations to those of the modulus mediation $m_0 \equiv F^T/(T+\overline{T})$,

$$\frac{F^C}{C} = m_0\alpha_m \ln\frac{M_p}{m_{3/2}}, \tag{3.14}$$

$$\frac{F^X}{X} = \alpha_g\frac{F^C}{C} = m_0\alpha_m\alpha_g\ln\frac{M_p}{m_{3/2}}, \tag{3.15}$$

where $m_{3/2}$ is the gravitino mass. The soft parameters can be rewritten by using these ratios as,

$$M_a(M_{\rm GUT}) = m_0 \left[1 + \frac{g_0^2}{16\pi^2} b'_a \alpha_m \ln \frac{M_p}{m_{3/2}}\right], \tag{3.16}$$

$$A^{ijk}(M_{\rm GUT}) = m_0 \left[(3 - n_i - n_j - n_k) + \left[y^{ljk}\gamma_l{}^i + (i \leftrightarrow j,\ k)\right]\alpha_m \ln \frac{M_p}{m_{3/2}}\right], \tag{3.17}$$

$$m^2{}_i{}^j(M_{\rm GUT}) = {m_0}^2 \left[(1 - n_i)\delta_i{}^j - 2\theta_i{}^j \alpha_m \ln \frac{M_p}{m_{3/2}} + \frac{1}{2}\dot{\gamma}_i^j \left(\alpha_m \ln \frac{M_p}{m_{3/2}}\right)^2\right], \tag{3.18}$$

and the threshold corrections at the messenger scale are

$$\Delta M_a(M_{\rm mess}) = -m_0 N_{\rm mess} \frac{g_a^2(M_{\rm mess})}{16\pi^2} \alpha_m (1 + \alpha_g) \ln \frac{M_p}{m_{3/2}}, \tag{3.19}$$

$$\Delta m^2{}_i{}^j(M_{\rm mess}) = {m_0}^2 \sum_a 2c_a(Q_i) N_{\rm mess} \frac{g_a^4(M_{\rm mess})}{(16\pi^2)^2} \left[\alpha_m (1 + \alpha_g) \ln \frac{M_p}{m_{3/2}}\right]^2 \delta_i{}^j. \tag{3.20}$$

Values of $\alpha_m,\ \alpha_g$ are dependent on how the moduli fields are stabilized. Moduli fields are massless modes originated from extra-dimensional vectors or tensors, but such massless fields should be heavy enough to be consistent with cosmological observations and to fix values of the Yukawa and the gauge coupling constants. Thus some mechanism is necessary to generate a potential for moduli fields, called a moduli stabilization mechanism. The KKLT model is one of a few examples of moduli stabilization mechanisms. We do not show details of the moduli stabilization, but potentials are generated by fluxes or non-perturbative effects, like the gaugino condensation in supersymmetric Yang-Mills theory. It is important that value of α_m could be fixed only by discrete parameters, like the number of fluxes, D-branes, intersections and so on. Thus its value would be irrelevant to the fine-tuning problem.

The original KKLT model predicts $\alpha_m = 1$ [17], but some modifications, like moduli-mixing superpotential, of KKLT-type models can allow various values $\alpha_m \leq \mathcal{O}(4\pi)$ [18]. A case of $\alpha_m = 2$ has been studied intensively, because the mirage unification scale is around TeV scale in this case. The mirage unification is a feature of the special case of the mirage mediation where values of soft parameters have the same values as the modulus mediated contributions at the mirage unification scale. Thus gaugino masses are always unified at this scale, and scalar masses and A-terms are also unified if values of the modular weights are the same for all the squarks and sleptons.

The mirage unification scale is given by,

$$M_{\rm mirage} = M_{\rm GUT} \left(\frac{m_{3/2}}{M_p}\right)^{\alpha_m/2}. \tag{3.21}$$

Since the gravitino mass is $\mathcal{O}(16\pi^2 m_0)$ in the KKLT-type models, then the mirage unification scale is at around TeV scale when $\alpha_m \simeq 2$. The mirage unification occurs only when the

condition

$$\sum_{l=i,j,k}(1-n_l)=1 \tag{3.22}$$

is satisfied for sizable Yukawa coupling constants y^{ijk}, like the top Yukawa coupling constant, where i,j,k correspond to each matter field part of the Yukawa coupling constant y^{ijk}. For example, $3-n_{H_u}-n_Q-n_u=1$ has to be satisfied for the top Yukawa coupling. Since the modulus mediated contributions to the soft mass for the MSSM matter Q_i are proportional to $(1-n_i)$, the value of $m_{H_u}^2$ at the EW scale can be small if $n_{H_u}=1$ and the mirage unification condition is satisfied.

This case with $n_{H_u}=1$ is interesting and has been well-studied, but one problem is that it is hard to explain the Higgs boson mass. If the mirage unification is satisfied, A_t and $M_{\rm st}$ at the TeV scale are $A_t=m_0$ and $M_{\rm st}^2=(1-n_Q)(1-n_u)m_0^2$, and then $A_t/M_{\rm st}\leq\sqrt{2}$. Thus this requires $m_0\gtrsim 5$ TeV and then fine-tuning for input parameters other than the μ-parameter would be necessary.

The value of α_g can have an $\mathcal{O}(1)$ value shown in Ref. [19]. If the non-perturbative or higher dimensional superpotential for X is generated, the F-term of X is induced by the supersymmetry breaking effect. For instance, if the superpotential is monotonic,

$$W_1(X)=\frac{X^n}{\Lambda^{n-3}}, \tag{3.23}$$

where Λ is a cut-off scale ($n>3$) or a scale which a gauge coupling constant blows-up ($n<0$). The above superpotential fixes the ratio $\alpha_g=-2/(n-1)$. Incidentally, the mirage unification occurs even when the gauge mediation works and RG-flows are deflected. The mirage unification scale is

$$M_{\rm mirage}=M_{\rm GUT}\left(\frac{m_{3/2}}{M_{\rm P}}\right)^{\frac{\alpha_m\rho}{2}}, \tag{3.24}$$

where ρ is defined as

$$\rho=\frac{1+\frac{2N_{\rm mess}{g_0}^2}{16\pi^2}\ln\frac{M_{\rm GUT}}{M_{\rm mess}}}{1-\alpha_m\alpha_g\frac{N_{\rm mess}{g_0}^2}{16\pi^2}\ln\frac{M_P}{m_{3/2}}}. \tag{3.25}$$

3.3 Mass spectrum of deflected mirage mediation

3.3.1 Parameter assumptions and overview of analysis

It is difficult to realize the 125 GeV Higgs boson mass when the top squark mass is about 1 TeV, if the mirage condition was satisfied. From the analysis in Chapter 2, we know that the most important ingredient to reduce the degree of tuning is the relatively large wino mass. Thus we investigate more general class of the mirage mediation.

In our analysis, we assume that the modular weights for the quark and lepton supermultiplets, denoted by n_Q are universal, while those for up- and down-type Higgs supermultiplets, denoted by n_H, can have a different value from modular weights for other matters. This parameterization is motivated from GUT theories, that is, quarks and leptons can be embedded into one representation of GUT gauge symmetries, but the Higgs bosons do not. The values of $n_Q,\ n_H$ can have $0,\ 1/2,\ 1$ as expected from superstring models. We fix $\tan\beta = 15$. We treat the size of modulus mediation m_0 and the ratio of anomaly mediated contribution to modulus mediated contribution α_m as free parameters.

Parameters of the messenger sector are the number of the messenger pairs $N_{\rm mess}$, the messenger scale $M_{\rm mess}$ where the messengers are decoupled and the ratio of the gauge mediated contributions to the anomaly mediated contributions α_g. We take $N_{\rm mess} = 0,\ 3,\ 6$ and $M_{\rm mess} = 10^6,\ 10^{12}$ GeV. The case with $N_{\rm mess} = 0$ corresponds to the pure mirage mediation.

In total, we have 7 parameters

$$m_0,\ \alpha_m,\ \alpha_g,\ n_Q,\ n_H, N_{\rm mess},\ M_{\rm mess}. \tag{3.26}$$

m_0 controls an overall scale of sparticles. $\alpha_m,\ \alpha_g$ control the ratio of soft parameters, especially α_m determines gaugino mass ratio at the unification scale. $n_Q,\ n_H$ control relations among soft masses and A-terms. Since modulus mediated contributes to a soft mass m_{Q_i} is $(1-n_i)m_0$ and those to an A-term A_{ijk} is $m_0\sum_{l=i,j,k}(1-n_l)$, then these are correlated with each other. The larger ratio of A-term to soft masses can be obtained for smaller modular weights. We study four cases of modular weights,

$$(n_Q,\ n_H) = (0,\ 0), (0,\ 1/2),\ (1/2,\ 1/2),\ (1/2,\ 1). \tag{3.27}$$

We calculated values of soft parameters at the EW scale by solving the 1-loop renormalization group equations which are listed in Appendix B. The explicit values of Yukawa matrices that are used in the analysis are also shown in this Appendix. We evaluated the Higgs boson mass with quantum corrections by the RG-improved effective potential method displayed in Appendix A. The sparticles masses are evaluated at tree-level.

3.3.2 Mass spectrum of mirage mediation

First, we study the case with $N_{\rm mess} = 0$, hence the gauge mediated contributions are absent.

Figure. 3.1 shows the Higgs boson mass and the degree of tuning of the μ-parameter with modular weights $(n_Q,\ n_H) = (0, 0),\ (0, 0.5)$.

A Higgs boson mass in the range $124.4 \leq m_h \leq 126.6$ GeV is obtained in the red region, while it becomes heavier than 126.6 GeV in the yellow region. We can see that the Higgs boson mass reaches about 125 GeV if $m_0 \gtrsim 1.1$ TeV for $(n_Q,\ n_H) = (0, 0)$, and $m_0 \gtrsim 1.3$ TeV for $(n_Q,\ n_H) = (0, 0.5)$. The blue lines indicate the lightest top squark mass, and their values are not so different for these cases. The Higgs boson mass is slightly heavier for $(n_Q,\ n_H) = (0, 0)$ case due to the larger A-term.

The black dashed lines indicate the degree of tuning and the correct electroweak symmetry breaking (EWSB) cannot occur in the dark gray region because of large positive, rather than

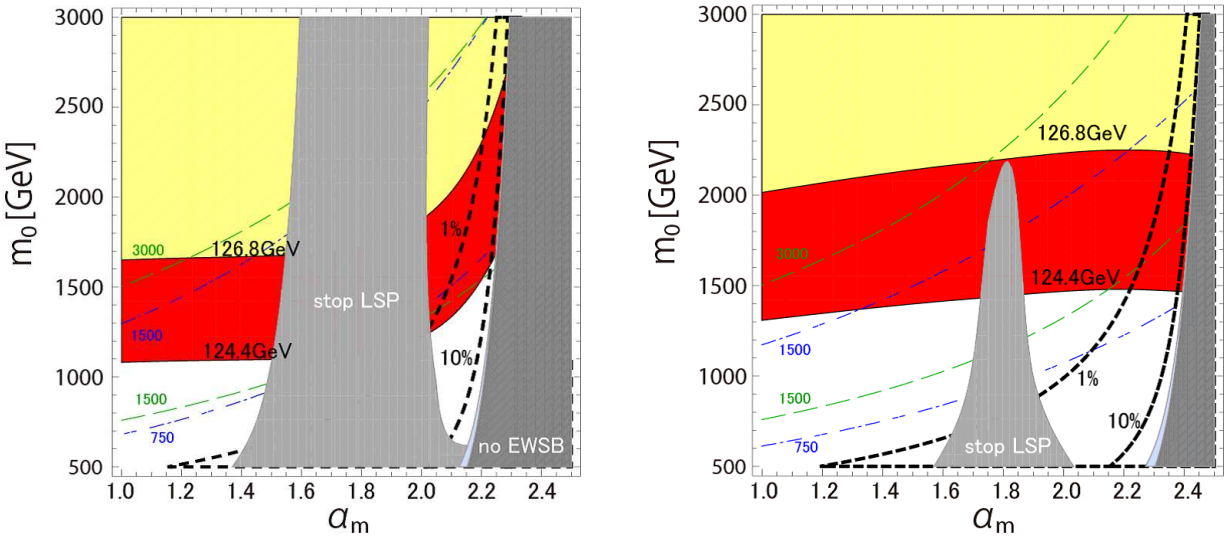

Figure 3.1: The Higgs boson mass m_h [GeV] and the degree of tuning the μ-parameter, $|\Delta_\mu|^{-1} \times 100\%$ with modular weights $(n_Q, n_H) = (0, 0)$ (left), $(0, 0.5)$ (right) on $\alpha_m - m_0$ plane.

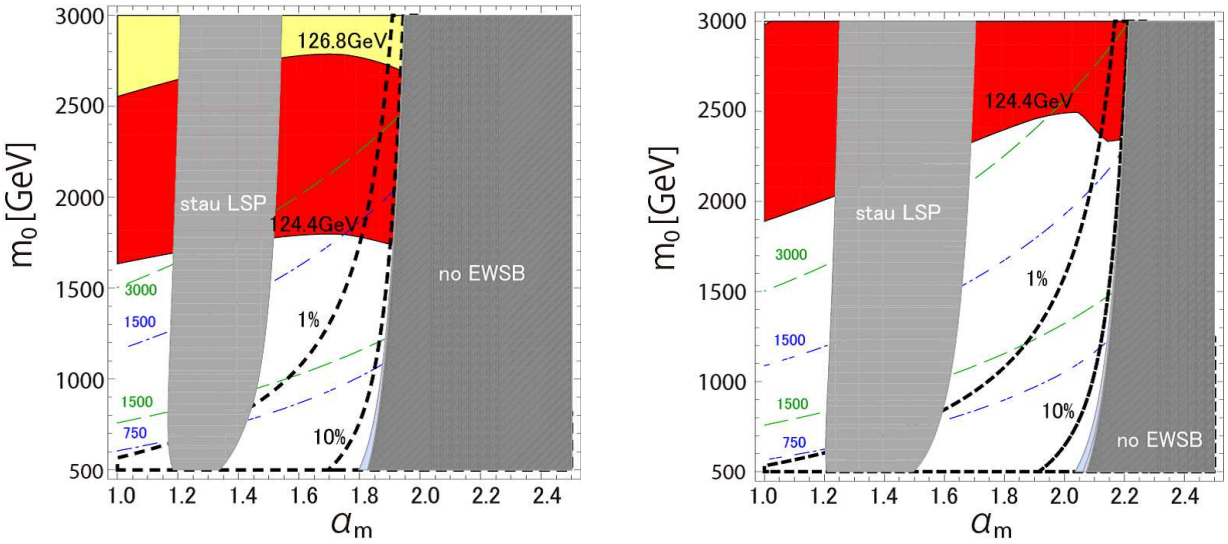

Figure 3.2: The results for the cases of $(n_Q, n_H) = (0.5, 0.5)$ (left), $(0.5, 1)$ (right).

	sample points			
input parameters	M1	M2	M3	M4
(n_Q, n_Q)	(0,0)	(0,0.5)	(0.5,0.5)	(0.5,1)
α_m	2.26	2.42	1.91	2.14
m_0[GeV]	2000	2000	2000	2000
output parameters	values			
$100 \times \lvert\Delta_\mu^{-1}\rvert$ (%)	53.5	28.4	7.54	2.31
m_h[GeV]	125.4	126.2	125.2	123.5

Table 3.1: The mass of SM-like Higgs boson and the degree of tuning μ parameter, $100 \times |\Delta_\mu^{-1}|$ (%) at several sample points.

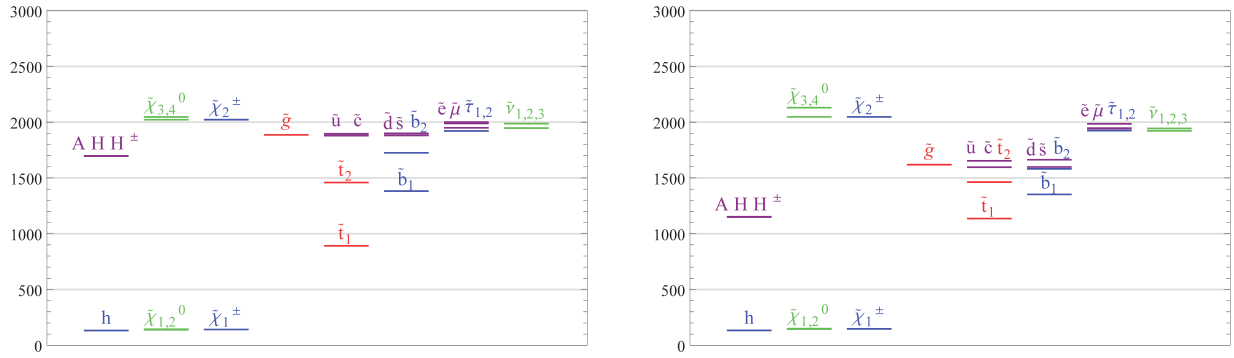

Figure 3.3: The mass spectrum at the sample points M1 (left) and M2 (right). The vertical axes represent the masses (GeV). The subscript 1, 2 for the first- and second-generation squarks and sleptons are omitted for simplicity, because their masses are quite degenerated.

negative as it should be for the realistic EWSB, values of $m_{H_u}^2$. As α_m is increased, $m_{H_u}^2$ gets a smaller negative value due to the larger ratio of wino to gluino masses, thus relaxing the degree of tuning of μ-parameter for larger values α_m. Since $m_{H_u}^2$ takes a smaller positive value at the unification scale, larger values of α_m are favored from the naturalness viewpoint for $(n_Q,\ n_H) = (0, 0.5)$ compared with $(n_Q,\ n_H) = (0, 0)$.

The LSP is represented by bino, top squark or higgsino for $\alpha_m \lesssim 1.5$, $1.5 \lesssim \alpha_m \lesssim 2.0$, $\alpha_m \gtrsim 2.0$, respectively. The gaugino masses are universal at the unification scale at $\alpha_m = 0$ and the bino becomes the LSP. As the parameter α_m increases, the bino mass increases while the μ-parameter decreases, and the higgsino becomes LSP for $\alpha_m \simeq 2$. Since the top squark becomes LSP, the intermediate region where both of the higgsino and bino are relatively heavy is inconsistent with cosmological observations.

We can find a parameter region with a relaxed degree of tuning where the Higgs boson mass is about 125 GeV for $\alpha_m \simeq 2.0$ and $1.5 \lesssim m_0 \lesssim 2.0$ TeV. The degree of tuning can be relaxed more than 1% in not a narrow region for $m_0 \lesssim 2.0$ TeV, but the region where it is relaxed above 10% is narrow, although the value of α_m would be determined only by discrete parameters in

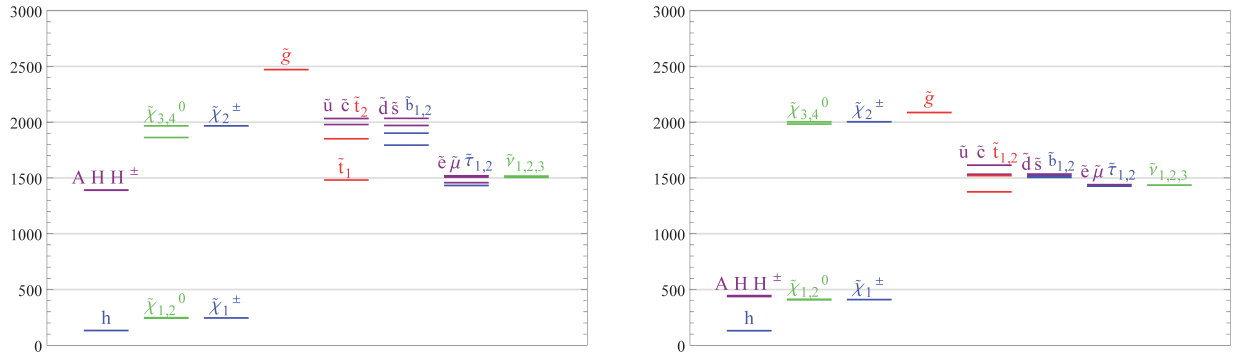

Figure 3.4: The mass spectrum at the sample points M3 (left) and M4 (right).

some superstring models.

Figure 3.2 show similar plots as Figs. 3.1, but values of the modular weights are different $(n_Q,\ n_H) = (0.5, 0.5),\ (0.5, 1)$. The latter case satisfies the mirage unification condition and has been studied intensively [15, 37–40]. At the mirage unification scale, a scalar mass squared for Q_i is given by $(1 - n_i)m_0^2$ and an A-term by m_0. If $\alpha_m \simeq 2$, the mirage unification scale is around TeV scale. The value of $m_{H_u}^2$ can be almost vanishing at this scale if $n_H = 1$. However, the Higgs boson mass can reach about 125 GeV only at $m_0 \gtrsim 3.0$ TeV, since the A-term to scalar mass ratio is $\sqrt{2}$ at the unification scale. Thus the degree of tuning the μ-parameter can be relaxed unless the value of α_m is fixed at suitable range with high accuracy.

The stau instead of the top squark tends to be the LSP in the intermediated values of α_m for $n_Q = 0.5$. The soft scalar masses at the unification scale are smaller for larger values of modular weights n_Q and the slepton mass terms are not so increased by the RG evolution. Thus the stau remains light in these cases.

Table. 3.1 shows values of the degree of tuning of the μ-parameter and the Higgs boson mass at several sample points M1-4 with $m_0 = 2.0$ TeV. The Higgs boson mass can not reach 125 GeV for the last case M4. Figures 3.3 and 3.4 show mass spectrum at these sample points.

For $n_Q = 0$, the top squark mass is around 1.0 TeV, while it is around 1.5 TeV for $n_Q = 0.5$. The mass relation between squarks and sleptons is dependent on gaugino mass ratio, or equivalently α_m. The gluino mass is larger than bino and wino masses for small α_m, while it gets relatively smaller for large α_m. If the gluino mass is heavier than the bino and wino masses, squarks tend to be heavier than sleptons, and vice versa. The modular weight for the Higgs bosons n_H influences the value of m_{H_d}, especially the heavy-states of the Higgs bosons are as light as higgsinos for the sample point M4. This can be understood as a consequence of the mirage unification, that predicts a degenerate value of m_{H_u} and m_{H_d} around the unification scale. Then the charged Higgs boson could be seen at a direct search for the extra Higgs boson search or the flavor physics. The gluino mass can be lighter than 2.0 TeV and the top squark can be lighter than 1.0 TeV for $n_Q = 1.0$, thus these are testable at the LHC in near future.

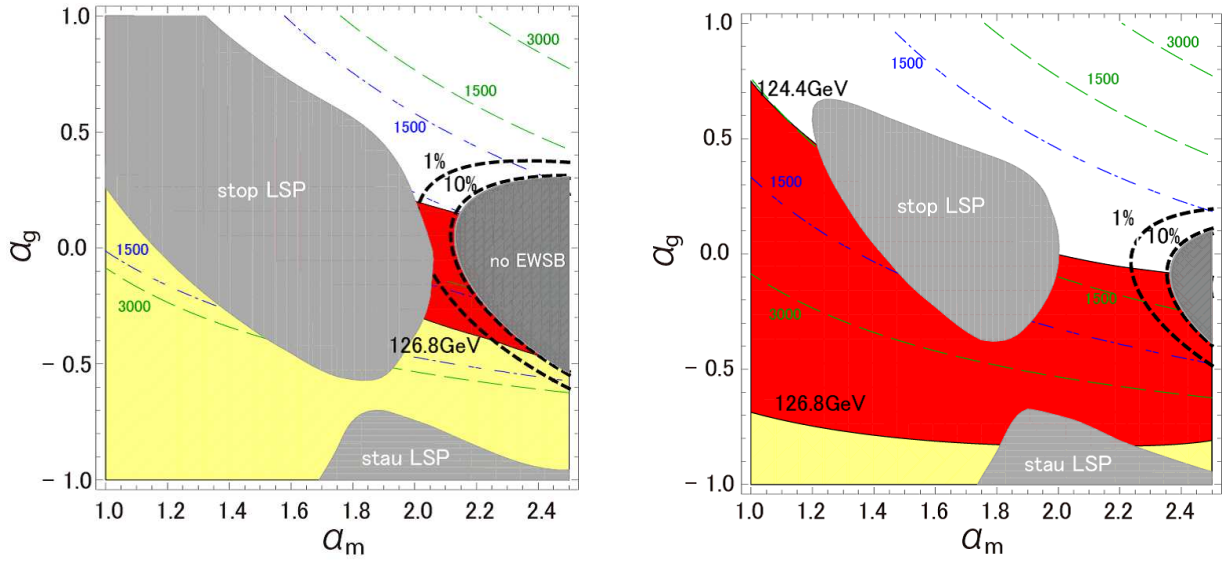

Figure 3.5: The results on $\alpha_m - \alpha_g$ plane for the case of $(n_Q, n_H) = (0, 0)$ (left) and $(0, 0.5)$ (right) with $m_0 = 2000$ GeV, $M_{\rm mess} = 10^{12}$ GeV and $N_{\rm mess} = 3$. The meanings of the lines and colored regions are same as in Fig.3.1.

3.3.3 Mass spectrum of deflected mirage mediation

We consider the case with gauge mediated contributions, namely $N_{\rm mess} = 3,\ 6$. We fix $m_0 = 2.0$ TeV to put the Higgs boson mass around 125 GeV. Note that the Landau pole for the gauge coupling constants appears below the unification scale if the number of messengers $N_{\rm mess}$ is too large or the messenger scale $M_{\rm mess}$ is too low energy. Here we consider three cases with $(N_{\rm mess},\ M_{\rm mess}) = (3, 10^{12}\ {\rm GeV}),\ (3, 10^{6}\ {\rm GeV}),\ (6, 10^{12}\ {\rm GeV})$. Values of α_g can take both signs. For instance, the stabilization potential Eq. (3.23) leads $\alpha_g = -2/(n-1)$, where $n < 0$ or > 3.

Figures 3.5 and 3.6 show the Higgs boson mass and the degree of tuning as in Figs. 3.1, 3.2, but on the α_m-α_g plane. Meanings of the colored regions and the lines are the same as in the previous figures. Impacts from the messenger sector are not only through the threshold corrections for the gaugino masses Eq. (3.19) and scalar masses Eq. (3.20), but also values of the gauge coupling constants through the RG-evolution. Thus low energy spectrum is different from cases with $N_{\rm mess}$ even if $\alpha_g = 0$.

The Higgs boson mass can be larger than 125 GeV only for $\alpha_g \lesssim 0$. For $\alpha_g > 0$, the gaugino masses are reduced while the scalar masses are enhanced by the gauge mediated contributions, and then the effects due to the large wino-to-gluino masses are weakened. On the other hand, gaugino masses are enhanced, but the ratio of wino-to-gluino masses is decreased for negative α_g. Moreover, the gauge mediation gives contributions only for scalar masses, but not for A-terms, then the Higgs boson mass is never enhanced by gauge mediated contributions. Again, the Higgs boson mass tends to be larger for $n_Q = 0$ than $n_Q = 0.5$ similarly to the cases with $N_{\rm mess} = 0$.

The degree of tuning is relaxed for $\alpha_m \gtrsim 2,\ -0.5 \lesssim \alpha_g \lesssim 0$. The favored value of α_m becomes larger when α_g deviates from 0, since $m_{H_u}^2$ is increased by the gauge-mediated contributions.

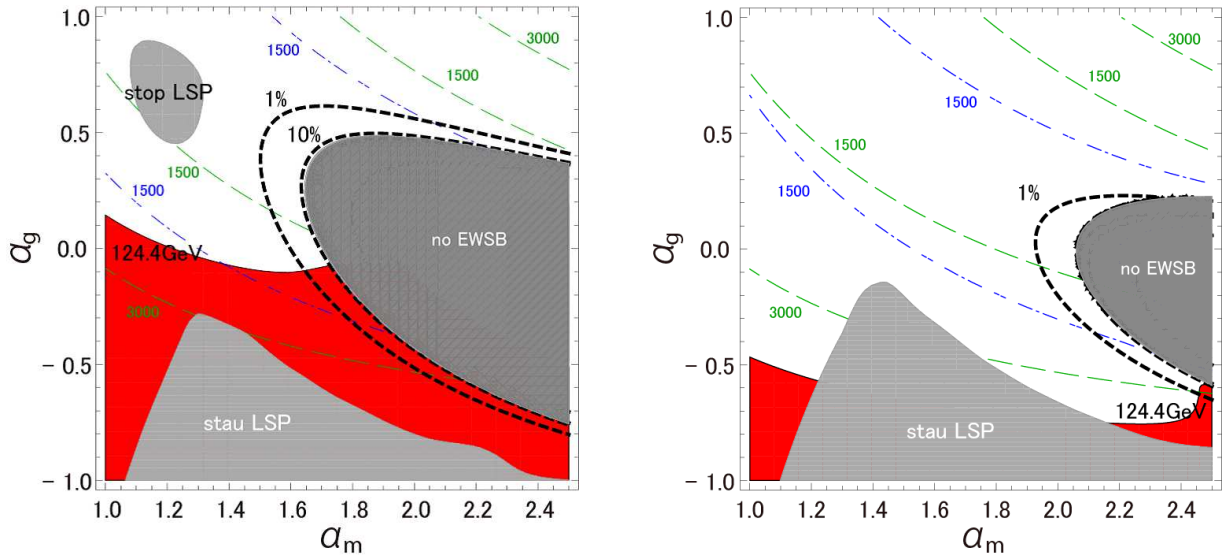

Figure 3.6: The results for the case of $(n_Q, n_H) = (0.5, 0.5)$ (left) and $(0.5, 1)$ (right) with $m_0 = 3000$ GeV, $M_{\rm mess} = 10^{12}$ GeV and $N_{\rm mess} = 3$.

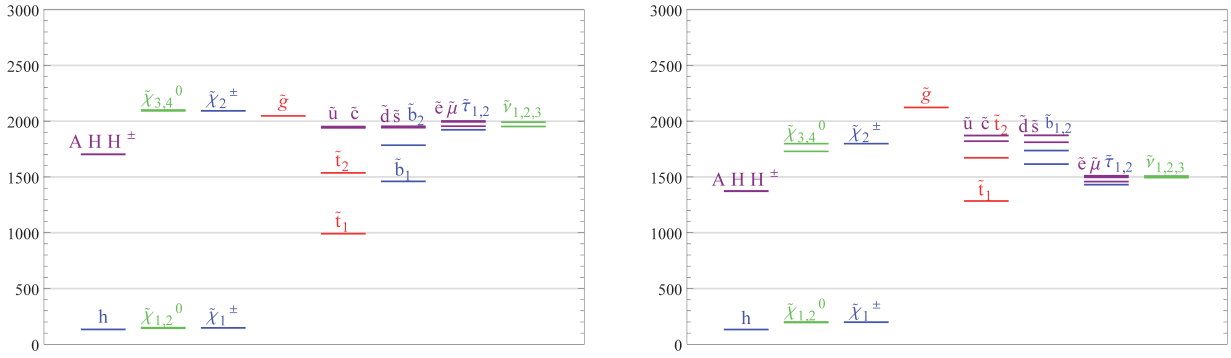

Figure 3.7: The mass spectrum at the sample points D1(left) and D3(right).

	sample points			
input parameters	D1	D2	D3	D4
(n_Q, n_H)	(0,0)	(0,0.5)	(0.5,0.5)	(0.5,1)
m_0[GeV]	2000	2000	2000	2000
$(N_{\rm mess}, M_{\rm mess}$[GeV])	(3,10^{12})	(3,10^{12})	(3,10^{12})	(3,10^{12})
(α_m, α_g)	(2.3,-0.35)	(2.4,-0.25)	(1.8,-0.20)	(2.5,-0.60)
output parameters	values			
$100 \times \lvert\Delta_\mu^{-1}\rvert$ (%)	30.5	12.1	10.6	4.95
m_h[GeV]	125.7	126.1	124.8	124.5

Table 3.2: The mass of SM-like Higgs boson and the degree of tuning μ parameter $100 \times |\Delta_\mu^{-1}|$ (%) at the sample points.

All of these four figures would indicate that natural region exists even without the modulus mediated contributions, namely at large α_m limit and $\alpha_g \simeq -1$. This case is known as the deflected anomaly mediation [45, 46]. We expect the cancellation between anomaly and gauge-mediated contributions to the gluino masses, and the sizable ratio of wino-to-gluino masses can be obtained. However, the A-term is not so large that the Higgs boson mass reaches 125 GeV if the top squark is around 1 TeV.

The Higgs boson mass and the degree of tuning of the μ-parameter at the sample points are listed in Table 3.2, and the sparticle and Higgs boson spectrum at the sample points D1 (left) and D3 (right) are shown in Fig. 3.7. The typical spectrum is quite similar for the pure mirage mediation, once we focus on the parameter space where the degree of tuning is relaxed. Squarks except top squark and sleptons have almost degenerate masses respectively, and their values are controlled by gluino mass and bino, wino masses respectively. Thus the mass spectrum is roughly controlled only by α_m once we require the μ-parameter to be small.

We also varied the messenger sectors. Figure 3.8 shows a similar plot as Fig. 3.5, but $N_{\rm mess} = 6$. In this case, the beta functions for gauge coupling constants are changed, and then the gauge coupling constants are enhanced at high scales. The most significant effect is that it enhances the gauge mediated contribution, since it is proportional to $N_{\rm mess}$ directly. The soft parameters become more sensitive to the value of α_g in this case. Thus these figures look like squeezed along the α_g direction. Incidentally, the chargino is lighter than the LEP bound in the blue region. This is due to a cancellation happening among the three mediation mechanisms for the wino mass parameter.

Figure 3.9 shows similar plot as Fig. 3.5, but $M_{\rm mess} = 10^6$ GeV. Note that the range of the vertical axis is shifted from other figures. The natural region shifts and gets closer to $\alpha_g \simeq -1.0$ compared with $M_{\rm mess} = 10^{12}$ GeV. The distance between the messenger scale and the unification scale gets longer for lower messenger scale, then the value of strong gauge coupling constant at the messenger scale becomes larger while it becomes smaller for the weak gauge coupling constants. Since the gauge-mediated contributions are proportional to $\alpha_g + 1$, the ratio α_g

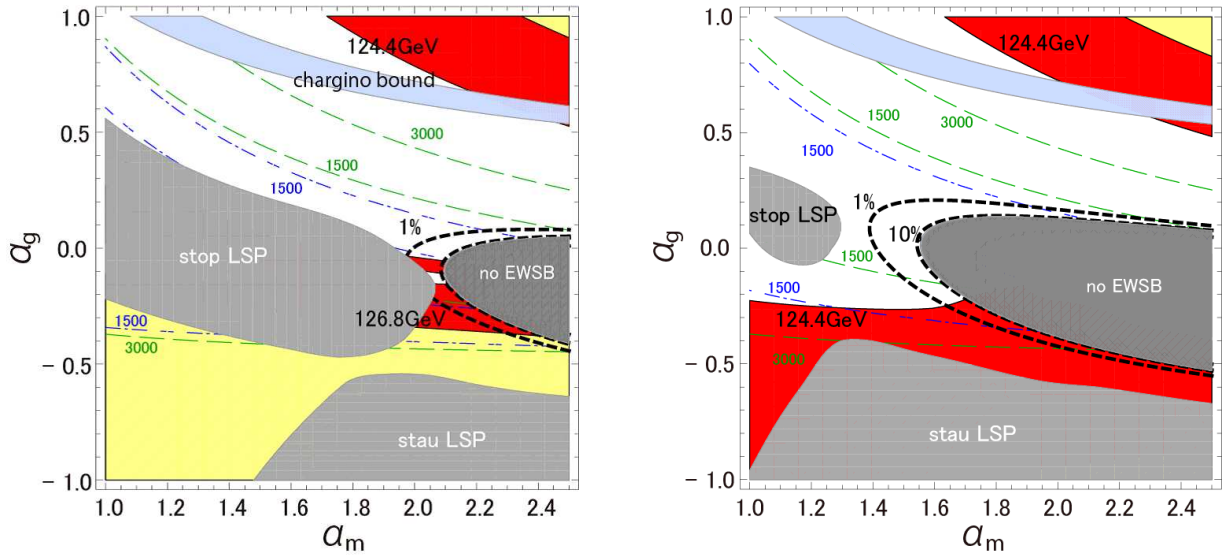

Figure 3.8: The results for the case of $M_{\rm mess} = 10^{12}$GeV, $N_{\rm mess} = 6$ with $(n_Q, n_H) = (0, 0), m_0 =$ 2000 GeV (left), $(n_Q, n_H) = (0.5, 0.5), m_0 = 3000$ GeV (right).

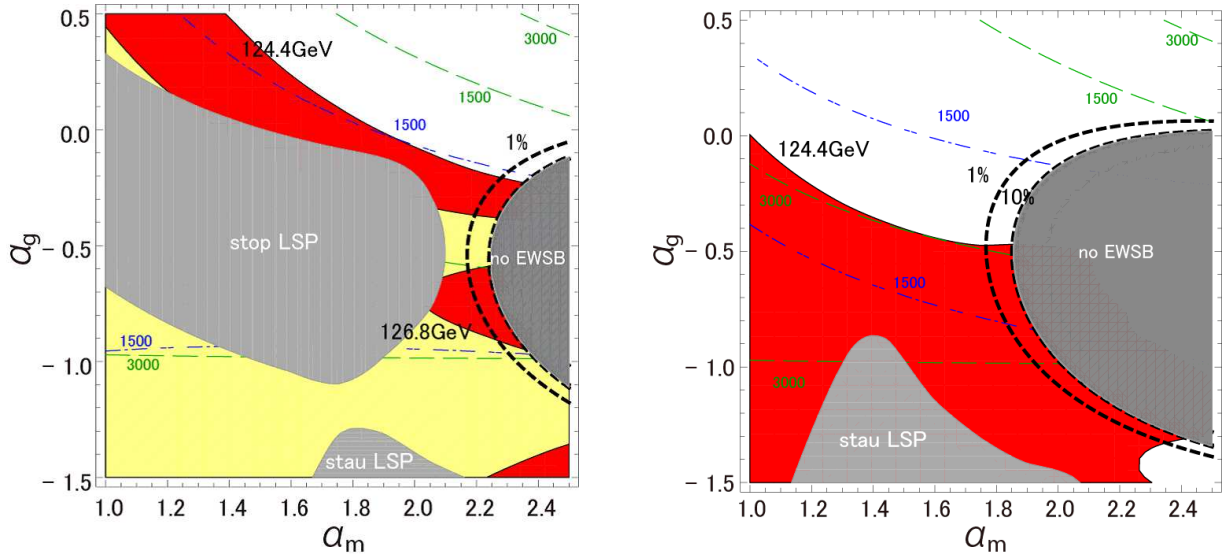

Figure 3.9: The results for the case of $M_{\rm mess} = 10^{6}$GeV, $N_{\rm mess} = 3$ with $(n_Q, n_H) = (0, 0), m_0 =$ 2000 GeV (left) , $(n_Q, n_H) = (0.5, 0.5), m_0 = 3000$ GeV (right). Note that the origin of the vertical axis is different from the other figures.

	sample points			
input parameters	D5	D6	D7	D8
(n_Q, n_H)	$(0, 0)$	$(0.5, 0.5)$	$(0, 0)$	$(0.5, 0.5)$
m_0[GeV]	2000	2000	2000	2000
$(N_{\rm mess}, M_{\rm mess}$[GeV])	$(6, 10^{12})$	$(6, 10^{12})$	$(3, 10^6)$	$(3, 10^6)$
(α_m, α_g)	$(2.20, -0.26)$	$(1.8, -0.29)$	$(2.25, -0.66)$	$(1.9, -0.77)$
output parameters	values			
$100 \times \lvert\Delta_\mu^{-1}\rvert$ (%)	9.17	6.91	11.6	18.1
m_h[GeV]	124.5	124.6	125.5	125.4

Table 3.3: The mass of SM-like Higgs boson and the degree of tuning μ parameter at the sample points.

should get closer to -1.0 to compensate the correction for gaugino mass ratio at the messenger scale. The Higgs boson mass and the degree of tuning at several sample points are listed in Table 3.3.

3.3.4 Mirage mediation without tachyonic masses

There are some subtleties for the mirage mediation. One is the so-called moduli-induced gravitino problem [47], although this is a problem for the KKLT moduli stabilization mechanism, rather than the mirage mediation itself. Historically, one of the benefits of the mirage mediation is that the size of gravitino mass is $\mathcal{O}(4\pi^2 m_0) = \mathcal{O}(100\text{TeV})$ for TeV-scale sparticles $m_0 \simeq \mathcal{O}(1\text{TeV})$. Thus it can solve the well-known gravitino problem induced by the gravitino with a mass of $\mathcal{O}(1\text{TeV})$ that the late-time gravitino decay after the Big-Bang breaks nucleons and ruins the success of the Big-Bang scenario. However, the modulus mass predicted by the KKLT scenario is $\mathcal{O}(100\text{TeV})$ and the LSP overcloses the universe produced by the decay of the modulus through the decay of the gravitino. This is the moduli-induced gravitino problem that the LSP abundance produced non-thermally excesses the observed value. Solutions for this problem can be categorized into three ways. One is diluting the produced LSP, and another is preparing other LSP candidate. Candidates for dilution are Q-balls and/or thermal inflation, and the LSP candidate is an axino [40]. Third possibility is to consider other moduli stabilization mechanism that the moduli will not decay to the gravitino while the sparticle spectrum is determined by mixture of the moduli and anomaly mediations.

The other subtlety is on tachyonic masses at high energies. Although all of the sfermions have definitely large masses at low energies, most of them are tachyonic at high energies. When we consider the thermal history of the universe, the thermal mass lifts up such negative mass squared, and become cosmologically safe. Moreover, it has been also discussed that such a tachyonic mass does not change structure of the scalar potential of the MSSM significantly if the scale where the tachyonic mass appears is enough far from the TeV scale [48]. Thus the

tachyonic mass would not be problematic but whether if it is true would depend on the thermal history of the universe. It might be worth probing a possibility that any tachyonic masses are absent at any scale until the unification scale.

Actually, we can avoid tachyonic masses for the third-generation quark due to the large contributions proportional to the top Yukawa coupling constant for $(n_Q,\ n_H) = (0, 0)$ even if $\alpha_m \simeq 2$. However, the first- and second-generation squark masses squared must be negative at the unification scale. Fortunately, we know that masses of the first- and second-generation squarks are less important for the Higgs boson mass and the naturalness argument, and modification of their masses will not spoil the attractive features of the mirage mediation discussed above. One candidate to give contributions to soft masses is a D-term mediated supersymmetry breaking. Effects from the D-term mediation to the mirage mediation are studied in Ref. [49]. We note that flavor-dependent moduli mediation would cause too large flavor violation due to the mixing terms of the moduli and anomaly mediations even if the modulus mediation is flavor diagonal and has no mixing. This can be seen in the general formula of the soft masses presented in Appendix D.

The D-term supersymmetry breaking could be caused by an anomalous $U(1)_A$, and it could be flavor dependent if the $U(1)_A$ is the flavor symmetry in some sense, for instance, like the Froggatt-Nielsen mechanism [50]. We assume additional D-term contributions only for the first- and second-generation sfermions,

$$(\Delta_D m^2)_i{}^j = \delta_i{}^j \times (2.0\text{TeV})^2, \tag{3.28}$$

where $i,\ j = 1, 2$ are flavor indices of sfermions. Note that this type of contribution cannot be hierarchically large, because it will reduce the third-generation squark masses and $m_{H_d}^2$ due to the mixing through the Yukawa matrices. The third-generation squark masses are significant for the running of $m_{H_u}^2$ and the $m_{H_d}^2$ should be enough large to keep the curvature of the D-flat direction of the Higgs potential positive. Thus these parameters must not be changed by introducing the D-term contribution in order not to spoil the success of the mirage mediation shown in previous sections.

With the D-term contribution, we can avoid any tachyonic masses at the unification scale. The explicit values of soft parameters at the unification scale are listed in Table 3.4. We can see that the values of Δ_μ and the Higgs boson mass are not so changed, but we can avoid any tachyonic masses. Figure 3.10 shows a sample low energy spectrum at the sample point. The first- and second-generation sfermions have masses above 3 TeV. This would help to evade the flavor violations. A remarkable feature is that, the tachyonic masses can be avoid only when $(n_Q,\ n_H) = (0,\ 0)$.

3.4 Summary

In this chapter, we studied an interesting way to realize a certain gaugino mass ratio. The mirage mediation is a mixed mechanism of the moduli and anomaly mediations, and the gauge mediation co-exists for the deflected mirage mediation. A suitable gaugino mass ratio can be obtained in these mediation mechanisms.

sparticles	mass [GeV]	particles, parameter	mass [GeV], value
$m_{\tilde{Q}_1}$	980.9	$m_{\tilde{E}_1}$	582.4
$m_{\tilde{Q}_2}$	1319	$m_{\tilde{E}_2}$	2059
$m_{\tilde{Q}_3}$	1334	$m_{\tilde{E}_3}$	2083
$m_{\tilde{U}_1}$	1769	M_{H_u}	3089
$m_{\tilde{U}_2}$	1775	M_{H_d}	738.8
$m_{\tilde{U}_3}$	2337	$(A_u)_{33}$	3810
$m_{\tilde{D}_1}$	746.5	$M_{\tilde{B}}$	4968
$m_{\tilde{D}_2}$	2098	$M_{\tilde{W}}$	2446
$m_{\tilde{D}_3}$	2116	$M_{\tilde{g}}$	650.9
$m_{\tilde{L}_1}$	426.9	$m_h(m_Z)$	125.3
$m_{\tilde{L}_2}$	2021	$m_H(m_Z)$	1638
$m_{\tilde{L}_3}$	2021	$100 \times \lvert\Delta_\mu^{-1}\rvert(\%)$	48.32

Table 3.4: The sparticle masses $m_{\tilde{\phi}_i}$, Higgs masses $M_{H_{u,d}}$, A-term for the top squark $(A_u)_{33}$, gaugino masses $M_{\tilde{G}}$ at the GUT scale, the Higgs masses at the EW scale $m_{h,H}$ and the degree of tuning of μ parameter where $M^2_{H_{u,d}} = |\mu|^2 + m^2_{H_{u,d}}$. The subscripts $\tilde{\phi}_i$ denote the mass eigenstates, $\tilde{Q}_i$: left-handed squarks, $\tilde{U}_i$, $\tilde{D}_i$: up- and down-type right-handed squarks, $\tilde{L}_i$, $\tilde{E}_i$: left- and right-handed sleptons, $\tilde{B}$: bino, $\tilde{W}$: wino, $\tilde{g}$: gluino, h, H: CP-even lighter and heavier Higgs bosons. The values of input parameters are the same as the sample point M1: $(n_Q, n_H) = (0, 0)$, $m_0 = 2000$ GeV and α_m=2.26.

The requirement of the 125 GeV Higgs boson mass constrains the parameter space of the mediation scenario significantly. If the mirage unification is to be satisfied, the size of the modulus mediation m_0 must be larger than 2.5 TeV. In this case, the parameter region is quite narrow where the degree of tuning the μ-parameter is relaxed above 1%.

Smaller values of modular weights are favored to enhance the Higgs boson mass, while the gaugino masses are independent of the modular weights. Hence, we also studied other patterns of modular weights and found the parameter region where the Higgs boson mass is about 125 GeV, but the parameter space with the small μ-parameter can be obtained. Such a region appears always around $\alpha_m \sim 2$ for any choice of modular weights.

Since the gauge messengers sometimes appear when the MSSM is embedded into some superstring models, we studied the case that the gauge mediation also contributes to the soft parameters. We found a parameter region with the 125 GeV Higgs boson mass and the small μ-parameter, where $-1 \lesssim \alpha_g \lesssim 0$ and $\alpha_m \gtrsim 2$. Interestingly, the resultant mass spectrum of sparticles and Higgs bosons is almost the same as that in the case of pure mirage mediation and is controlled by the value of α_m, once we restrict the case with small μ-parameter.

The typical mass spectrum can be summarized as follows. The LSP is higgsino-like since we choose the small μ-parameter. All the gauginos, sleptons and squarks except top squark have roughly the same masses due to the large bino and wino masses at the unification scale. Since

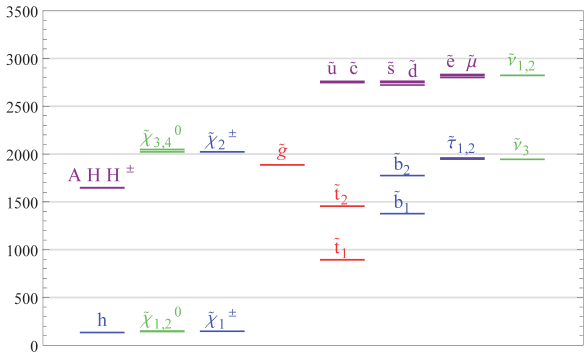

Figure 3.10: The mass spectrum for the case that the first- and second-generation sfermion soft masses receive the D-term mediated contributions Eq. (3.28) in addition to the mirage mediated contributions with $(n_Q, n_H) = (0, 0)$, $m_0 = 2000$ GeV and α_m=2.26.

it is reduced by the top Yukawa coupling through the RG runnings, the top squark mass can be lighter than other sparticle masses. These features are mainly due to the gaugino mass ratios at the unification scale rather than scalar masses. Thus experimental studies of the general NUGM scenario in the following chapters could be applied to the (deflected) mirage mediation in this chapter.

Chapter 4

LHC phenomenology with non-universal gaugino masses

4.1 General features of LHC

The NUGM scenario is testable at the LHC, since the sparticle masses can be lighter than TeV scale even with the 125 GeV Higgs boson mass due to the sizable ratio of $A_t/M_{\rm st}$. It is worth studying expected signals and possibility of discovery or exclusion potential of the NUGM scenario at the LHC [51, 52]. In general, the colored sparticles are easier to be produced than the color-singlet sparticles, because protons are collided at the LHC, although the color-singlet sparticles tend to give cleaner signals like tri-leptons than that of colored sparticles. All of sparticles finally decay to the LSP as a consequence of the R-parity and the LSP must be both electrically and color neutral to be consistent with the cosmological observations. Thus expected signals from sparticle productions are accompanied with large missing energy. The run-I of the LHC finished with center of mass energies of 7 and 8 TeV, and now the run-II is running with center of mass energy reaching 13 TeV. The center of mass energy will reach to 14 TeV during the run-II and it continues to run until 2023 and collect data with an integrated luminosity of 100 fb^{-1} until the end of run-II.

This chapter is organized as follows. First, we show characteristics of the sparticles in the NUGM scenario, especially their mass spectrum and decay modes, which are important for collider signals in Section 4.2. Then, we study exclusion limits obtained in the run-II data of the LHC in Section 4.3. Finally, we summarize this chapter in Section 4.4.

4.2 Masses and Decays

4.2.1 Boundary conditions

The right-handed top squark and the higgsinos tend to be lighter than other sparticles in the NUGM scenario. A key ingredient of the NUGM scenario is a suitably large wino mass parameter at the unification scale. The value of wino mass term around the EW scale is the same

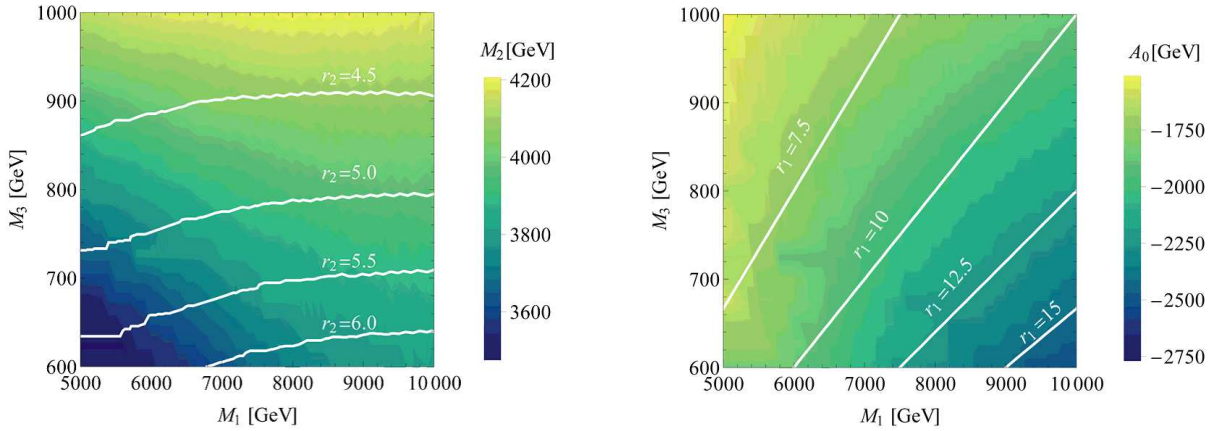

Figure 4.1: Boundary conditions at the unification scale, where $m_0 = 1.0$ TeV, $\tan\beta = 15$.

as the gluino mass parameter at the EW scale in this case. This leads sleptons to be as heavy as squarks unlike the cases with universal gaugino masses at the unification scale. Since the gluino has the largest production cross section for proton-proton collision, lower bounds on squarks, sleptons and gauginos are given by the exclusion limits from gluino searches. Exceptions are the right-handed top squark and the higgsinos. The large wino mass term reduces the right-handed top squark mass and the value of μ-parameter due to the RG-effects as discussed in the previous chapter.

Figure 4.1 shows values of boundary conditions and the gaugino mass ratios $r_{1,2} = M_{1,2}/M_3$ at the unification scale. We fixed $\tan\beta = 15$, $m_0 = 1.0$ TeV and the values of M_2 and A_0 are fixed to realize $\mu = 300$ GeV and the SM-like Higgs boson mass in a range $m_h = 125.09 \pm 0.24$ GeV. The Higgs boson masses and sparticles mass spectrum with the above condition is calculated by using SOFTSUSY-3.5.1 [53]. A suitable value of r_2 is found to be 6 for $M_3 \sim 600$ GeV and decreases as M_3 increases. This is due to the larger radiative corrections from the top squarks to the Higgs potential minimization condition. The value of A-term A_0 is within $\mathcal{O}(1-3$ TeV) and is not so different from the other soft parameters. Suitable values of A_0 are mainly correlated with r_1.

Table 4.1 and Table 4.2 show sample mass spectrum and the branching fractions of the sparticles with light higgsinos in the NUGM scenario. Note that complex conjugates of particles are dropped for simplicity. The branching fractions are calculated by using SDECAY [54]. The boundary conditions at the unification scale are listed in Table 4.1. Since the gluino mass contribution to the right-handed top squark mass $m_{\tilde{u}_3}$ is canceled by that of the wino mass when the same cancellation occurs for $m^2_{H_u}$, the bino mass parameter mainly determines the lightest top squark mass. The sample points ST1, ST2, SB1 and SB2 have the light top squark, but GL1 and GL2 have the light gluino. The bino mass parameter should be large to reduce the gluino mass about 1 TeV while keeping the top squark mass squared positive. Hence the top squark mass is about 1.5 TeV at the sample points GL1 and GL2.

We also consider $\tan\beta = 50$ for the sample points SB1 and SB2. In this case, the bottom Yukawa coupling is as strong as the top Yukawa coupling, and the right-handed bottom squark

input [GeV]	ST1	ST2	SB1	SB2	GL1	GL2
$\mu(m_Z)$	150	300	300	300	300	800
$\tan\beta$	15	15	50	50	15	15
A_0	-1469	-1283	-1908	-2259	-2448	-2570
M_1	5000	2000	5000	10000	12000	12000
M_2	4156	3995	4085	4100	3886	3554
M_3	1000	1000	1000	1000	750	750
mass [GeV]						
m_h	125.03	125.03	125.03	125.02	125.00	125.03
m_H	2668	2453	898.7	1200	3168	3101
$m_{\widetilde{d}_L}$	3327	3234	3296	3342	3040	2877
$m_{\widetilde{d}_R}$	2161	2092	2169	2399	2217	2221
$m_{\widetilde{u}_L}$	3326	3233	3295	3342	3039	2876
$m_{\widetilde{u}_R}$	2399	2131	2405	3180	3353	3355
$m_{\widetilde{b}_1}$	2075	2012	1070	1301	2111	2117
$m_{\widetilde{b}_2}$	2895	2864	2574	2402	2320	2150
$m_{\widetilde{t}_1}$	793.9	409.1	861.7	1837	1964	1990
$m_{\widetilde{t}_2}$	2903	2871	2583	2424	2355	2226
$m_{\widetilde{e}_L}$	2963	2742	2922	3335	3450	3301
$m_{\widetilde{e}_R}$	2094	1241	2095	3809	4521	4520
$m_{\widetilde{\tau}_1}$	2029	1161	1245	2928	3408	3258
$m_{\widetilde{\tau}_2}$	2940	2725	2669	3066	4457	4456
$m_{\widetilde{g}}$	2232	2224	2229	2248	1745	1744
$m_{\widetilde{\chi}_1^0}$	152.6	302.8	305.6	306.8	307.0	812.2
$m_{\widetilde{\chi}_2^0}$	155.8	308.6	308.9	309.5	309.7	815.3
$m_{\widetilde{\chi}_3^0}$	2215	881.5	2225	3343	3162	2897
$m_{\widetilde{\chi}_4^0}$	3375	3247	3329	4468	5350	5359
$m_{\widetilde{\chi}_1^\pm}$	154.4	306.0	307.5	308.3	308.5	813.7
$m_{\widetilde{\chi}_2^\pm}$	3375	3248	3329	3343	3162	2897

Table 4.1: Values of input parameters, sparticle masses and Higgs boson masses at several sample points. A universal soft mass m_0 of 1 TeV is assumed here.

becomes as light as the right-handed top squark. The cancellation between the wino and gluino mass parameters is not so strict for the right-handed bottom squark mass that is as light as the top squark, since the small μ-parameter requires cancellation for $m^2_{H_u}$ but for $m^2_{H_d}$. Thus the

Branching fractions	ST1	ST2	SB1	SB2	GL1	GL2
1st mode $\widetilde{t}_1$	$b\widetilde{\chi}_1^+$	$b\widetilde{\chi}_1^+$	$b\widetilde{\chi}_1^+$	$b\widetilde{\chi}_1^+$	$b\widetilde{\chi}_1^+$	$t\widetilde{\chi}_{1,2}^0$
BR	0.52	1.0	0.52	0.50	0.43	0.44
2nd mode $\widetilde{t}_1$	$t\widetilde{\chi}_{1,2}^0$	-	$t\widetilde{\chi}_{1,2}^0$	$t\widetilde{\chi}_{1,2}^0$	$t\widetilde{\chi}_{1,2}^0$	$b\widetilde{\chi}_1^+$
BR	0.48	0.0	0.48	0.50	0.46	0.31
1st mode $\widetilde{b}_1$	$t\widetilde{\chi}_1^-$	$t\widetilde{\chi}_1^-$	$t\widetilde{\chi}_1^-$	$t\widetilde{\chi}_1^-$	$\widetilde{g}b$	$\widetilde{g}b$
BR	0.50	0.40	0.49	0.49	0.84	0.80
2nd mode $\widetilde{b}_1$	$b\widetilde{\chi}_{1,2}^0$	$b\widetilde{\chi}_{1,2,3}^0$	$b\widetilde{\chi}_{1,2}^0$	$b\widetilde{\chi}_{1,2}^0$	$b\widetilde{\chi}_{1,2}^0$	$t\widetilde{\chi}_1^-$
BR	0.50	0.60	0.51	0.51	0.08	0.13
1st mode $\widetilde{g}$	$\widetilde{t}_1 t$	$\widetilde{t}_1 t$	$\widetilde{t}_1 t$	$\widetilde{b}_1 b$	$tb\widetilde{\chi}_1^\pm$	$tb\widetilde{\chi}_1^\pm$
BR	0.97	0.93	0.54	0.84	0.52	0.55
2nd mode $\widetilde{g}$	$\widetilde{t}_1 t$	$\widetilde{b}_1 b$	$\widetilde{b}_1 b$	$\widetilde{t}_1 t$	$t\bar{t}\widetilde{\chi}_{1,2}^0$	$t\bar{t}\widetilde{\chi}_{1,2}^0$
BR	0.03	0.04	0.45	0.16	0.44	0.39
1st mode H (A)	$b\bar{b}$	$b\bar{b}$	$b\bar{b}$	$b\bar{b}$	$b\bar{b}$	$b\bar{b}$
BR	0.77(0.77)	0.63(0.63)	0.88(0.88)	0.87(0.87)	0.80(0.80)	0.80(0.80)
2nd mode H (A)	$\tau\bar{\tau}$	$\widetilde{\chi}_{1,2}^0\widetilde{\chi}_3^0$	$\tau\bar{\tau}$	$\tau\bar{\tau}$	$\tau\bar{\tau}$	$\tau\bar{\tau}$
BR	0.13(0.13)	0.18(0.20)	0.12(0.12)	0.13(0.13)	0.14(0.14)	0.13(0.13)
1st mode H^+	$t\bar{b}$	$t\bar{b}$	$t\bar{b}$	$t\bar{b}$	$t\bar{b}$	$t\bar{b}$
BR	0.83	0.67	0.86	0.85	0.85	0.85
2nd mode H^+	$\bar{\tau}\nu_\tau$	$\widetilde{\chi}_1^+\widetilde{\chi}_3^0$	$\bar{\tau}\nu_\tau$	$\bar{\tau}\nu_\tau$	$\bar{\tau}\nu_\tau$	$\bar{\tau}\nu_\tau$
BR	0.13	0.22	0.14	0.14	0.14	0.15

Table 4.2: Branching fractions at the sample points.

lightest bottom squark mass also significantly depends on the gluino mass parameter. Flavor constraints and the heavy Higgs boson searches would be important for the large $\tan\beta$ case in addition to the sparticle searches.

4.2.2 Higgs bosons

Let us comment on the Higgs bosons in our scenario. In this chapter, we require the SM-like Higgs boson mass to be in the range $m_h = 125.09 \pm 0.24$ GeV. The sparticles will change the couplings of the SM-like Higgs boson to the SM fermions or SM gauge bosons. Furthermore, sparticles also change the decay properties of the SM-Higgs boson from the SM prediction [55]. These will be tested precisely in future collider experiments, like the HL-LHC or ILC. These points are enough interesting to investigate more precisely, which we leave as a future work.

There are heavy Higgs bosons in the MSSM, A, H, $H^\pm$, which are CP-odd, CP-even neutral and charged Higgs bosons, respectively. They have almost similar masses and in a typical case

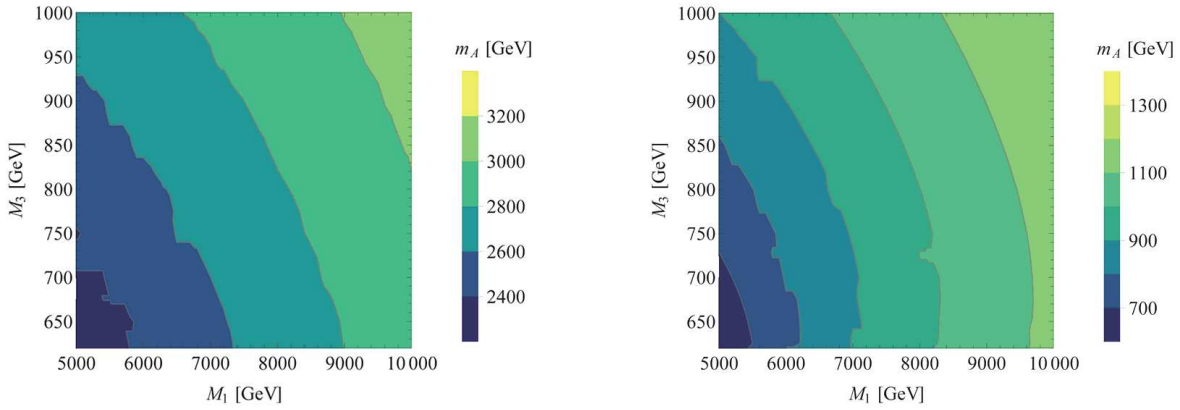

Figure 4.2: m_A [GeV] with $\tan\beta = 15$ (left), 50 (right).

of the MSSM, where $m^2_{H_u} < 0$, $m^2_{H_d} > 0$, these masses are controlled by $m^2_{H_d}$. This occurs if the bottom Yukawa coupling constant is enough small, or equivalently $\tan\beta$ is moderately small. These heavy Higgs boson masses tend to be enhanced by the bino and wino masses and they would be heavier than 2-3 TeV and far above the current exclusion limits of the LHC [56]. Similarly, the sleptons are too heavy to be probed by the LHC.

On the other hand, we have to care about the heavy Higgs boson masses if $\tan\beta$ is so large that the bottom Yukawa coupling constant is as large as the top Yukawa coupling constant. Such a bottom Yukawa coupling reduces $m^2_{H_d}$ as $m^2_{H_u}$ is reduced by the top Yukawa coupling through the RG effects. The heavy Higgs boson can be lighter than TeV scale as shown in the right panel of Fig. 4.2. We also calculated branching fractions of the heavy Higgs bosons as

$$\mathrm{BR}(H, A \to bb) \gtrsim 0.85, \tag{4.1}$$
$$\mathrm{BR}(H, A \to \tau\tau) \gtrsim 0.13, \tag{4.2}$$
$$\mathrm{BR}(H^\pm \to tb) \gtrsim 0.85, \tag{4.3}$$
$$\mathrm{BR}(H^\pm \to \tau\nu_\tau) \gtrsim 0.14. \tag{4.4}$$

Other decay modes are highly suppressed unless the bino is sufficiently lighter than the Higgs bosons. If the bino is light, the Higgs boson can decay into a higgsino-like and a bino-like neutralino as in the sample point ST2.

In this case, we have to care about not only direct searches for the heavy Higgs bosons and the bottom squark as discussed above, but also indirect searches for new physics such as flavor experiments, and measurements of Higgs properties. Superstring models and GUT models tend to favor the same large bottom Yukawa coupling as the top Yukawa coupling at the unification scale. Thus a large-$\tan\beta$ scenario looks worth studying in more detail from the theoretical point of view in addition to the phenomenological viewpoint, which can be our future work.

4.2.3 Neutralino and chargino

As we can see from Table 4.1, higgsino-like neutralinos $\tilde{\chi}^0_1$, $\tilde{\chi}^0_2$ and charginos $\tilde{\chi}^\pm_1$ have almost degenerate masses and their mass differences are at most 4 GeV, $m_{\tilde{\chi}^0_2} - m_{\tilde{\chi}^0_1} \lesssim 4$ GeV. The

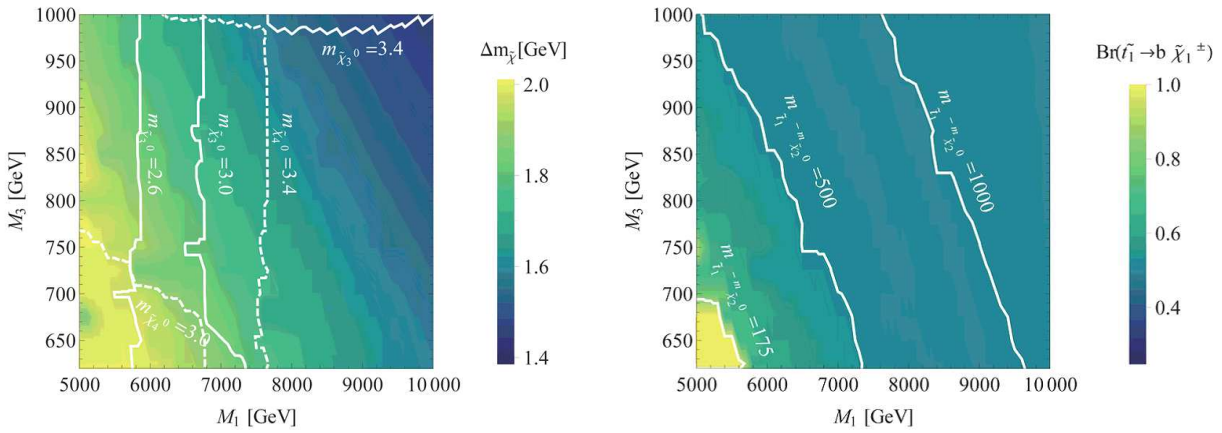

Figure 4.3: Mass difference between the higgsinos (left) and branching fraction of $\widetilde{t}_1 \to b\widetilde{\chi}_1^{\pm}$ (right). The white lines represent the third lightest neutralino mass [TeV] (left) and the mass difference between the lightest top squark and the second lightest neutralino [GeV] (right).

left panel of Fig. 4.3 shows the mass difference between the lightest neutralino and the lightest chargino $\Delta m_{\tilde{\chi}} \equiv m_{\tilde{\chi}_1^{\pm}} - m_{\tilde{\chi}_1^0}$ obtained by the same analysis as those of Fig. 4.1. The mass difference is always smaller than 2 GeV. The mass differences among higgsinos are usually induced by the mixings with bino and wino in the mass matrices. The mass differences are quite suppressed due to larger values of bino and wino masses. This fact indicates that decays of heavier higgsinos are effectively invisible for the detector, because SM particles decayed from the higgsinos are too soft to be reconstructed in the experimental analysis at the collider. Thus the neutralino/chargino searches would be inefficient to look the higgsinos in this scenario.

Furthermore, it is also difficult to see the higgsino-like chargino by using charged track which can be used efficiently to search for a wino-like chargino [57]. The mass difference between the chargino and the lightest neutralino is $\mathcal{O}(100$ MeV) for the wino-like chargino, and the lifetime of the chargino is so long that the chargino can be detected as a charged track. On the other hand, the lifetime of the higgsino with the mass difference of $\mathcal{O}(1$ GeV) is too short to be detected. Therefore, all of the higgsinos are effectively invisible in the collider experiments.

4.2.4 Colored sparticles

Figure 4.4 shows the masses of lighter third-generation squarks, which are almost right-handed, and the gluino. The red (blue) lines correspond to the physical masses of the top squark (gluino) and the background colors correspond to the bottom squark mass. We can see that the top squark mass depends on M_1, while the bottom squark mass depends on both M_1 and M_3. The bottom squark can easily become lighter than TeV scale if $\tan\beta = 50$.

The top squarks couple to the third-generation quarks and the higgsinos through the Yukawa couplings,

$$y_t Q_3 \cdot \widetilde{H}_u \widetilde{t}_R + y_t \widetilde{Q}_3 \cdot \widetilde{H}_u t_R + y_b \widetilde{Q}_3 \cdot \widetilde{H}_d b_R, \tag{4.5}$$

where y_t, y_b are the top and bottom Yukawa coupling constants, $\widetilde{H}_u = (\tilde{H}_u^+,\ \tilde{H}_u^0)$, $\widetilde{H}_d =$

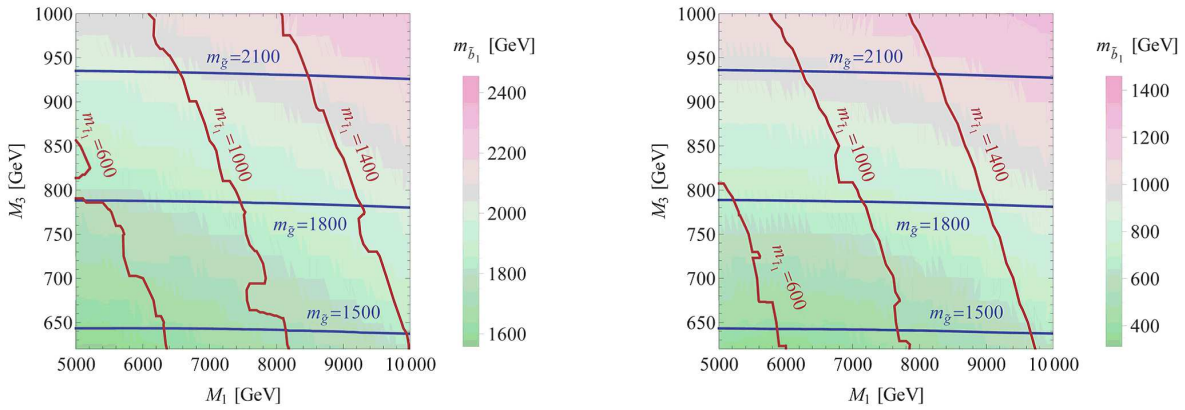

Figure 4.4: Masses of the colored sparticles at $\tan\beta = 15$ (left) $= 50$ (right) and $\mu = 300$ GeV, $m_0 = 1.0$ TeV. The red (blue) lines represent the lightest top squark (gluino) mass [GeV].

$(\tilde{H}_d^0,\ \tilde{H}_d^-)$, $\widetilde{Q}_3 = (\tilde{t}_L,\ \tilde{b}_L)$ are the up-type higgsino doublet, down-type higgsino doublet, third-generation squark doublet, respectively. The dots mean contraction of $SU(2)_L$ indices by the anti-symmetric tensor. Note that these interactions are in the gauge basis and they should be rotated to mass eigenstates. In the NUGM scenario, the lightest top squark is almost right-handed $\tilde{t}_1 \simeq \tilde{t}_R$ and the neutralinos and charginos are almost higgsino-like $\tilde{\chi}_{1,2}^0 \simeq \tilde{H}_{u,d}^0$, $\tilde{\chi}_1^\pm \simeq \tilde{H}_{u,d}^\pm$.

The right-handed top squark couples to $b\tilde{\chi}_1^+$ and $t\tilde{\chi}_{1,2}^0$ through the first term of Eq. (4.5), and both of the couplings are given by the top Yukawa coupling. This fact leads to branching fractions of the top squark of almost 50%

$$\mathrm{BR}(\tilde{t}_1 \to t\tilde{\chi}_{1,2}^0) \simeq \mathrm{BR}(\tilde{t}_1 \to b\tilde{\chi}_1^\pm) \simeq 0.5, \tag{4.6}$$

if mass difference between the top squark and the higgsino is sufficiently large. $\mathrm{BR}(\tilde{t}_1 \to b\tilde{\chi}_1^\pm)$ increases as the mass difference decreases. We can see this in the right panel of Fig. 4.3. Similar arguments can be applied for the right-handed bottom squark with large $\tan\beta$. The values of branching fractions at the samples points are listed in Table 4.2.

The gluino decays to a top squark and a top quark through the D-term interaction $g_3\bar{t}_R\tilde{g}\tilde{t}_R$, and finally decays like $\tilde{g} \to t\tilde{t}_1 \to tt\tilde{\chi}_{1,2}^0/tb\tilde{\chi}_1^\pm$, where the second decay is nothing but the top squark decay discussed above. If the mass difference between the gluino and the higgsinos are as small as $m_t + m_b$, the tree-level decay $\tilde{g} \to tb\tilde{\chi}_1^\pm$ is suppressed and a loop-induced decay $\tilde{g} \to g\tilde{\chi}_{1,2}^0$ dominates the decay of the gluino. The values of branching fractions at the sample points GL1 and GL2 are listed in Table 4.2.

4.3 Exclusion limits on non-universal gaugino mass scenario

The branching fractions of the top squark and the gluino vary with input parameters and more than two decay modes can be sizable. Thus the experimental exclusion limits from the top squark searches [58–60] and the gluino searches [61] can not be valid for our scenario since such simplified models usually assume that one decay mode dominates.

Here we execute Monte-Carlo simulations of the NUGM scenario. We used MadGraph5 [62] to generate signal events from top squark and gluino pair production up to one additional parton at the matrix element level. The generated events are passed to PYTHIA6 [63] for showering and hadronizing partons. The MLM scheme [64] is used to avoid double counting of events with initial state and/or final state jets between the matrix element level events and those after showering. We carry out fast detector simulation by DELPHES3 [65] to reconstruct objects like leptons, jets or missing energies. Jets are reconstructed from the hadrons by the anti-k_T jet clustering algorithm [66] with the radius parameter $\Delta R = 0.4$ as in the analysis of the ATLAS collaborations. Finally, the generated events are normalized on the basis of production cross sections of the sparticle pair productions with an accuracy of Next-to-Leading-Order + Next-to-Leading-Log calculated by Prospino2.1 [67].

4.3.1 Top squark search

A pair-produced top squarks decay to two third-generation quarks and higgsinos counted as missing energies. If the mass difference between the top squark and the higgsino is enough large, a quarter of the pair-produced top squark decay to $tt + \not{E}_T$ and $bb + \not{E}_T$ and a half decays to $tb + \not{E}_T$. Reference [68] summarizes results of the third-generation squark searches in the LHC run-I at the ATLAS detector. Search for $bb + \not{E}_T$ is based on the data with the integrated luminosity ~ 3.2 fb^{-1} [58]. The analyses in Refs. [59, 60] aim at finding signals from $tt + \not{E}_T$ using the data taken in the run-II with the integrated luminosity ~ 13 fb^{-1}.

We evaluate exclusion limits based on the experimental data shown in Ref. [58] for the $bb + \not{E}_T$ search, and definitions of the signal regions are listed in Table 4.3. Two signal regions SRA and SRB are used in the analysis, where the SRA aims at heavy top squarks and large mass difference to the LSP, while the SRB aims at small mass difference between the top squark and the LSP.

Basically, there are two b-tagged jets from the top squark pair production, if both of them decay as $\tilde{t}_1 \to b\tilde{\chi}_1^{\pm}$, although initial and/or final state radiations can produce additional jets. Then two energetic b-tagged jets are required for the SRA, and events with more than four energetic jets and with any signal lepton are vetoed. The latter reduces backgrounds from the top quark pair production. A large $\not{E}_T$ is required as usual in sparticle searches, since the LSP produces large $\not{E}_T$.

The cuts for $\Delta\phi^j_{\rm min}$ and $\not{E}_T/m_{\rm eff}$ are applied for both signal regions. $\Delta\phi^j_{\rm min}$ is defined as the minimum azimuthal angle difference between $\not{E}_T$ and two (three) leading jets for SRA (SRB). The effective mass $m_{\rm eff}$ is the scalar sum of $\not{E}_T$ and p_T of the two (three) leading jets for SRA

variable	SRA	SRB
lepton veto	no e/μ with $p_T > 10$ GeV	
$\not{E}_T$	> 250 GeV	> 400 GeV
$p_T(j_1)$	> 130 GeV	> 300 GeV
$p_T(j_2)$	> 50 GeV	> 50 GeV
fourth jet veto	no fourth jet with $p_T(j_4) > 50$ GeV	
$\Delta\phi^j_{\rm min}$	> 0.4	> 0.4
$\Delta\phi(j_1, \not{E}_T)$	-	> 2.5
b-tagging	j_1 and j_2	j_2 and (j_3 or j_4)
$\not{E}_T/m_{\rm eff}$	> 0.25	> 0.25
$m_{\rm CT}$	$> 250,\ 350,\ 450$ GeV	-
m_{bb}	> 200 GeV	-

Table 4.3: Definitions of signal regions for $bb + \not{E}_T$ [58] search.

(SRB). These values tend to be large for events including missing particles in final states, while these are small for multi-jet background.

In addition to the cuts above, the so-called contransverse mass $m_{\rm CT}$ and the invariant mass of the two b-tagged jets are useful to discriminate signals from backgrounds. The contransverse mass is defined as

$$m^2_{\rm CT}(v_1,\ v_2) \equiv (E_T(v_1) + E_T(v_2))^2 - (\mathbf{p}_T(v_1) - \mathbf{p}_T(v_2))^2, \tag{4.7}$$

where $v_1,\ v_2$ are two visible particles in an event. The contransverse mass has an upper bound for events with semi-invisible decay of heavy particles as,

$$m^{\rm max}_{\rm CT} = \frac{m^2_{\rm heavy} - m^2_{\rm invisible}}{m_{\rm heavy}}, \tag{4.8}$$

where $m_{\rm heavy}$ is a mass of a heavy particle which decays to an invisible particle and the visible particle v_1 or v_2. $m_{\rm invisible}$ is a mass of the invisible particle. In the case of the top squark decay, heavy particle is the top squark, invisible particle is the chargino and visible particle is the bottom quark. Note that the chargino is higgsino-like and effectively invisible in the NUGM scenario. Then the value of $m_{\rm CT}$ for the event tends to be large for the heavy top squark. On the other hand, the upper bound is 135 GeV for tt events, where heavy, visible, invisible particles are top quark, bottom quark and W-boson that its daughter leptons or jets are failed to be reconstructed, respectively. Thus the contransverse mass is a powerful tool to discriminate events with semi-invisibly decaying heavy particles from backgrounds.

SRB targets the small mass difference between the top squark and the LSP. In this case, the missing energy and the two b-tagged jets from the top squark decay will not have sufficiently high p_T that can be used to discriminate from the SM backgrounds. Thus SRB targets a pair-produced top squarks in association with one initial state jet with very high p_T. Hence, the

Signal Region	Variable	common cut		
	jet p_T	$> 80,\ 80,\ 40,\ 40$ GeV		
	b-tag	1 of 4 leading jets		
	lepton	veto		
	$\not{E}_T$	> 250 GeV		
	$\min_{i=1,2} \lvert\Delta\phi(j_i,\ \not{E}_T)\rvert$	> 0.4		
	$E_T^{\text{miss,track}}$	>30 GeV and $\lvert\Delta\phi(\not{E}_T, E_T^{\text{miss,track}})\rvert < \pi/3$		
Signal Region	Variable	TT	TW	T0
	$m^1_{R=1.2}$	> 120 GeV		
	$m^2_{R=1.2}$	> 120 GeV	$60 - 120$ GeV	< 60 GeV
SRA	$m^1_{R=0.8}$	> 60 GeV		
	b-tag jet	≥ 2		
	$m_T^{b,\text{min}}$	> 200 GeV		
	τ jet	veto		
	$\not{E}_T$	> 400 GeV	> 450 GeV	> 500 GeV
SRB	b-tag jet	≥ 2		
	$m_T^{b,\text{min}}$	> 200 GeV		
	$m_T^{b,\text{max}}$	> 200 GeV		
	τ jet	veto		
	$\Delta R(b,b)$	> 1.2		
	$\not{E}_T$	> 250 GeV		
Signal Region	Variable	low	med	high
SRC	jet p_T	$p_T >$150, 100, 40, 40 GeV		
	b-tag jet	2 of leading 4 jets		
	m_{bjj}	> 250 GeV		
	$p_T(j_1)$	> 150 GeV	> 200 GeV	> 250 GeV
	$p_T(j_2)$	> 100 GeV	> 150 GeV	> 150 GeV
	$m_T^{b,\text{min}}$	> 250 GeV	> 300 GeV	> 350 GeV
	$m_T^{b,\text{max}}$	> 350 GeV	> 450 GeV	> 500 GeV
	$\Delta R(b,b)$	> 0.8		
	$\not{E}_T/\sqrt{H_T}$	$[5,12]\sqrt{\text{GeV}}$	$[5,12]\sqrt{\text{GeV}}$	$[5,17]\sqrt{\text{GeV}}$
	$\not{E}_T$	> 250 GeV		

Table 4.4: Definitions of signal regions for searching hadronic $tt + \not{E}_T$ [59].

Common cut					
lepton	exactly one signal lepton				
jets	at least four jets and $\min_{i=1,2} \lvert\Delta\phi(j_i,\ \not{E}_T)\rvert > 0.4$				
Hadronic τ	veto events with hadronic τ and $m^{\tau}_{\mathrm{T2}} < 80$ GeV				
Variable	tN-high	bC2x-diag	bC2x-med	DM-low	DM-high
Number of b-jets	≥ 1	≥ 2	≥ 2	≥ 1	≥ 1
$p_T(j_{1,2}) >$ [GeV]	120 80	70 60	170 110	60 60	50 50
$p_T(j_{3,4}) >$ [GeV]	50 50	55 25	25 25	40 25	50 25
b-tag jet $p_T >$ [GeV]	-	25 25	105 100	-	-
$\not{E}_T >$ [GeV]	450	230	210	300	330
$E^{\mathrm{miss}}_{T,\perp} >$[GeV]	180	-	-	-	-
$H^{\mathrm{miss}}_{T,\mathrm{sig}} >$	22	14	7	14	9.5
$m_T >$ [GeV]	210	170	140	120	220
$am_{T2} >$ [GeV]	175	170	210	140	170
$\Delta R(b, l) <$	2.4	-	-	-	-
1^{st} large R jet p_T [GeV]	>290	-	-	-	-
1^{st} large R jet mass [GeV]	>70	-	-	-	-
$\Delta\phi(\mathbf{p}^{\mathrm{miss}}_T, 2^{\mathrm{nd}}$ large R jet)	> 0.6	-	-	-	-
$\lvert\Delta\phi(\mathrm{jet}_1), \mathbf{p}^{\mathrm{miss}}_T\rvert >$	-	1.2	1.0	-	-
$\lvert\Delta\phi(\mathrm{jet}_2), \mathbf{p}^{\mathrm{miss}}_T\rvert >$	-	0.8	0.8	-	-
$\min_{i=1-4} \lvert\Delta\phi(\mathrm{j}_i,\ \mathbf{p}^{\mathrm{miss}}_T)\rvert$	-	-	-	1.4	0.8
$\Delta\phi(\mathbf{p}^{\mathrm{miss}}_T, l) >$	-	-	-	0.8	-

Table 4.5: Definitions of signal regions for searching $tt + \not{E}_T$ with one lepton [60].

b-tagging is required for sub-leading jets. Since the direction of leading jet is expected to be opposite against the top squark pairs that decay to the LSP counted as $\not{E}_T$, azimuthal angle between the leading jet and $\not{E}_T$ is required to be large.

Table 4.6 exhibits the number of observed events, the number of background events, its total systematic uncertainties and 95 % C.L upper bounds on signal events in each signal regions by referring to the data obtained at the run-II of the ATLAS experiment with the integrated luminosity 3.2 fb^{-1}.

Next, we consider two analyses searching for the top squarks decaying to a top quark and a neutralino. Analysis in Ref. [59] is prepared for such a top squark that the daughter top quarks decay hadronically, while the analysis in Ref. [60] targets events that one of the top quarks decays leptonically. We refer to these two analyses as hadronic $tt + \not{E}_T$ search and leptonic $tt + \not{E}_T$ search. Note that both of the top quarks can decay leptonically and two leptons are produced, but the probability to produce such a signal from a pair-produced top quark is less

signal region	SRA 250	SRA 350	SRA 450	SRB
observed events	22	6	1	5
bkg events	40	9.5	2.2	13.1
bkg uncertainty	8	2.6	0.6	3.2
$S^{95\%\text{C.L.}}$	8.8	6.1	3.7	5.0

Table 4.6: The number of observed events, the number of background events, their total systematic uncertainties and 95 % C.L upper bounds on signal events in each signal region.

than 10% and this dileptonic channel generically gives a weaker limit. Hence, we do not consider such dileptonic channels and leptonic $tt + \not{E}_T$ channel always indicates the signal events having exactly one lepton in our analysis. Definitions of signal regions for the hadronic search and the leptonic search are listed in Table 4.4 and Table 4.5, respectively.

We can see that the events are required to have at least 4 jets with $p_T \geq 40$ GeV and two of the four leading jets have to be b-tagged. This means that the processes $\widetilde{t}_1\widetilde{t}_1 \to t(\to bjj)b + \not{E}_T$ will contribute to the signal events in our scenario. This seems to be an advantage of this channel against $bb + \not{E}_T$ search although this channel is not completely optimized for $tb + \not{E}_T$. Events with leptons and $\not{E}_T \leq 250$ GeV are vetoed. The leading two jets have to be separated from the missing momentum in order to reduce hadronic tt and multi-jets events. $E_T^{\text{miss,track}}$ is constructed from the vector sum of reconstructed tracks in the detector. To mimic the analysis, we calculate this quantity from all objects with tracks in the lhco-format file [69], although this requirement hardly reduces signal events.

SRA (SRB) is optimized for large (moderately small) mass difference between the top squark and the neutralinos. Events are categorized by using masses of re-clustered jets which may correspond to the top squark.

The signal jets in a event clustered by the anti-k_T algorithm with the radius parameter $\Delta R = 0.4$ are re-clustered into larger R-jets again by the anti-k_T algorithm but with the radius parameter $\Delta R = 1.2$. The mass of re-clustered jet, which is defined by the four-momentum of the re-clustered jet, is expected to be about the top quark mass, so that at least one of the large radius jets have the mass larger than 120 GeV. The events are categorized according to how the mass of the second large radius jet is re-constructed likely to the top quark (TT) or the W-boson (TW) or unlikely to both of these (T0). If the mass difference is large, decay particles from the top quark would be more collimated. Hence, a mass of the re-clustered jet with smaller radius parameter $\Delta R = 0.8$ is considered in the SRA.

The transverse mass is defined as

$$m_T = \sqrt{2 p_T \not{E}_T (1 - \cos\Delta\phi(\mathbf{p}_T^{\text{miss}},\ \mathbf{p}_T))}, \tag{4.9}$$

where $\mathbf{p}_T$, $\mathbf{p}_T^{\text{miss}}$ are a transverse momentum vector of the lepton or the b-tagged jet and that of the missing transverse momentum, respectively. $\Delta\phi(\not{E}_T,\ \mathbf{p}_T)$ is a difference of the azimuthal angle between those two transverse momenta. The transverse masses are widely used to distinguish semi-invisible particles in background events. For instance, the transverse mass

signal region	A-TT	A-TW	A-T0	B-TT	B-TW	B-T0	C-low	C-med	C-high
observed events	8	5	16	17	18	84	36	14	9
bkg events	5.2	5.7	11.3	10.6	16.7	60	23.9	9.4	10.5
bkg uncertainty	1.4	1.6	2.6	2.3	3.6	14	7.5	3.5	3.7
$S^{95\%\text{C.L.}}$	9.5	6.1	14.0	15.5	12.9	52.1	29.1	14.6	8.8

Table 4.7: The number of observed events, the number of background events, their total systematic uncertainty and 95 % C.L upper bounds on signal events in each signal region shown in Ref. [59].

of a lepton is bounded from above by the leptonically decaying W-boson. $m_T^{\text{b,min}}$ is a transverse mass for the b-tagged jet closest in ϕ to $\mathbf{p}_T^{\text{miss}}$ and can discriminate an event containing a top quark that its daughter W-boson is mis-reconstructed. $m_T^{\text{b,max}}$ is a similar quantity, but the b-tagged jet is the farthest from $\mathbf{p}_T^{\text{miss}}$. The events with the hadronically decaying τ lepton is vetoed to reduce the backgrounds from tt. The signal events hardly contain τ leptons.

SRC is optimized for $\widetilde{t}_1 \to b\widetilde{\chi}^{\pm}$, so that there is no top quark in the process. The invariant mass m_{bjj} is used to drop the tt background. In Ref. [59], a pair of non b-tagged jets that have the smallest $\Delta R(j,j)$ are selected from all jets except two jets having the highest b-tagging weight. Then, the pair of two jets are combined and the b-tagged jet is identified by selecting the closest b-tagged jet from this combined jet. In our analysis, all b-tagged jets in the event are considered to be a candidate for the first procedure, instead of using b-tagging weight information that we cannot obtain from the fast detector simulation. m_{bjj} is expected to be about the top quark mass for tt backgrounds.

Table 4.7 shows the experimental results obtained from the data with $\sqrt{s} = 13$ TeV and 13.3 fb^{-1} [59]. Note that signal regions TT, TW, T0 are exclusive to each other, and the exclusion limits are obtained by combining data of these three signal region for the SRA and SRB, respectively.

In order to extract exclusion limits, we have to calculate CL_s [70]. We follow the method in Ref. [71] which is based on the asymptotic formula derived in [72]. The likelihood function $\mathcal{L}(\text{data}|\mu,\theta)$ is defined as

$$\mathcal{L}(\text{data}|\mu,\theta) = \text{Pois}(\text{data}|\mu s(\theta) + b(\theta)) \cdot p(\theta|\tilde{\theta}), \tag{4.10}$$

where data will be obtained by experiments or MC-simulations, and s, b, μ are the numbers of signals, background events and the so-called signal strength modifier, respectively. θ is a set of nuisance parameters obeying a distribution $p(\tilde{\theta}|\theta)$. Pois is the Poisson distribution,

$$\Pi_i \frac{(\mu s_i + b_i)^{n_i}}{n_i} e^{-(\mu s_i + b_i)}, \tag{4.11}$$

where i corresponds to bins of data such as TT, TW, T0, and n_i is the number of events in each bin i obtained from the data.

The test statistic $\tilde{q}_\mu$ is introduced by using the likelihood function,

$$\tilde{q}_\mu = -2\log\frac{\mathcal{L}(\text{data}|\mu,\hat{\hat{\theta}}_\mu)}{\mathcal{L}(\text{data}|\hat{\mu},\hat{\theta})}, \tag{4.12}$$

where $\hat{\mu},\hat{\theta}$ are obtained by maximizing the likelihood with $0 \leq \hat{\mu} \leq \mu$, while $\hat{\hat{\theta}}_\mu$ is obtained to maximize the likelihood for a given μ.

The $CL_s(\mu)$ is defined as

$$CL_s(\mu) = \frac{p_\mu}{1-p_b}, \tag{4.13}$$

where p_μ, p_b are p-values for the signal+background and background-only hypothesis in association with the observed data. These are defined by

$$p_\mu = P(\tilde{q}_\mu \geq \tilde{q}_\mu^{obs}|\text{signal+background}) = \int_{\tilde{q}_\mu^{obs}}^{\infty} f(\tilde{q}_\mu|\mu,\hat{\hat{\theta}}_\mu^{obs})d\tilde{q}_\mu, \tag{4.14}$$

$$1-p_b = P(\tilde{q}_\mu \geq \tilde{q}_\mu^{obs}|\text{background-only}) = \int_{\tilde{q}_0^{obs}}^{\infty} f(\tilde{q}_\mu|0,\hat{\hat{\theta}}_\mu^{obs})d\tilde{q}_\mu, \tag{4.15}$$

where $f(\tilde{q}_\mu|\mu,\hat{\hat{\theta}}_\mu^{obs})$ is a probability distribution function of the test statistic $\tilde{q}_\mu$ that will be obtained by some toy Monte Carlo experiment. $\tilde{q}_\mu^{obs}$, $\hat{\hat{\theta}}_\mu^{obs}$ are obtained from the observed data by the experiment.

The asymptotic formula for $f(\tilde{q}_\mu|\mu,\hat{\hat{\theta}}_\mu^{obs})$ is derived in Ref. [72]. In the asymptotic regime, the CL_s can be written as

$$CL_s(\mu) = \frac{1-\Phi(\sqrt{q_\mu})}{\Phi(\sqrt{q_{\mu,A}}-\sqrt{q_\mu})}, \tag{4.16}$$

where Φ is a cumulative function of the standard Gaussian distribution. $q_{\mu,A}$ is the value of test static based on the so-called Asimov dataset. The signal+background hypothesis is excluded 95% C.L., if $CL_s(\mu=1) \leq 0.05$ for the expected background is assigned to the Asimov dataset.

In our analysis, we assume that there is only one nuisance parameter that determines overall normalization of the background, and it obeys the normal Gaussian distribution. Concretely, the likelihood function is given by

$$\mathcal{L}(\text{data}|\mu,\theta) = \Pi_i \frac{(\mu s_i + (b_i^0 + \theta\sigma_i^b))^{n_i}}{n_i} e^{-(\mu s_i + (b_i^0+\theta\sigma_i))} \cdot \text{Gauss}(\theta|0,1), \tag{4.17}$$

where b_i^0, σ_i are the number of SM background events and its uncertainty in each bin. Note that we truncate the Gaussian distribution where the number of background is negative.

We also study $tt + \not{E}_T$ search where one of the top quarks decays leptonically [60]. The definitions of signal regions are listed in Table 4.5. TN-high targets top squarks that become $tt + \not{E}_T$, bC2x-diag (-med) targets a pair of top squarks that become $bb + \widetilde{\chi}^{\mp}\widetilde{\chi}^{\pm}$ with small (medium) mass difference. DM-low (high) targets more generic dark matter production in

signal region	tN-high	bC2x-diag	bC2x-med	DM-low	DM-high
observed events	5	37	14	35	21
bkg events	3.8	22	13	17	15
bkg uncertainty	0.8	3	2	2	2
$S^{95\%\text{C.L.}}$	7.2	27.5	9.9	28.3	15.6

Table 4.8: The number of observed events, the number of background events, their total systematic uncertainties and 95 % C.L upper bounds on signal events in each signal region shown in Ref. [60].

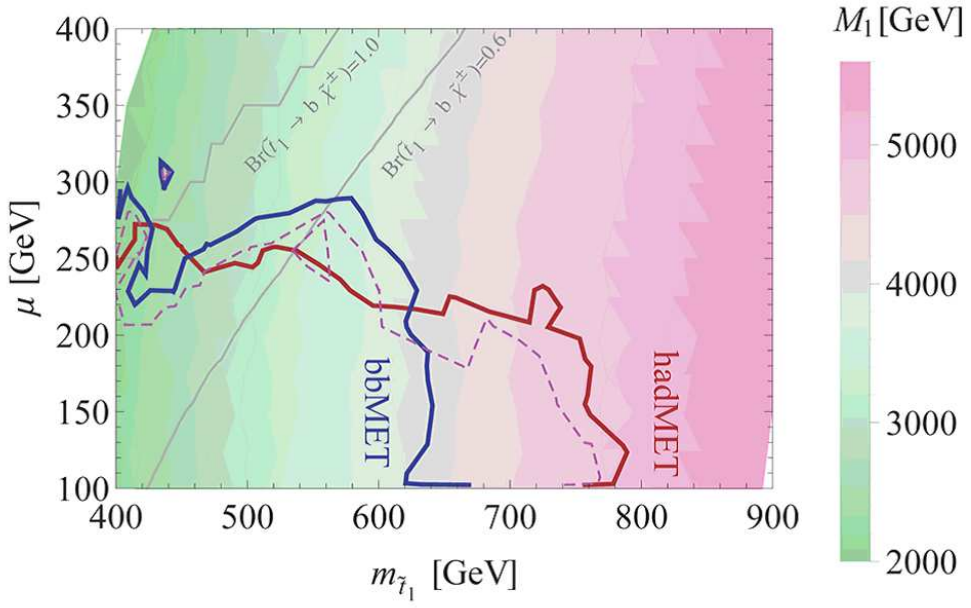

Figure 4.5: Exclusion limits on the top squark mass and the μ-parameter plane. The lower-left region of the lines are excluded.

association with top quarks with lower (higher) masses. These signal regions require more than four jets in addition to one signal lepton, then $tb + \not{E}_T$ will not give contributions to the signal regions. The result of the analysis in Ref [60] is represented in Table 4.8.

We compared the number of signal events at points in the NUGM scenario for $bb+\not{E}_T$ search and leptonic $tt + \not{E}_T$ search, while we directly calculate CL_s for the hadronic $tt + \not{E}_T$ search. If we additionally require $p_T(j_4) > 50$ GeV in the hadronic $tt + \not{E}_T$ search, the signal regions are orthogonal to those of $bb + \not{E}_T$ search. Obviously, signal regions in the leptonic $tt + \not{E}_T$ search have no overlaps with the others. We extract the exclusion limits by combining results of the most sensitive signal regions in each search, and the fourth jet requirement is added to the hadronic $tt + \not{E}_T$ channel. This would give slightly conservative limits due to the additional requirement only for signal events.

Figure 4.5 shows exclusion limits on the top squark mass and μ-parameter plane. The blue

Variable	Gbb-A	Gbb-B	Gtt-0lA	Gtt-0lB	Gtt-1lA	Gtt-1lB	Gtt-1lC
$N_{\rm lepton}^{\rm candidate}$	0		-		-		
$N_{\rm lepton}^{\rm signal}$	-		0		1		
$N^{\rm jet} \geq$	4		8		6		
$N^{\rm b-jet} \geq$	3	4	3		3	3	4
$p_T^{\rm jet} >$	70	30	30		30		
$\not{E}_T >$	450	300	400		200	350	200
$\Delta\phi_{\rm min}^{j} >$	0.4		0.4		-		
$m_T >$	-		-		200	200	150
$m_{\rm T,min}^{\rm b-jets} >$	-		80		120	120	80
$m_{\rm eff}^{\rm incl} >$	-		2000	1250	2000	1500	500
$m_{\rm eff}^{\rm 4j} >$	1900	1000	-		-		
$m_J^{\Sigma} >$	-		200	-	200	150	-

Table 4.9: Definitions of signal regions searching for gluino decays to the top quark and the top squark. All dimensional parameters are in units of GeV.

(red) solid line shows the exclusion limits from the $bb + \not{E}_T$ search (hadronic $tt + \not{E}_T$ search) and the purple dashed line corresponds to the exclusion limit by the combined analysis. The lower-left region of the exclusion limits are excluded. Note that inclusion of the leptonic $tt+\not{E}_T$ search slightly improves the exclusion limits although it itself does not give exclusion limits. The background colors indicate the bino mass parameter at the unification scale. The gray lines show the branching fraction of the top squark decay $\widetilde{t}_1 \to b\widetilde{\chi}_1^{\pm}$.

The hadronic $tt+\not{E}_T$ search gives the most stringent bound on the small μ-parameter region, and it excludes top squark lighter than around 800 GeV. On the other hand, $bb+\not{E}_T$ gives the most stringent bound on the mass-degenerate region. Note that the integrated luminosity of the data is different for these two searches. Once the $bb+\not{E}_T$ search is updated, this bound and also combined limits will be tightened, and it could give a stronger bound than the hadronic $tt+\not{E}_T$. Analysis dedicated to $tb+\not{E}_T$ with leptonically decaying top quark or inclusive searches as done in the CMS collaboration [73] will be important in addition to these analyses.

4.3.2 Gluino search

The gluino search will also give a significant bound on the NUGM scenario and its lower bound gives those for most of the sparticles. A pair produced gluinos finally decay to four third-generation quarks, where two of them are the top quarks and the others depend on the decay of the top squark. We referred to the data used in the analysis in Ref. [61] targeting signals with four b-tagged jets and large $\not{E}_T$.

The definitions of signal regions are shown in Table 4.9. The signal regions Gbb target gluino decays to the two bottom quarks through bottom squark and they are not completely

signal region	Bbb-A	Gbb-B	Gtt-0lA	Gtt-0lB	Gtt-1lA	Gtt-1lB	Gtt-1lC
observed events	2	15	1	11	1	2	4
bkg events	1.6	21	0.94	5.0	1.0	1.1	7.0
bkg uncertainty	0.7	5.0	0.31	1.5	0.6	0.4	2.8
$S^{95\%\text{C.L.}}$	4.6	10.0	3.8	13.3	3.8	4.9	5.7

Table 4.10: The number of observed events, the number of background events, their total systematic uncertainties and 95 % C.L upper bounds on signal events in each signal region shown in Ref. [61].

suited for seeing the gluino in the NUGM scenario. The signal regions Gtt aim at gluino decays to two top quarks, and Gtt-0l (Gtt-1l) targets events with no lepton (one lepton). Gbb-A, Gtt-0lA, Gtt-1lA are optimized for large mass splitting between the gluino and the LSP, and Gbb-B, Gtt-0lB, Gtt-1lC (B) aim at small (medium) mass splitting.

Signal leptons are required to satisfy tighter conditions than candidate leptons. For instance, the former must have $p_T > 30$ GeV and the latter must have $p_T > 20$ GeV. These details are shown in Ref. [61]. The different numbers of jets with $p_T > 30$ GeV are required in all signal regions except Gbb-A, and p_T requirement is tightened to 70 GeV for Gbb-A. Cuts for $\not{E}_T$ and $\Delta\phi^j_{\text{min}}$ are applied for the same purpose as the top squark search.

m_T and $m^{\text{b-jets}}_{\text{T,min}}$ are the transverse masses defined as Eq. (4.9). $m^{\text{b-jets}}_{\text{T,min}}$ is the minimal one among the transverse masses for three leading b-tagged jets. For leptonically decaying W-boson, the transverse mass is always less than the W-boson mass. Hence, $m^{\text{b-jets}}_{\text{T,min}}$ can reduce backgrounds from tt and $W+$ jets. For a top quark with mis-reconstructed W-boson, $m^{\text{b-jets}}_{\text{T,min}}$ is bounded from above by the top quark mass and then this can discriminate tt backgrounds. $m^{\text{incl}}_{\text{eff}}$ ($m^{\text{4j}}_{\text{eff}}$) is the effective mass defined as a scalar sum of $\not{E}_T$ and lengths of transverse momenta of all signal leptons and jets (leading four jets). These values tend to be large for events with heavy sparticle.

m^{Σ}_J is defined as

$$m^{\Sigma}_J = \sum_{i \leq 4} m_{J,i}, \tag{4.18}$$

where $m_{J,i}$ is the mass of re-clustered jets with a large radius. The large radius re-clustered jets are formed from the jets with a small radius parameter by the anti-k_T algorithm with a radius parameter $\Delta R = 0.8$, then the re-clustered jets are trimmed by dropping sub-jets with p_T less than $f_{\text{cut}} = 10\%$ of the original large radius jet. These large-radius jets are required to have $p_T > 100$ GeV and $|\eta| < 2.0$, where η is the pseudo-rapidity. m^{Σ}_J discriminates signals from tt events with leptons.

Table 4.10 exhibits the numbers of observed events, fitted background events and their uncertainties, and the 95 % C.L. upper limits on signal events. Figure 4.6 shows our result. The blue line is the 95 % C.L. exclusion limits obtained by comparing the generated events with the upper limits on the number of signal events. The red line is obtained by directly calculating the CL_s by combining signal regions Gbb, Gtt-0l and Gtt-1l. To separate signal

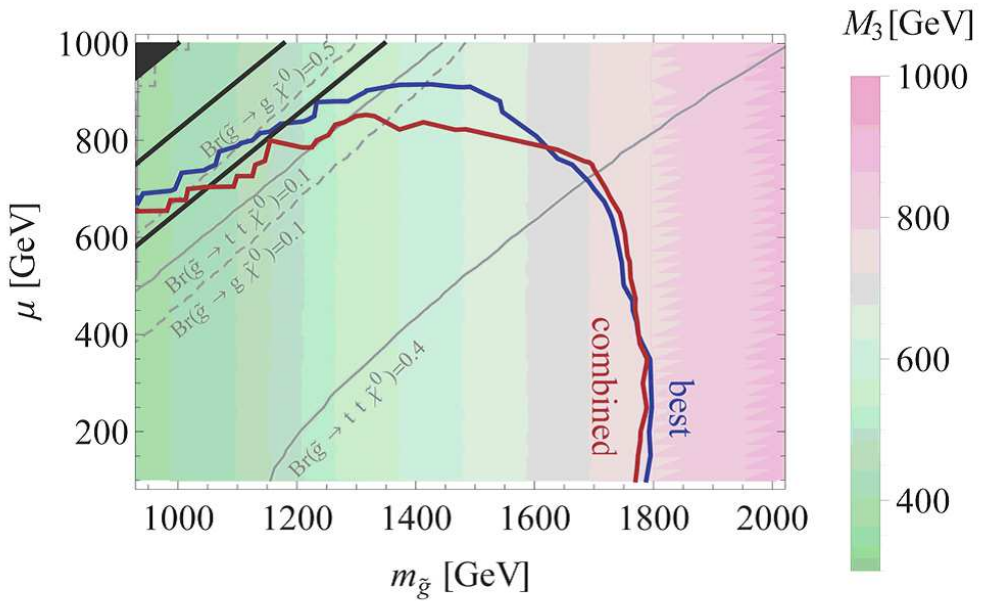

Figure 4.6: Exclusion limits on the gluino mass and the μ-parameter plane with $M_1 = 12$ TeV at the unification scale. The lower-left region than the lines are excluded.

regions in Gbb and Gtt-0l, we require events in Gbb do not have more than 8 jets with $p_T > 35$ GeV. The background colors indicate the gluino mass at the unification scale. The gray solid and dashed lines show the branching fractions BR($\tilde{g} \to tt\tilde{\chi}^0$) and BR($\tilde{g} \to g\tilde{\chi}^0$), respectively. The latter decay mode is induced by loop corrections and dominates if $m_{\tilde{g}} \lesssim m_{\tilde{\chi}} + m_t + m_b$. This region could be covered by the $jj + \not{E}_T$ search [74], but it would not give stringent bounds. We can see that the gluino mass less than 1.8 TeV is excluded if $\mu \lesssim 800$ GeV.

4.4 Summary

In this chapter, we studied expected signals of the NUGM scenario at the LHC. Typical spectrum of the NUGM is characterized by the light higgsino LSP, relatively light right-handed top squark and other sparticles having almost the same masses.

The higgsino is hard to be detected at the LHC. The mass differences among the higgsinos are suppressed due to the heavy wino and binos. This makes decays of heavier states of the higgsinos effectively invisible at the detector. Furthermore, its lifetime is too short to be counted as charged tracks. Thus the higgsino is really hard to be seen at the LHC.

The light right-handed top squark is the specific property of the NUGM scenario and then is important. The right-handed top squark decays to both top and bottom quark, then the situation is different from the simplified model usually assumed in experimental analysis. The hadronic top squark search is efficient in a region with large mass difference between the top squark and the higgsino. The $bb + \not{E}_T$ channel also gives severe bounds on the NUGM, especially for a mass degenerate region where the branching fraction to the bottom squark approaches to

unity. The top squark lighter than 800 GeV has been excluded if $\mu \lesssim 200$ GeV. This bound can be interpreted as lower bounds on the bino mass parameter at the unification scale $M_1 \gtrsim 5$ TeV.

The gluino has the largest cross section among all the sparticles, then the gluino search also gives an important bound. The gluino in the NUGM scenario decays through the top squark, so the expected signal is four third-generation quarks, two of them are top quark and large missing momentum. The gluino lighter than 1.8 TeV has been excluded if $\mu \lesssim 800$ GeV. This bound can be interpreted as a lower bound on the gluino mass parameter at the unification scale $M_3 \gtrsim 800$ GeV.

Let us comment on another possibility to probe our scenario at the LHC. As shown in Fig.4.4, the bottom squark can be lighter than TeV scale and the bottom squark pair production will give contribution to the top squark search. This occurs only if the $\tan\beta$ is so large that the bottom Yukawa coupling constant is as large as the top Yukawa coupling constant. In this case, the heavy Higgs bosons also become lighter than 1 TeV as shown in Fig. 4.2. However, such a large $\tan\beta$ is severely constrained by flavor experiments and our sample values are on the edge of the exclusion limit. Thus it is worth studying large $\tan\beta$ region interplaying collider and flavor physics, which is our future work.

To reduce the μ-parameter, the wino mass is most important, and the bino can be light as long as the top squark is sufficiently heavy. We investigate this case in the next chapter, which involves dark matter physics.

Chapter 5

Dark matter phenomenology with non-universal gaugino masses

5.1 Dark matter scenarios

In this chapter, let us discuss dark matter physics of the NUGM scenario based on Ref. [75]. One of the strong motivations to consider the MSSM is that it provides a certain dark matter candidate. The LSP is higgsino-like neutralino in most of parameter regions of the NUGM scenario with the small μ-parameter. It is known that such a light higgsino-like neutralino is less produced by the thermal production than the observed value $h^2\Omega \simeq 0.01188 \pm 0.1$ [76, 77]. There are several ways to explain the observed relic density of the dark matters with the light higgsinos.

In general, the gravitino mass is not so different from the MSSM particles, since the mass correlates with the supersymmetry breaking scale. The gravitino couples to the MSSM particles only through Planck-suppressed operators, and its lifetime can be long enough so that it survives after thermal decoupling of the LSP. If the lifetime is so long that it survives after Big-Bang Nucleon (BBN) synthesis, the decay of gravitino spoils the success of the BBN scenario, which is known as the gravitino problem. The gravitino problem can be avoided if the gravitino mass is sufficiently heavy, typically $\gtrsim \mathcal{O}(10\text{TeV})$, and the lifetime is short enough. Although we should care about such a cosmological problem, there are other sources to produce relic abundance of the LSP, often called non-thermal productions [78].

The other approach to explain the relic abundance is to suppose that there are other particles which behave as dark matters in addition to the LSP. A possible candidate is an axion that was introduced to solve the strong CP problem in the QCD, but it is known that imaginary parts of moduli can remain in low energy effective theories of superstring models and behave like the axion dark matter.

Still another approach is to extend the MSSM. For instance, the Next-to-MSSM (NMSSM) is an interesting possibility [79]. The NMSSM is an extension of the MSSM where a singlet field that couples to the Higgs supermultiplets is introduced. A fermionic component of the singlet field, the so-called singlino, can be the sizable fraction of the LSP and could explain the relic density by the thermal production. The other candidate of the LSP in the extended MSSM

is an axino, the superpartner of the axion. The axino always appears if axion exists in the model owing to the supersymmetry [80,81]. In Ref. [40], the axino LSP is studied in the mirage mediation scenario.

These three possibilities seem to be reasonable and are interesting enough, but they are less predictable and depend on details of supersymmetry breaking, how the MSSM is embedded into superstring models or how to extend the MSSM. Therefore it is more attractive due to its predictability and simplicity to explain the dark matter relic by the thermal production in the MSSM.

A certain wino-to-gluino mass ratio is the most important ingredient to relax the fine-tuning and enhance the Higgs boson mass simultaneously. This indicates that the bino mass parameter can be small without spoiling the benefit of the NUGM scenario. Such a small bino mass is interesting, because the thermal relic density of the LSP can be raised due to the sizable fraction of the bino component [82]. We should care about the top squark mass, because it can be tachyonic easily for a light bino mass.

Even if the relic abundance is not explained by the thermally produced LSP, direct detections of the dark matter are important to probe the light higgsinos. The direct searches for the higgsinos are quite difficult at the LHC, especially for the NUGM scenario due to the small mass differences among higgsino-like neutralinos. On the other hand, the direct detections are efficient to see the higgsinos directly. For the direct detections, the size of bino mass parameter is crucial even if the LSP is mostly higgsino-like, and there would be non-negligible contributions from other sparticles.

Collider signals of sparticles could be different from the case that the LSP is purely higgsino-like for the light bino case. Since the mass differences among higgsinos are suppressed by the heavy bino and wino mass parameters, the mass difference could be sizable for the case of light bino. This would make decays of higgsinos detectable and also affects the decays of heavier sparticles. For instance, a decay channel of the top squark $\tilde{t}_1 \to t\tilde{\chi}_3^0$ opens up and then the branching ratio $\mathrm{BR}(\tilde{t}_1 \to b\tilde{\chi}_1^\pm)$ is reduced. The signal from the top squark decay $\tilde{t}_1 \to b\tilde{\chi}_1^\pm$ can be changed by decays of the chargino if the mass differences between the chargino and the lighter neutralinos becomes sizable.

In this chapter, we study dark matter physics in the NUGM scenario, and assess whether the collider signals are changed for a light-bino region from the case with heavy-bino where the LSP is mostly higgsino-like. In Section 5.2, we discuss conditions to obtain light binos without suffering from tachyonic or too light top squarks. Then we study dark matter physics by scanning parameter region of bino mass from light to heavy in Section 5.3. We also discuss whether the light binos influence the collider signals in Section 5.4. Section 5.5 summarizes this chapter.

5.2 Mass spectrum with light bino

We considered larger values of bino mass parameters in the previous chapters to lift up the top squark mass. When the μ-parameter is around the EW scale, contributions to the right-handed top squark mass from the gluino and the wino mass terms are canceled to each other. Thus

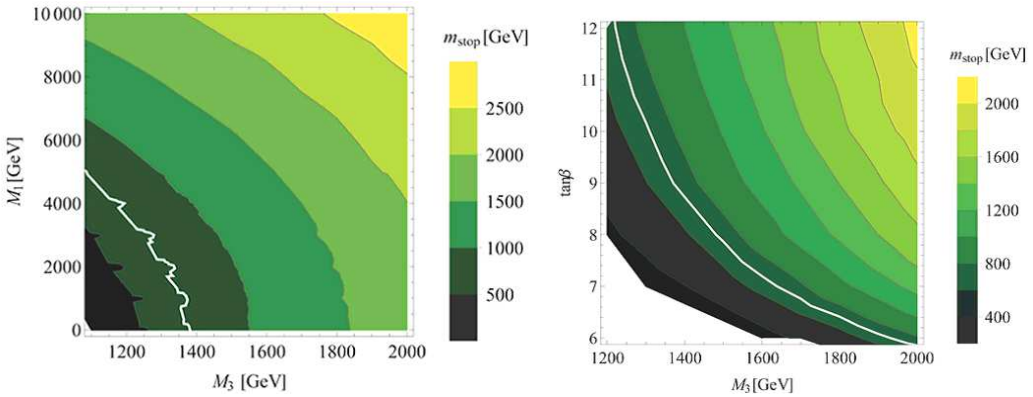

Figure 5.1: The top squark mass on M_1-M_3 plane (left) and M_3-$\tan\beta$ plane (right).

the top squark mass correlates with the bino mass parameter, and becomes easily too small to evade from the exclusion limits at the LHC or even becomes tachyonic.

Figure 5.1 shows the lightest top squark mass for small bino mass parameters. The left panel shows it on the M_1-M_3 plane. Values of parameters at the unification scale are fixed to $m_0 = 1.0$ TeV, $\mu = 300$ GeV and $\tan\beta = 10$. The right panel shows top squark mass on the M_3-$\tan\beta$ plane with $m_0 = 1.0$ TeV, $\mu = 300$ GeV and $M_1 = 2.5$ TeV. Values of the universal A-term A_0 and the wino mass term M_2 are chosen to realize the Higgs boson mass in a range $m_h = 125.04 \pm 0.6$ GeV and the μ-parameter is at 300 GeV. The top squark mass is 700 GeV on the white lines, which corresponds to the current experimental lower limit.

From the left panel, we see that the top squark mass increases as the bino or the gluino mass is increased. The gluino mass has to be larger than 1.4 TeV at the unification scale, or equivalently larger than about 4.0 TeV at the TeV scale, if the bino mass is around 1 TeV at the unifications scale. The top squark mass is lifted up by differences of contributions between the gluino and the wino mass parameter in cases of the light bino.

We also calculated the top squark mass for smaller $\tan\beta$, because it is important not only for the Higgs boson mass, but also for the direct detections as will be discussed later. The tree-level Higgs boson mass reduces for $\tan\beta \lesssim 10$, and the larger values of $A_t/M_{\rm st}$ are necessary to enhance the radiative correction. Thus the lighter right-handed top squark mass is induced by a smaller $\tan\beta$. The gluino mass term has to be larger than 1.2 TeV even for $\tan\beta \gtrsim 12$ to obtain the top squark heavier than 700 GeV with $M_1 = 2.5$ TeV.

5.3 Dark matter observations

5.3.1 Parameter settings

We consider two scenarios that the LSP saturates the whole dark matter abundance. One is that the LSP dark matter is produced only by the thermal process, and the other is that the LSP is produced non-thermally like the gravitino decay. The LSP saturates whole relic

density of dark matter in both cases. We assume that there is no entropy production after the thermal production of the LSP. Hence we consider such a parameter region is inconsistent with observations where the thermal abundance exceeds the observed relic density.

We study both cases with a positive or a negative μ-parameter, because its sign is especially relevant for cross sections of the LSP with nucleus. As pointed out in Ref. [83], there are several parameter regions, the so-called blind spots, where the spin-independent (SI) cross section or the spin-dependent (SD) cross section vanishes. The blind spots for SI cross section appears if a condition

$$m_{\tilde{\chi}} + \mu \sin 2\beta = 0 \tag{5.1}$$

is satisfied, and SD cross section vanishes at $\tan\beta = 1$. The blind spot for the SD cross section is hardly satisfied if we are interested in sparticles near TeV scale, because the tree-level Higgs boson mass also vanishes and the top squark mass must be much heavier than the EW scale.

Equation (5.1) can be satisfied if the signs of $M_{1,2}$ and μ are opposite to each other and comparable. The SI cross section can be reduced even when the condition Eq. (5.1) does not hold exactly. In our analysis, we employ a notation M_1 for a positive bino mass and the μ-parameter can have both signs. Smaller values of $\tan\beta$ are favored for satisfying the condition Eq. (5.1), but $\tan\beta \lesssim 7$ is hardly obtained with the experimentally allowed top squark mass as can be seen in Fig. 5.1. Although the cross section cannot vanish completely, it reduces for smaller values of $\tan\beta$ if the signs of μ and M_1 are opposite, while it enhances for smaller $\tan\beta$ if these have the same sign.

5.3.2 Constraints from dark matter observations

We evaluate the thermal relic density of the LSP, which is bino-like or higgsino-like or their mixture and the SI and SD cross sections constrained by the direct detections. These observables are calculated by using micrOmega-2 [84]. We refer to current exclusion limits for the cross sections given by the LUX [85–87], and future expected exclusion limits given by the XENON1T project [88, 89].

Figure 5.2 shows the thermal relic density and the exclusion limits from the direct detections. $m_0 = 1.0$ TeV, $M_3 = 1.5$ TeV and $\tan\beta = 10$ are assumed in this figure and values of M_2 and A_0 are decided to realize the Higgs bosom mass ~ 125 GeV and values of the μ-parameter which is varied along the vertical axis. The thermal relic density is in the observed range $h^2\Omega \simeq 0.01188 \pm 0.00001$ on the red lines, and it overcloses the universe below the red lines and the brown region. The blue regions are excluded by the LUX experiment measuring the SI cross section. The excluded regions by the SD cross section are fully covered by those of the SI cross section. The blue dashed lines correspond to the future expected exclusion limits for th SI cross section by the XENON1T experiment, and the purple solid line is that for the SD cross section. The background colors indicate the top squark mass. The LEP experiment excluded a chargino lighter than about 90 GeV by the mono-photon search [90] and such a region is in light gray. The top squark is lighter than the neutralinos and then becomes the LSP in the dark gray region.

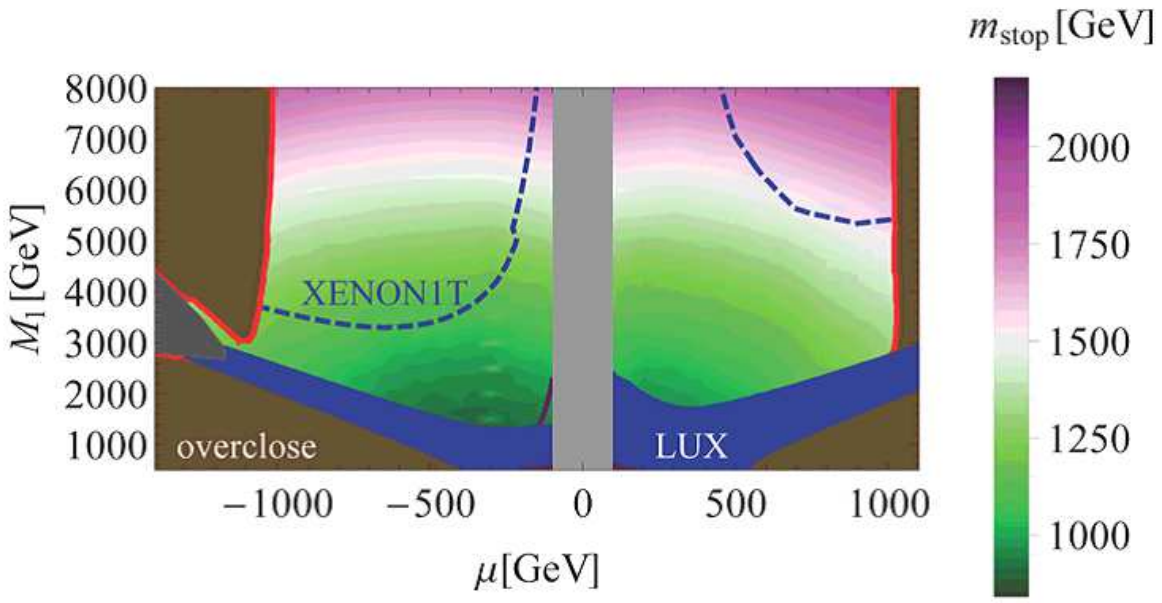

Figure 5.2: Allowed regions by dark matter observations on M_1-μ plane with $M_3 = 1.5$ TeV, $\tan\beta = 10$.

The LSP becomes a mixture of the bino and the higgsino below $M_1 \sim 3.0$ TeV and the observed relic density can be explained by the thermal production of the LSP, but such a region has already been excluded by the LUX experiment. Thus the thermal relic can be in the observed range only for the purely-higgsino LSP with the mass around 1 TeV. Even in this case, the bino must be heavier than 4.0 TeV for a negative μ-parameter and 6.0 TeV for a positive μ-parameter. This is because the SI cross sections enhanced significantly by the mixing between the bino and the higgsino. Note that there are contributions from the wino-higgsino mixing because the wino-like neutralino is in sub-TeV range and it does not decouple completely. The thermal relic can be reduced to the observed value around the top squark LSP region, colored in dark gray. The co-annihilation process between the higgsino and the top squark works efficiently.

5.4 Collider signals

Before closing, let us mention about collider signals for a small bino mass region. The situation could be changed significantly if the bino is the main component of the lightest neutralino instead of the higgsino, and the higgsino search will be available or decays of the top squark differ from the case that the LSP is purely higgsino-like. However, such light bino region has been inconsistent with the cosmological observations as shown in the previous section and it

seems not to be worth studying collider signals in detail *. Thus our remaining interest to this region is whether the bino mixing to the higgsino LSP rather than bino itself affects collider signals.

The higgsino search is not efficient due to the small mass differences among the higgsinos suppressed by the heavy bino and wino masses. In other words, the higgsino search can be efficient if the bino mass can be so small where the mass difference is large enough. However, we showed that the mass difference can not be larger than about 5-10 GeV and the higgsino search will be still inefficient once we take the exclusion limits from the direct detections into account. Note that bino search is also inefficient, because its production cross section is quite small due to the fact that the bino is singlet under the SM gauge group.

A remaining possibility is to rely on the effects caused by decays of heavier particles, especially the top squark. The top squark can decay to the bino if the bino is lighter than the top squark. This increases the branching fraction to the top quark, $\mathrm{BR}(\tilde{t}_1 \to t\widetilde{B})$. However, the bino couples to the top squark through the weak gauge coupling and its coupling is weaker than that of the higgsino to the top squark through the top Yukawa coupling. Hence, the $\mathrm{BR}(\tilde{t}_1 \to t\widetilde{B})$ can not be sizable unless this decay mode is kinematically favored, namely the bino is lighter than the higgsino. Again, such light bino region is excluded by the dark matter observations, and the light bino cannot change the top squark decay from the case with the purely-higgsino LSP.

From the above discussion, the collider signals are almost the same as the analysis in the previous chapter once we concentrate on the parameter region allowed by dark matter observations.

5.5 Summary

In this chapter, we investigate dark matter prospects in the NUGM scenario. Even if the LSP is mostly higgsino-like, the bino mass parameter is also important for the character of the LSP dark matter. The bino mass parameter plays a key role to lift up the top squark mass, and it can be small only for large gluino mass parameter $M_3 \gtrsim 1.5$ TeV.

The thermal relic density can be raised by the sizable bino component, but such a bino-higgsino dark matter is severely constrained by the direct detections. The direct detections are sensitive to a little mixing to the higgsino LSP from the bino. Thus tight limits are expected for light binos in future observations.

The remaining ways to explain the relic abundance are to consider the higgsino about 1 TeV or existence of the non-thermal productions with the higgsino lighter than 1 TeV. Sensitivity of direct detections for such higgsinos is significantly dependent on the sign of μ-parameter and bino mixing. It is possible that co-annihilation of the top squark and the higgsinos could allow to explain the thermal relic even if they are lighter than 1 TeV.

*There are small rooms to explain the thermal relic abundance by the bino-higgsino LSP, but the LSP-nucleon cross sections are enough small as intensively studied in Ref. [91]. The thermal relic abundance can be reduced by the Z- or Higgs-boson resonance and the cross sections can be suppressed by their blind spot nature even if the LSP has a sizable bino component.

Since the bino can not be the LSP to avoid too much LSPs and well mixes with the higgsino, expected signals from higgsino production will not be so changed from the case that the LSP is purely higgsino. Moreover, the top squark decay is not so changed by the bino lighter than the top squark, because the bino couples to top squark much weaker than the higgsinos. Therefore, expected signals for lighter bino will be quite similar to the heavier binos studied in the previous chapter.

Chapter 6

Conclusion

In this thesis, we studied the non-universal gaugino mass (NUGM) scenario. A certain wino-to-gluino mass ratio at the unification scale enhances the Higgs boson mass and relaxes the degree of tuning of the μ-parameter at the same time. This scenario is particularly attractive, because the relatively large wino mass reduces the μ-parameter and simultaneously enhances the Higgs boson mass owing to the large top squark mixing induced by the wino mass. It allows the sparticle masses below or near TeV scale, and this scenario is testable at experiments and observations.

An interesting mechanism to realize such gaugino masses is the mirage mediation of supersymmetry breaking, which is the mixture of the moduli and anomaly mediations. The mirage mediation scenario is supported by a certain class of superstring models. The comparable contributions from moduli and anomaly mediations can be realized by the KKLT-type moduli stabilization mechanism. The moduli mediated contributions depend on how the moduli couples to the MSSM field and are controlled by the modular weights. Since the modular weights do not affect the gaugino masses, they can be chosen to increase the Higgs boson mass individually. We specified the parameter space where the Higgs boson mass is 125 GeV while the μ-parameter is near the EW scale for several patterns of the modular weights. The modular weights are determined by, e.g., the way how the MSSM particles are embedded into D-brane configurations. Then we will be able to know the structure of superstring models behind the MSSM, once we observe the sparticle spectrum and specify the modular weights.

The mass spectrum of the NUGM scenario is characterized by the light higgsino LSP and a right-handed top squark while all the other sparticles have roughly the same masses. We studied expected signals of the NUGM at the collider experiment. The higgsino is quite difficult to be probed at the LHC due to its certainly small mass difference. The right-handed top squark decays to both top and bottom quarks plus the higgsinos. Since all of the higgsinos behave as invisible particles, the expected signals are only two third-generation quarks and missing energy. The event topology with two bottom quarks and missing energy is particularly important for testing spectra with a small mass difference between the top squark and the higgsinos. The gluino is also important due to its large production cross section and a large multiplicity of the associated jets. The gluino decays to or through a top squark and a top quark, then the top squark subsequently decays to a third-generation quark and higgsinos. The gluino pair

production makes the signal with four third-generation quarks, where two of them are top quarks, and missing energy.

The dark matter observations are important to probe the light higgsino which is quite difficult for the LHC. The higgsino dark matter is less produced by the thermal processes than is required, unless its mass is about 1 TeV. Hence, the non-thermal production through, e.g., the gravitino decay or the sizable mixing with the light bino is necessary to explain the observed relic density of the dark matter. We examined dark matter physics in a wide range from the light bino comparable with the higgsino to the heavy bino decoupled from the higgsino. The top squark is kept heavy enough due to the RG-contributions from the bino, because those from the gluino and wino are mostly canceled each other. If the bino mass is small and can not contribute to the top squark mass, the gluino has to be heavy enough to keep the top squark mass non-tachyonic even though most contributions from the gluino are canceled by those of the wino mass. The bino-higgsino LSP can explain the adequate thermal relic density, but such an LSP has already been excluded by the direct detections. Even if we adopt 1 TeV higgsino or non-thermal productions, direct detection will give considerable bounds due to the bino-higgsino mixing. If the bino mass is quite heavy and the mixing is highly suppressed, the gluino mass can be light because it does not have to be heavy to keep the top squark mass. This case is easier to be probed by the LHC while the direct detection experiment is efficient for the light-bino cases. Thus they play complemental roles to each other.

The naturalness is a guiding principle to consider new physics. Supersymmetry gives an elegant solution to the naturalness problem of the SM, but the recent LHC results have constrained parameter space favored from the naturalness in the MSSM. The non-universal gaugino masses with certainly large wino is at a corner of such parameter space favored from the naturalness but still surviving. The LHC and direct detections are now probing this parameter space and will guide us to construct physics beyond the SM.

Acknowledgment

Firstly, I would like to thank my supervisor, professor Hiroyuki Abe (Waseda Univ.) for giving me valuable advices and stimulating discussions. I greatly thank associate professor Yuji Omura (KMI) for meaningful discussions and collaborations. I thank professor Hiromichi Nakazato (Waseda Univ.) for helpful advices and comments. I thank professor Kohei Yorita (Waseda Univ.) for valuable advices. I also thank Hajime Otsuka and Keigo Sumita for collaborations and all members in Nakazato-Abe laboratory.

Appendix A

The SM-like Higgs boson mass in the MSSM

In this appendix, the explicit formulae for the SM-like Higgs boson mass of the MSSM which are used in Chapter 2 and 3 are shown. We basically follow the RG-improved effective potential method used in Ref. [23,92]. The mass matrices for the third-generation squarks and the Higgs boson are shown in Section A.1. In Section A.2, the Higgs boson mass for the case with $m_A \gtrsim m_{\rm SUSY}$ is shown, while the case with $m_A < m_{\rm SUSY}$ is considered in Section A.3.

A.1 Higgs boson and third-generation squark sector

In the MSSM, there are two Higgs $SU(2)_L$ doublets and they have 2 CP-even neutral ($h,\ H$), 1 CP-odd neutral (A) and 2 charged ($H^\pm$) degrees of physical freedom. The other three degrees of freedom are unphysical and can be absorbed into the Weak gauge bosons. The masses of the physical degrees of freedom can be written at tree-level,

$$m_A^2 = \frac{2b}{\sin 2\beta} = 2|\mu|^2 + m_{H_u}^2 + m_{H_d}^2, \tag{A.1}$$

$$m_{h,H}^2 = \frac{1}{2}\left(m_A^2 + m_Z^2 \mp \sqrt{(m_A^2 - m_Z^2)^2 + 4m_Z^2 m_A^2 \sin^2 2\beta} \right), \tag{A.2}$$

$$m_{H^\pm}^2 = m_A^2 + m_W^2, \tag{A.3}$$

where

$$m_Z = \frac{1}{4}\left(g_2^2 + \frac{3}{5} g_1^2 \right) v^2, \tag{A.4}$$

$$m_W = \frac{1}{4} g_2^2 v^2, \tag{A.5}$$

and $v \simeq 174$ GeV. The lighter CP-even neutral Higgs boson corresponds to the SM-like Higgs boson that has the mass of about 125 GeV.

In a limit of $m_A \gg m_Z$, the so-called decoupling limit, the Higgs bosons except the SM-like one decouples from the EW sector, and the Higgs sector consists only of the SM-like Higgs boson. The SM-like Higgs boson mass in this limit becomes

$$m_h^2 = m_Z^2 \cos^2 2\beta \leq m_Z^2 \simeq (91.2\text{GeV})^2. \tag{A.6}$$

Thus it is obvious that radiative corrections are important to explain the observed Higgs boson mass. In the decoupling limit, the two Higgs doublets $H_u,\ H_d$ in the MSSM contribute to the SM-like Higgs boson h as $H_u \to \sin\beta h$ and $H_d \to -\cos\beta \epsilon h^*$.

The radiative corrections to the Higgs boson masses are governed by the third-generation squarks. Their mass matrices are given by

$$M_{\tilde{t}}^2 = \begin{pmatrix} m_Q^2 + y_t^2|H_u|^2 + \frac{1}{4}(g_2^2 - \frac{1}{5}g_1^2)(|H_d|^2 - |H_u|^2) & y_t(A_t H_u - \mu H_d^*) \\ y_t^*(A_t H_u - \mu H_d^*)^* & m_u^2 \ + y_t^2|H_u|^2 + \frac{1}{5}g_1^2(|H_d|^2 - |H_u|^2) \end{pmatrix}, \tag{A.7}$$

$$M_{\tilde{b}}^2 = \begin{pmatrix} m_Q^2 + y_b^2|H_d|^2 - \frac{1}{4}(g_2^2 + \frac{1}{5}g_1^2)(|H_d|^2 - |H_u|^2) & y_b(A_b H_d - \mu H_u^*) \\ y_b^*(A_b H_d - \mu H_u^*)^* & m_d^2 + y_b^2|H_d|^2 - \frac{1}{10}g_1^2(|H_d|^2 - |H_u|^2) \end{pmatrix}, \tag{A.8}$$

where $M_{\tilde{t}}^2,\ M_{\tilde{b}}^2$ are mass squared matrices for the top squark and the bottom squark. Note that contributions from the bottom squark become important only when $\tan\beta$ is large and y_b is sizable compared with the top Yukawa coupling constant. These will be used later to calculate the radiative corrections by the effective potential.

A.2 Higgs boson mass for $m_{\rm SUSY} \gtrsim m_A$

A.2.1 Tree-level relations

Let us consider the case with $m_{\rm SUSY} \gtrsim m_A$. We define the SUSY scale depending on mass spectra as,

$$m_{\rm SUSY} = \sqrt{m_Q m_u}, \tag{A.9}$$

in order to reduce the renormalization scale dependence of radiative corrections, because the top squarks will give the most important contributions to many quantities, including the SM-like Higgs boson mass.

In the NUGM scenario, the right-handed top squark can be lighter than the other scalars including the heavy Higgs bosons. Hence, the effective theory below $m_{\rm SUSY}$, where most of the sparticles decouple from the theory, consists of the SM particles, the higgsinos $\tilde{H}_{u,d}$ and the right-handed top squark $\tilde{t}_R$. The scalar and the higgsino part of Lagrangian below the SUSY threshold can be written as,

$$\begin{aligned} \mathcal{L}_{\rm scalar,higgsino} &= m_H^2 H^\dagger H - \frac{\lambda_1}{2}(H^\dagger H)^2 - h_t \bar{Q}_3 \epsilon H^* t_R - h_b \bar{Q}_3 H b_R + f_t \overline{\widetilde{H}}_u \epsilon Q \widetilde{t}_R \\ &\quad -\mu \widetilde{H}_u^T \epsilon \widetilde{H}_d - m_U^2 |\widetilde{t}_R|^2 - \lambda_2 |\widetilde{t}_R|^2 |H|^2 - \frac{\lambda_3}{2}|\widetilde{t}_R|^4 + \text{h.c.}. \end{aligned} \tag{A.10}$$

Values of the coupling constants are connected to the MSSM parameters at $m_{\rm SUSY}$

$$\lambda_1(m_{\rm SUSY}) = \frac{1}{4}\left(g_2^2+\frac{3}{5}g_1^2\right)\cos^2 2\beta + \Delta\lambda, \tag{A.11}$$

$$h_t(m_{\rm SUSY}) = y_t \sin\beta, \tag{A.12}$$

$$f_t(m_{\rm SUSY}) = y_t, \tag{A.13}$$

$$\lambda_2(m_{\rm SUSY}) = y_t^2\sin^2\beta + \frac{1}{5}g_1^2\cos 2\beta - \frac{m_u}{m_Q}y_t^2\sin^2\beta\widetilde{X}_t^2, \tag{A.14}$$

$$\lambda_3(m_{\rm SUSY}) = \frac{1}{3}\left(g_3^2+\frac{4}{5}g_1^2\right), \tag{A.15}$$

where $\tilde{X}_t = (A_t - \mu\cot\beta)/\sqrt{m_Q m_u}$. These relations are at tree-level except $\Delta\lambda$ which represents loop induced threshold corrections.

A.2.2 Threshold correction

The threshold corrections come from wave-function renormalization and proper corrections to quartic couplings. We have to calculate the 1-loop corrections to the self-energies in order to obtain the wave-function renormalization part.

For the Higgs quartic couplings, the most important correction come from wave-function renormalization induced by trilinear couplings. The 1-loop correction to a self-energy $\Pi(p)$ of scalar field induced by a trilinear coupling A mediated by two scalars having masses m_1, m_2 is given by

$$\Pi^{\rm Tri}(p) = -\frac{A^2}{16\pi^2}\int_0^1 dx \log\left[\frac{x m_1^2 + (1-x)m_2^2 - x(1-x)p^2}{Q^2}\right], \tag{A.16}$$

and the threshold corrections to the wave-function renormalizations can be read as

$$\Delta Z_\phi^{\rm Tri} = \left.\frac{\partial\Pi^{\rm Tri}}{\partial p^2}\right|_{p^2=0} = \frac{1}{16\pi^2}\frac{A^2}{m_1 m_2}\frac{1}{6}F_5\left(\frac{m_1}{m_2}\right), \tag{A.17}$$

where the definition of F_5 will be shown later. In the case of the SM-like Higgs boson, the trilinear coupling and the scalar masses are $A = y_t\sin\beta(A_t - \mu\cot\beta)$, $m_1 = m_u$, $m_2 = m_Q$. The threshold corrections from the Higgs self-energy contributes to the Higgs quartic coupling as

$$\frac{1}{4}\left(g_2^2+\frac{3}{5}g_1^2\right)\cos^2 2\beta \times 12\left(-\frac{1}{2}\Delta Z_h^{\rm Tri}\right). \tag{A.18}$$

The proper corrections to the quartic coupling can be obtained by the usual diagrammatic approach, but it can be also obtained by expanding the effective potential. For instance, if a mass squared matrix of a complex scalar field has a form

$$\mathcal{M}^2 = \begin{pmatrix} M^2 + \frac{1}{2}\alpha\phi^2 & -X\frac{1}{\sqrt{2}}\phi \\ -X\frac{1}{\sqrt{2}}\phi & m^2 + \frac{1}{2}\beta\phi^2 \end{pmatrix}, \tag{A.19}$$

second derivative of the effective potential with respect to ϕ^2 at $\phi^2 = 0$ is

$$\begin{aligned}\left.\frac{d^2}{d\phi^2 d\phi^2} V_{\rm eff}^{1l}(\phi^2)\right|_{\phi^2=0} &= \frac{1}{32\pi^2}\left[\frac{\alpha^2}{2}\log\frac{M^2}{Q^2} + \frac{\beta^2}{2}\log\frac{m^2}{Q^2} - \frac{X^4}{12m^2M^2}F_2\left(\frac{M}{m}\right)\right. \\ &+ \left.\frac{X^2}{(M^2-m^2)^2}\left((\alpha-\beta)(M^2-m^2) - (\alpha m^2 - \beta M^2)\log\frac{M^2}{m^2}\right)\right].\end{aligned} \tag{A.20}$$

where the 1-loop effective potential induced by fields i with spin s_i is given by

$$V_{\rm eff}^{1l}(\phi^2) = \frac{1}{64\pi^2}\sum_i (-1)^{2s_i}(2s_i+1)\ {\rm Tr}\left[\mathcal{M}^4\left(\log\frac{\mathcal{M}^2}{Q^2} - \frac{3}{2}\right)\right], \tag{A.21}$$

where we adopt the dimensional reduction scheme [93]. The quartic coupling λ above and below the threshold are related as

$$\frac{\lambda_{\rm LE}}{8} + \frac{1}{2}\left.\frac{d^2}{d\phi^2 d\phi^2} V_{\rm LE}^{1l}(\phi^2)\right|_{\phi^2=0} = \frac{\lambda_{\rm HE}}{8} + \frac{1}{2}\left.\frac{d^2}{d\phi^2 d\phi^2} V_{\rm HE}^{1l}(\phi^2)\right|_{\phi^2=0}, \tag{A.22}$$

where LE, HE represent Lower-Energy and Higher-Energy than the threshold scale, respectively.

For the Higgs quartic coupling, the third-generation squarks give the dominant corrections which are $\mathcal{O}(y_{t,b}^4)$. Hence, we consider contributions from the top squark and the bottom squark mass matrices Eq. (A.8) but $H_u,\ H_d$ are replaced to $1/\sqrt{2}\phi\sin\beta,\ 1/\sqrt{2}\phi\cos\beta$, respectively.

Finally, we obtain the threshold corrections to the Higgs quartic coupling $\Delta\lambda$ at the $m_{\rm SUSY}$,

$$\begin{aligned}16\pi^2\Delta\lambda &= 3\left\{h_t^4 + \frac{1}{2}h_t^2\left(g_2^2 - \frac{1}{5}g_1^2\right)\cos 2\beta\right\}\log\frac{m_Q^2}{m_{\rm SUSY}^2} \\ &+3\left\{h_b^4 - \frac{1}{2}h_b^2\left(g_2^2 + \frac{1}{5}g_1^2\right)\cos 2\beta\right\}\log\frac{m_Q^2}{m_{\rm SUSY}^2} \\ &+3\left(h_t^4 + \frac{2}{5}h_t^2 g_1^2\cos 2\beta\right)\log\frac{m_u^2}{m_{\rm SUSY}^2} \\ &+3\left(h_b^4 - \frac{1}{5}h_b^2 g_1^2\cos 2\beta\right)\log\frac{m_d^2}{m_{\rm SUSY}^2} \\ &+6h_t^4\tilde{X}_t^2\left(F_1\left(\frac{m_Q}{m_u}\right) - \frac{\tilde{X}_t^2}{12}F_2\left(\frac{m_Q}{m_u}\right)\right) \\ &+6h_b^4\tilde{X}_b^2\left(F_1\left(\frac{m_Q}{m_d}\right) - \frac{\tilde{X}_b^2}{12}F_2\left(\frac{m_Q}{m_d}\right)\right) \\ &+\frac{3}{4}h_t^2\cos 2\beta\tilde{X}_t^2\left(\frac{3}{5}g_1^2F_3\left(\frac{m_Q}{m_u}\right) + g_2^2F_4\left(\frac{m_Q}{m_u}\right)\right) \\ &-\frac{3}{4}h_b^2\cos 2\beta\tilde{X}_b^2\left(\frac{3}{5}g_1^2F_3'\left(\frac{m_Q}{m_d}\right) + g_2^2F_4\left(\frac{m_Q}{m_d}\right)\right) \\ &-\frac{1}{4}h_t^2\cos^2 2\beta\tilde{X}_t^2\left(\frac{3}{5}g_1^2 + g_2^2\right)F_5\left(\frac{m_Q}{m_u}\right)\end{aligned} \tag{A.23}$$

$$
\begin{aligned}
&-\frac{1}{4}h_b^2\cos^2 2\beta\tilde{X}_b^2\left(\frac{3}{5}g_1^2+g_2^2\right)F_5\left(\frac{m_Q}{m_d}\right)\\
&-3\lambda_2^2\log\frac{m_u^2}{m_{\rm SUSY}^2},
\end{aligned}
$$

where $\tilde{X}_t=(A_t-\mu\cot\beta)/\sqrt{m_Q m_u}$, $\tilde{X}_b=(A_b-\mu\tan\beta)/\sqrt{m_Q m_d}$. Here, we drop the $\mathcal{O}(g_{1,2}^4)$ terms. Note that the last term comes from low energy part of Eq. (A.22) when the right-handed top squark remains in the low-energy theory and it is canceled with the third line. This result is consistent with Ref. [94] when the right-handed top squark mass is also considered to be decoupled at $m_{\rm SUSY}$.

The loop functions are defined as

$$
\begin{aligned}
F_1(x) &= \frac{x\log x^2}{x^2-1}, && \text{(A.24)}\\
F_2(x) &= \frac{6x^2[2-2x^2+(1+x^2)\log x^2]}{(x^2-1)^3}, && \text{(A.25)}\\
F_3(x) &= \frac{2x[5(1-x^2)+(1+4x^2)\log x^2]}{3(x^2-1)^2}, && \text{(A.26)}\\
F_3'(x) &= \frac{2x[1-x^2+(2x^2-1)\log x^2]}{3(x^2-1)^2}, && \text{(A.27)}\\
F_4(x) &= \frac{2x[x^2-1-\log x^2]}{(x^2-1)^2}, && \text{(A.28)}\\
F_5(x) &= \frac{3x[1-x^4+2x^2\log x^2]}{(1-x^2)^3}. && \text{(A.29)}
\end{aligned}
$$

A.2.3 Renormalization group

We want to know the Higgs boson mass at the top quark mass scale. Hence, we need a value of $\lambda(m_t)$ by solving RGEs. Anomalous dimensions and beta functions at 2-loop order for dimensionless couplings in a general gauge theory with real scalars and fermions are derived in Refs. [95–97].

First, we extract beta functions for the general model having interaction terms

$$
-\mathcal{L}_{\rm int}=-\mathcal{L}_{\rm gauge}+\frac{1}{2}y^{Ijk}\phi_I\psi_j\psi_k+\frac{1}{2}y^I_{jk}\phi_I\bar{\psi}^j\bar{\psi}^k+\frac{1}{4}\lambda^{IK}_{JL}\phi_I\phi^J\phi_K\phi^L, \qquad \text{(A.30)}
$$

where complex scalars are represented by ϕ_I, $\phi^J=(\phi_J)^*$ and two component spinors are denoted by ψ_i, $\bar{\psi}^j$. The beta function for the Yukawa coupling y^{Ijk} is

$$
\begin{aligned}
16\pi^2\beta_y^{Ijk} &= 2y^{Kjl}y^I_{lm}y_K^{mk}+\frac{1}{2}(y^{Ilk}Y(F)^j_l+y^{Ijm}Y(F)^k_m)+y^{Kjk}Y(S)^I_K \qquad \text{(A.31)}\\
&\quad -3\sum_a g_a^2\{C_a(F),\ y^I\}^{jk},
\end{aligned}
$$

and those for quartic coupling λ^{IK}_{JL} is

$$\begin{aligned}16\pi^2\beta^{IK}_{JL} =&\lambda^{IK}_{MN}\lambda^{MN}_{JL} + 2(\lambda^{IM}_{JN}\lambda^{NK}_{ML} + \lambda^{IM}_{LN}\lambda^{NK}_{MJ}) \\ &- 4\ \mathrm{tr}\big[Y^I Y_L^\dagger Y^K Y^\dagger{}_J + Y^{\dagger I} Y_L Y^{\dagger K} Y_J + (J \leftrightarrow L)\big] \\ &+ \lambda^{IK}_{JL} \sum_{S=I,J,K,L} (Y_2(S) - 3\sum_a g_a^2 C_a(S)) \\ &+ 3\sum_{a,b}\sum_{l,m} g_l^2 g_m^2 (\{\theta^a_l, \theta^b_m\}_J{}^I \{\theta^a_l, \theta^b_m\}_L{}^K + \{\theta^a_l, \theta^b_m\}_L{}^I \{\theta^a_l, \theta^b_m\}_J{}^K),\end{aligned} \tag{A.32}$$

where

$$(Y^I)_{ij} = y^I_{ij},\ (Y^{\dagger I})^{jk} = y^{Ijk}, \tag{A.33}$$

and

$$Y(S) = y_{Ikl}y^{Jkl} + y^{kl}_I y^J_{kl}, \quad Y(F) = y^I_{ik}y^{kj}_I, \tag{A.34}$$

$$C_a(S) = \theta^{aK}_I \theta^{aJ}_K, \qquad C_a(F) = T^{ak}_i T^{aj}_k, \quad C_a(G)\delta_{ab} = f_{acd}f_{bcd}, \tag{A.35}$$

$$T(S)\delta_{ab} = \mathrm{tr}\theta^a\theta^b, \qquad T(F)\delta_{ab} = \mathrm{tr}T^aT^b. \tag{A.36}$$

The upper indices for scalar fields are contracted to conjugate fields and summation for upper and lower indices should be understood as $A_K B^K = \sum_K (A_K B^K + A^K B_K)$. The indices a, b runs over gauge groups in the model and T^{ai}_j, θ^{aI}_J are the representation matrices of the scalar field ϕ_i and the fermion ψ_I, respectively.

Based on those formulae and the well-known beta function of a gauge coupling constant, we can obtain the beta functions for the model below the SUSY threshold. The beta functions of the gauge coupling constants are written as

$$16\pi^2\beta_{g_1} = \frac{3}{5}g_1^3\left[\frac{41}{6} + \frac{1}{6}\theta_H + \frac{2}{3}\theta_{\tilde{H}} + \frac{4}{9}\theta_{\tilde{u}} + \frac{26}{9}\theta_{\tilde{m}}\right], \tag{A.37}$$

$$16\pi^2\beta_{g_2} = g_2^3\left[-\frac{19}{6} + \frac{1}{6}\theta_H + \frac{2}{3}\theta_{\tilde{H}} + \frac{4}{3}\theta_{\tilde{W}} + 2\theta_{\tilde{m}}\right], \tag{A.38}$$

$$16\pi^2\beta_{g_3} = g_3^2\left[-7 + 2\theta_{\tilde{g}} + \frac{1}{6}\theta_{\tilde{u}} + \frac{11}{6}\theta_{\tilde{m}}\right], \tag{A.39}$$

where θ_ϕ is a step function that it is unity if the scale is above the mass of field ϕ while it vanishes below the mass of ϕ. H, $\tilde{H}$, $\tilde{u}$, $\tilde{W}$, $\tilde{g}$ denote the heavy Higgs bosons, higgsinos, right-handed top squark, wino and gluino, respectively. All the other sparticles are assumed to have similar masses and their contributions are denoted by $\tilde{m}$. The beta function of the Yukawa coupling constants are given by

$$16\pi^2 h_t = h_t\left[\frac{9}{2}h_t^2 + \frac{3}{2}h_b^2 + \frac{1}{2}f_t^2 - \left(\frac{17}{20}g_1^2 + \frac{9}{4}g_2^2 + 8g_3^2\right)\right], \tag{A.40}$$

$$16\pi^2 h_b = h_b\left[\frac{3}{2}h_t^2 + \frac{9}{2}h_b^2 + \frac{1}{2}f_t^2 - \left(\frac{1}{4}g_1^2 + \frac{9}{4}g_2^2 + 8g_3^2\right)\right], \tag{A.41}$$

$$16\pi^2 f_t = f_t\left[\frac{1}{2}h_t^2 + \frac{1}{2}h_b^2 + 4f_t^2 - \left(\frac{1}{2}g_1^2 + \frac{9}{2}g_2^2 + 4g_3^2\right)\right]. \tag{A.42}$$

The beta functions for the quartic couplings are

$$16\pi^2\beta_{\lambda_1} = 12\lambda_1^2 + 6\lambda_2^2 + 4\lambda_1\left(3h_t^2 + 3h_b^2 - \frac{9}{20}g_1^2 - \frac{9}{4}g_2^2\right) \tag{A.43}$$
$$-12(h_t^4 + h_b^4) + \frac{9}{4}\left(\frac{3}{25}g_1^4 + \frac{2}{5}g_1^2g_2^2 + g_2^4\right),$$
$$16\pi^2\beta_{\lambda_2} = \lambda_2(6\lambda_1 + 4\lambda_2 + 8\lambda_3) + \lambda_2\left(6h_t^2 + 6h_b^2 + 4f_t^2 - \frac{5}{2}g_1^2 - 9g_2^2 - 8g_3^2\right) \tag{A.44}$$
$$-4f_t^2(h_t^2 + h_b^2) + \frac{12}{25}g_1^4,$$
$$16\pi^2\beta_{\lambda_3} = 4\lambda_2^2 + 14\lambda_3^2 + 4\lambda_3\left(2f_t^2 - \frac{4}{5}g_1^2 - \frac{9}{4}g_2^2 - 4g_3^2\right) \tag{A.45}$$
$$-8f_t^4 + \frac{64}{75}g_1^4 + \frac{32}{15}g_1^2g_3^2 + \frac{13}{3}g_3^4.$$

(A.46)

The beta functions for quartic couplings can be obtained from the general formulae Eq.(A.32), but they can be also obtained by expanding and differentiating the effective potential [92] with respect to the Higgs boson and the renormalization scale, respectively. We confirmed both results are the same as it should be.

In our analysis, we assume that the higgsinos decouple at the same time as the right-handed top squark. Note that there is no threshold correction to the Higgs quartic self-coupling up to $\mathcal{O}(y_t^2 g_{1,2}^2)$, because it is given by the last term of Eq. (A.24) but $m_{\rm SUSY}$ is replaced by m_u. Finally, we can obtain $\lambda(m_t)$ by solving the SM RG equations below m_u. The beta-functions for the relevant SM coupling couplings are given by

$$16\pi^2\beta_{y_t} = y_t\left(\frac{9}{2}y_t^2 + \frac{3}{2}y_b^2 - \frac{17}{20}g_1^2 - \frac{9}{4}g_2^2 - 8g_3^2\right), \tag{A.47}$$
$$16\pi^2\beta_{y_b} = y_b\left(\frac{3}{2}y_t^2 + \frac{9}{2}y_b^2 - \frac{1}{4}g_1^2 - \frac{9}{4}g_2^2 - 8g_3^2\right), \tag{A.48}$$
$$16\pi^2\beta_{\lambda} = 12\lambda^2 + 4\lambda\left(3y_t^2 + 3y_b^2 - \frac{9}{20}g_1^2 - \frac{9}{4}g_2^2\right) \tag{A.49}$$
$$-12(y_t^4 + y_b^4) + \frac{9}{4}\left(\frac{3}{25}g_1^4 + \frac{2}{5}g_1^2g_2^2 + g_2^4\right).$$

After we obtain the quartic coupling constant at the top quark mass scale, we calculate the Higgs boson mass using the 1-loop effective potential $V_{\rm SM}^{1l}(\phi)$ based on the $\overline{\rm MS}$ scheme with neglecting the Yukawa couplings except the top Yukawa coupling as

$$m_h^2(p^2 = 0) = 2\lambda v^2 + \frac{d^2}{d\phi d\phi}V_{\rm SM}^{1l}(\phi)\Big|_{\phi=0} - \frac{1}{\sqrt{2}v}\frac{d}{d\phi}V_{\rm SM}^{1l}\Big|_{\phi=\sqrt{2}v}. \tag{A.50}$$

A.3 Higgs boson mass for $m_A < m_{\rm SUSY}$

If the m_A is smaller than the SUSY threshold, the Higgs potential still contains two Higgs doublets below $m_{\rm SUSY}$. We basically follow the calculation in Ref. [23], but we solve RG equations numerically rather than the log expansion.

The tree-level CP-even Higgs mass matrix is given by

$$M_h^2 = \begin{pmatrix} M_{11}^2 & M_{12}^2 \\ M_{21}^2 & M_{22}^2 \end{pmatrix} \tag{A.51}$$
$$= \begin{pmatrix} 2v^2\lambda_1\cos^2\beta + m_A^2\sin^2\beta & 2v^2\sin\beta\cos\beta(\lambda_3+\lambda_4) - m_A^2\sin\beta\cos\beta \\ 2v^2\sin\beta\cos\beta(\lambda_3+\lambda_4) - m_A^2\sin\beta\cos\beta & 2v^2\lambda_2\sin^2\beta + m_A^2\cos^2\beta \end{pmatrix},$$

where λ_{1-4} are defined as

$$V_{\rm quartic}^{\rm 2HDM} = \lambda_1(H_d^\dagger H_d)^2 + \lambda_2(H_u^\dagger H_u)^2 + \lambda_3(H_d^\dagger H_d)(H_u^\dagger H_u) + \lambda_4|H_u^\dagger \epsilon H_d|^2. \tag{A.52}$$

These coupling constants are related to the gauge coupling constants as $\lambda_1 = \lambda_2 = -(\lambda_3+\lambda_4) = (g^2+g'^2)/4$ at tree-level in the MSSM.

A.3.1 Threshold corrections

As $m_A \gtrsim m_{\rm SUSY}$, we calculate the Higgs boson mass at the top quark mass scale. Hence we have to evaluate the values of the quartic couplings at this scale. In addition, there are threshold corrections at $m_{\rm SUSY}$

$$\Delta^{\rm th}M_h(m_{\rm SUSY}) = \begin{pmatrix} \frac{1}{2}\left.\frac{\partial^2 V_{\rm th}^{1l}}{\partial h_d^2}\right|_{h_d=0} - \left.\frac{1}{v_d}\frac{\partial V_{\rm th}^{1l}}{\partial H_d}\right|_{H_d=v_d} & \frac{1}{2}\left.\frac{\partial^2 V_{\rm th}^{1l}}{\partial h_d \partial h_u}\right|_{h_d=h_u=0} \\ \frac{1}{2}\left.\frac{\partial^2 V_{\rm th}^{1l}}{\partial h_d \partial h_u}\right|_{h_d=h_u=0} & \frac{1}{2}\left.\frac{\partial^2 V_{\rm th}^{1l}}{\partial h_u^2}\right|_{h_u=0} - \left.\frac{1}{v_u}\frac{\partial V_{\rm th}^{1l}}{\partial H_u}\right|_{H_u=v_u} \end{pmatrix}, \tag{A.53}$$

where $H_u = v_u + h_u$, $H_d = v_d + h_d$, respectively. Since these are the values at the SUSY scale, the Higgs VEVs also have to be rescaled according to the anomalous dimensions

$$\gamma_{H_d} = \frac{1}{64\pi^2}\left[\left(9g_2^2 + 3g_1^2 - 12y_b^2\right)\theta_Z - 6g_2^2\theta_{\widetilde{W}}\theta_{\widetilde{H}} - \frac{6}{5}g_1^2\theta_{\widetilde{B}}\theta_{\widetilde{H}}\right], \tag{A.54}$$

$$\gamma_{H_u} = \frac{1}{64\pi^2}\left[\left(9g_2^2 + 3g_1^2 - 12y_t^2\theta_t\right)\theta_Z - 6g_2^2\theta_{\widetilde{W}}\theta_{\widetilde{H}} - \frac{6}{5}g_1^2\theta_{\widetilde{B}}\theta_{\widetilde{H}}\right], \tag{A.55}$$

where θ_X is the step function that is unity above m_X and is zero below m_X. We define anomalous dimension factors as

$$\xi_d = {\rm Exp}\left[\int_{\ln m_{\rm SUSY}/m_t}^0 \gamma_{H_d}(Q)d(\ln Q/m_t)\right], \tag{A.56}$$

$$\xi_u = {\rm Exp}\left[\int_{\ln m_{\rm SUSY}/m_t}^0 \gamma_{H_u}(Q)d(\ln Q/m_t)\right], \tag{A.57}$$

and the vacuum expectation values at the SUSY scale can be obtained as

$$v_i(m_{\rm SUSY}) = \xi_i v_i(m_t), \quad i = d, u. \tag{A.58}$$

Furthermore, we have to rescale the Higgs mass matrix as $\xi_i(\Delta^{\rm th}M_h^2)_{ij}\xi_j$, $(i,j=d,u)$.

The threshold corrections to the effective potential are read as

$$\begin{aligned} V_{\rm th}^{1l} &= V_{\rm HE}^{1l} - V_{\rm LE}^{1l} \\ &= \frac{3}{32\pi^2}\left[\sum_{\tilde{q}=\tilde{t}_{1,2},\tilde{b}_{1,2}} m_{\tilde{q}}^4\left(\log\frac{m_{\tilde{q}}^2}{Q^2}-\frac{3}{2}\right)\right] - \frac{3}{32\pi^2}m_{\tilde{t}_R}^4\left(\log\frac{m_{\tilde{t}_R}^2}{Q^2}-\frac{3}{2}\right), \end{aligned} \tag{A.59}$$

where $m_{\tilde{t}_{1,2},\tilde{b}_{1,2}}$ are eigenvalues of the mass matrices defined in Eq. (A.8) and $m_{\tilde{t}_R}^2 = (M_{\tilde{t}}^2)_{22}$

The threshold corrections from the top squarks at $M_{st} = {\rm Max}(m_Q^2+m_t^2,\ m_u^2+m_t^2)$ are given by

$$(\mathcal{M}_{\rm stop}^{\rm th})_{11}^2 = \frac{3}{8\pi^2v^2}\left[\frac{m_t^4}{\sin^2\beta}\left(\frac{\mu(-A_t+\mu\cot\beta)}{m_{\tilde{t}_1}^2-m_{\tilde{t}_2}^2}\right)^2 g(m_{\tilde{t}_1}^2,m_{\tilde{t}_2}^2) + m_Z^2 m_t\mu\cot\beta\ f_2^{\tilde{t}}\right], \tag{A.60}$$

$$\begin{aligned} (\mathcal{M}_{\rm stop}^{\rm th})_{22}^2 &= \frac{3}{8\pi^2v^2}\left[\frac{m_t^4}{\sin^2\beta}\left\{\log\left(\frac{m_{\tilde{t}_1}^2 m_{\tilde{t}_2}^2}{(m_Q^2+m_t^2)(m_u^2+m_t^2)}\right) + \frac{2A_t(A_t-\mu\cot\beta)}{m_{\tilde{t}_1}^2-m_{\tilde{t}_2}^2}\log\frac{m_{\tilde{t}_1}^2}{m_{\tilde{t}_2}^2}\right.\right. \\ &\left.\left. + \left(\frac{A_t(A_t-\mu\cot\beta)}{m_{\tilde{t}_1}^2-m_{\tilde{t}_2}^2}\right)^2 g(m_{\tilde{t}_1}^2,m_{\tilde{t}_2}^2)\right\} + m_Z^2[-2m_t^2 f_1^{\tilde{t}} + m_t A_t f_2^{\tilde{t}}]\right], \end{aligned} \tag{A.61}$$

$$\begin{aligned} (\mathcal{M}_{\rm stop}^{\rm th})_{12}^2 &= \frac{3}{8\pi^2v^2}\left[\frac{m_t^4}{\sin^2\beta}\frac{\mu(-A_t+\mu\cot\beta)}{m_{\tilde{t}_1}^2-m_{\tilde{t}_2}^2}\left\{\log\frac{m_{\tilde{t}_1}^2}{m_{\tilde{t}_2}^2}\right.\right. \\ &\left.\left. + \frac{A_t(A_t-\mu\cot\beta)}{m_{\tilde{t}_1}^2-m_{\tilde{t}_2}^2}g(m_{\tilde{t}_1}^2,m_{\tilde{t}_2}^2)\right\} + m_Z^2\left\{m_t^2\cot\beta f_1^{\tilde{t}} - m_t\frac{A_t\cot\beta+\mu}{2}f_2^{\tilde{t}}\right\}\right], \end{aligned} \tag{A.62}$$

where

$$g(m_1^2,m_2^2) = 2 - \frac{m_1^2+m_2^2}{m_1^2-m_2^2}\log\frac{m_1^2}{m_2^2}, \tag{A.63}$$

and

$$\begin{aligned} f_1^{\tilde{t}} &= \frac{m_Q^2-m_u^2}{m_{\tilde{t}_1}^2-m_{\tilde{t}_2}^2}\left(\frac{1}{2}-\frac{4}{3}\sin^2\theta_W\right)\frac{1}{2}\log\frac{m_{\tilde{t}_1}^2}{m_{\tilde{t}_2}^2} + \left(\frac{1}{2}-\frac{2}{3}\sin^2\theta_W\right)\log\frac{m_{\tilde{t}_1}m_{\tilde{t}_2}}{m_Q^2+m_t^2} \\ &+ \frac{2}{3}\sin^2\theta_W\log\frac{m_{\tilde{t}_1}m_{\tilde{t}_2}}{m_u^2+m_t^2}, \end{aligned} \tag{A.64}$$

$$f_2^{\tilde{t}} = m_t\frac{A_t-\mu\cot\beta}{m_{\tilde{t}_1}^2-m_{\tilde{t}_2}^2}\left[-\frac{1}{2}\log\frac{m_{\tilde{t}_1}^2}{m_{\tilde{t}_2}^2} + \left(\frac{4}{3}\sin^2\theta_W-\frac{1}{2}\right)\frac{m_Q^2-m_u^2}{m_{\tilde{t}_1}^2-m_{\tilde{t}_2}^2}g(m_{\tilde{t}_1}^2,m_{\tilde{t}_2}^2)\right]. \tag{A.65}$$

Similarly, the threshold corrections from the bottom squarks at $M_{sb} = \mathrm{Max}(m_Q^2+m_b^2,\ m_d^2+m_b^2)$ are

$$(\mathcal{M}^{\rm th}_{\rm sbottom})^2_{11} = \frac{3}{8\pi^2 v^2}\left[\frac{m_b^4}{\cos^2\beta}\left\{\log\left(\frac{m^2_{\tilde{b}_1}m^2_{\tilde{b}_2}}{(m_Q^2+m_b^2)(m_d^2+m_b^2)}\right)\right. \tag{A.66}$$
$$\left. + \frac{2A_b(A_b-\mu\tan\beta)}{m^2_{\tilde{b}_1}-m^2_{\tilde{b}_2}}\log\frac{m^2_{\tilde{b}_1}}{m^2_{\tilde{b}_2}} + \left(\frac{A_b(A_b-\mu\tan\beta)}{m^2_{\tilde{b}_1}-m^2_{\tilde{b}_2}}\right)^2 g(m^2_{\tilde{b}_1}, m^2_{\tilde{b}_2})\right\}$$
$$+ m_Z^2[2m_b^2 f_1^{\tilde{b}} - m_b A_b f_2^{\tilde{b}}]\Big],$$
$$(\mathcal{M}^{\rm th}_{\rm sbottom})^2_{22} = \frac{3}{8\pi^2 v^2}\left[\frac{m_b^4}{\cos^2\beta}\left(\frac{\mu(-A_b+\mu\tan\beta)}{m^2_{\tilde{b}_1}-m^2_{\tilde{b}_2}}\right)^2 g(m^2_{\tilde{b}_1}, m^2_{\tilde{b}_2}) - m_Z^2 m_b\mu\tan\beta\ f_2^{\tilde{b}}\right], \tag{A.67}$$
$$(\mathcal{M}^{\rm th}_{\rm sbottom})^2_{12} = \frac{3}{8\pi^2 v^2}\left[\frac{m_b^4}{\cos^2\beta}\frac{\mu(-A_b+\mu\tan\beta)}{m^2_{\tilde{b}_1}-m^2_{\tilde{b}_2}}\left\{\log\frac{m^2_{\tilde{b}_1}}{m^2_{\tilde{b}_2}} + \frac{A_b(A_b-\mu\tan\beta)}{m^2_{\tilde{b}_1}-m^2_{\tilde{b}_2}} g(m^2_{\tilde{b}_1}, m^2_{\tilde{b}_2})\right\}\right.$$
$$\left. - m_Z^2\left\{m_b^2\tan\beta f_1^{\tilde{b}} - m_b\frac{A_b\tan\beta+\mu}{2}f_2^{\tilde{b}}\right\}\right], \tag{A.68}$$

where

$$f_1^{\tilde{b}} = \frac{m_Q^2-m_d^2}{m^2_{\tilde{b}_1}-m^2_{\tilde{b}_2}}\left(-\frac{1}{2}+\frac{2}{3}\sin^2\theta_W\right)\frac{1}{2}\log\frac{m^2_{\tilde{b}_1}}{m^2_{\tilde{b}_2}} + \left(-\frac{1}{2}+\frac{1}{3}\sin^2\theta_W\right)\log\frac{m_{\tilde{b}_1}m_{\tilde{b}_2}}{m_Q^2+m_b^2} \tag{A.69}$$
$$-\frac{1}{3}\sin^2\theta_W\log\frac{m_{\tilde{b}_1}m_{\tilde{b}_2}}{m_d^2+m_b^2},$$
$$f_2^{\tilde{b}} = m_b\frac{A_b-\mu\tan\beta}{m^2_{\tilde{b}_1}-m^2_{\tilde{b}_2}}\left[\frac{1}{2}\log\frac{m^2_{\tilde{b}_1}}{m^2_{\tilde{b}_2}} + \left(\frac{1}{2}-\frac{2}{3}\sin^2\theta_W\right)\frac{m_Q^2-m_d^2}{m^2_{\tilde{b}_1}-m^2_{\tilde{b}_2}}g(m^2_{\tilde{b}_1}, m^2_{\tilde{b}_2})\right]. \tag{A.70}$$

Note that the $\mathcal{O}(g^4_{1,2})$ contributions are dropped.

A.3.2 Renormalization group

We have to evaluate the quartic coupling constants at $Q = m_t$. The beta functions for the gauge coupling constants have been already shown in Eq.(A.39). Those for the Yukawa coupling constants in the 2HDM are [98],

$$16\pi^2\beta_{y_t^2} = y_t^2\left(\frac{9}{2}y_t^2+\frac{1}{2}y_b^2-\frac{17}{12}g_1^2-\frac{9}{4}g_2^2-8g_3^2\right), \tag{A.71}$$
$$16\pi^2\beta_{y_b^2} = y_b^2\left(\frac{1}{2}y_t^2+\frac{9}{2}y_b^2+y_\tau^2-\frac{5}{12}g_1^2-\frac{9}{4}g_2^2-8g_3^2\right), \tag{A.72}$$
$$16\pi^2\beta_{y_\tau^2} = y_\tau^2\left(3y_b^2+\frac{5}{2}y_\tau^2-\frac{15}{4}g_1^2-\frac{9}{4}g_2^2\right). \tag{A.73}$$

The beta functions for the quartic coupling constants are

$$
\begin{aligned}
8\pi^2\beta_{\lambda_1} &= 6\lambda_1^2+\lambda_3^2+(\lambda_3+\lambda_4)^2+\frac{3}{8}\left\{2g_2^4+(g_1^2+g_2^2)^2\right\} \\
&+3\left[-2y_d^4+\left(y_d^2-\frac{1}{6}g_1^2\right)^2\theta_{\tilde{D}}+\left(\frac{1}{3}g_1^2\right)^2\theta_{\tilde{U}}\left\{y_d^4-\frac{1}{2}y_d^2\left(\frac{1}{3}g_1^2+g_2^2\right)\right.\right. \\
&\left.\left.+\frac{1}{8}\left(g_2^4+\frac{1}{9}g_1^4\right)\right\}\theta_{\tilde{Q}}\right]-\frac{5}{2}g_2^4\theta_{\tilde{H}}\theta_{\tilde{W}}-g_1^2g_2^2\theta_{\tilde{H}}\theta_{\tilde{B}}\theta_{\tilde{W}}-\frac{1}{2}g_1^4\theta_{\tilde{H}}\theta_{\tilde{B}} \\
&-\frac{\lambda_1}{2}[9g_2^2+3g_1^2-12y_b^2-4y_\tau^2-6g_2^2\theta_{\tilde{W}}\theta_{\tilde{H}}-2g_1^2\theta_{\tilde{B}}\theta_{\tilde{H}}],
\end{aligned}
\tag{A.74}
$$

$$
\begin{aligned}
8\pi^2\beta_{\lambda_2} &= 6\lambda_2^2+\lambda_3^2+(\lambda_3+\lambda_4)^2+\frac{3}{8}\{2g_2^4+(g_1^2+g_2^2)^2\} \\
&+3\left[-2y_u^4+\left(\frac{1}{6}g_1^2\right)^2\theta_{\tilde{D}}+\left(y_u^2-\frac{1}{3}g_1^2\right)^2\theta_{\tilde{U}}+\left\{y_u^4+\frac{1}{2}y_u^2\left(\frac{1}{3}g_1^2-g_2^2\right)\right.\right. \\
&\left.\left.+\frac{1}{8}\left(g_2^4+\frac{1}{9}g_1^4\right)\right\}\theta_{\tilde{Q}}\right]-\frac{5}{2}g_2^4\theta_{\tilde{H}}\theta_{\tilde{W}}-g_1^2g_2^2\theta_{\tilde{H}}\theta_{\tilde{W}}\theta_{\tilde{B}}-\frac{1}{2}g_1^4\theta_{\tilde{H}}\theta_{\tilde{B}} \\
&-\frac{\lambda_2}{2}[9g_2^2+3g_1^2-12y_t^2-6g_2^2\theta_{\tilde{W}}\theta_{\tilde{H}}-2g_1^2\theta_{\tilde{B}}\theta_{\tilde{H}}],
\end{aligned}
\tag{A.75}
$$

$$
\begin{aligned}
8\pi^2\beta_{\lambda_3} &= (\lambda_1+\lambda_2)(3\lambda_3+\lambda_4)+2\lambda_3^2+\lambda_4^2+\frac{3}{8}\{2g_2^4+(g_2^2-g_1^2)^2\} \\
&+3\left[-2y_u^2y_d^2+\frac{1}{6}g_1^2(y_d^2-\frac{1}{6}g_1^2)\theta_{\tilde{D}}+\frac{1}{3}g_1^2(y_u^2-\frac{1}{3}g_1^2)\theta_{\tilde{U}}+y_u^2y_d^2\theta_{\tilde{U}}\theta_{\tilde{D}}\right. \\
&\left.+\left\{y_u^2y_d^2-\frac{1}{4}y_u^2\left(\frac{1}{3}g_1^2+g_2^2\right)+\frac{1}{4}y_d^2\left(\frac{1}{3}g_1^2-g_2^2\right)+\frac{1}{8}\left(g_2^4-\frac{1}{3}g_1^4\right)\right\}\theta_{\tilde{Q}}\right] \\
&-\frac{5}{2}g_2^4\theta_{\tilde{W}}\theta_{\tilde{H}}+g_1^2g_2^2\theta_{\tilde{W}}\theta_{\tilde{B}}\theta_{\tilde{H}}-\frac{1}{2}g_1^4\theta_{\tilde{B}}\theta_{\tilde{H}} \\
&-\frac{\lambda_3}{2}[9g_2^2+3g_1^2-6y_t^2-6y_b^2-2y_\tau^2-6g_2^2\theta_{\tilde{W}}\theta_{\tilde{H}}-2g_1^2\theta_{\tilde{B}}\theta_{\tilde{H}}],
\end{aligned}
\tag{A.76}
$$

$$
\begin{aligned}
8\pi^2\beta_{\lambda_4} &= \lambda_4(\lambda_1+\lambda_2+4\lambda_3+2\lambda_4)+\frac{3}{2}g_2^2g_1^2 \\
&+3\left[2y_u^2y_d^2-y_u^2y_d^2\theta_{\tilde{U}}\theta_{\tilde{D}}-(y_u^2-\frac{1}{2}g_2^2)(y_d^2-\frac{1}{2}g_2^2)\theta_{\tilde{Q}}\right] \\
&+2g_2^4\theta_{\tilde{W}}\theta_{\tilde{H}}-2g_1^2g_2^2\theta_{\tilde{W}}\theta_{\tilde{B}}\theta_{\tilde{H}}-\frac{\lambda_4}{2}[9g_2^2+3g_1^2-6y_t^2-6y_b^2-2y_\tau^2-6g_2^2\theta_{\tilde{W}}\theta_{\tilde{H}}-2g_1^2\theta_{\tilde{B}}\theta_{\tilde{H}}].
\end{aligned}
\tag{A.77}
$$

In these expressions, we assume the SUSY relations for the quartic coupling constants involving the sfermions even below the scale where the sfermions decouple. Another notification is that we drop Higgs quartic couplings for $(H_d\epsilon H_u)^2+\text{h.c.}$, $(H_d^\dagger H_d)(H_d\epsilon H_u+\text{h.c.})$ and $(H_u^\dagger H_u)(H_d\epsilon H_u+\text{h.c.})$ which are absent at tree-level but will be induced by the trilinear couplings at loop-level.

Appendix B

Renormalization group equations

The 1-loop renormalization group equations (RGEs) are listed in this Appendix. These are used in the analyses in Chapter 2 and 3. The 1-loop RGEs for the dimensionless couplings and the soft parameters in the MSSM are derived in Refs. [24, 25], and those in the most general model with softly broken supersymmetry, which include the case of the MSSM with the flavor mixings, are derived in Ref. [26]. The 2-loop RGEs are obtained in Ref. [27].

The RGEs for Yukawa coupling constants squared for the third-generation fermions in the SM are given by,

$$\frac{d}{dt}y_t^2 = \frac{1}{8\pi^2}y_t^2\left[\frac{9}{2}y_t^2+\frac{3}{2}y_b^2+y_\tau^2-\frac{17}{20}g_1^2-\frac{9}{4}g_2^2-8g_3^2\right], \tag{B.1}$$

$$\frac{d}{dt}y_b^2 = \frac{1}{8\pi^2}y_b^2\left[\frac{3}{2}y_t^2+\frac{9}{2}y_b^2+y_\tau^2-\frac{1}{4}g_1^2-\frac{9}{4}g_2^2-8g_3^2\right], \tag{B.2}$$

$$\frac{d}{dt}y_\tau^2 = \frac{1}{8\pi^2}y_\tau^2\left[3y_t^2+3y_b^2+\frac{5}{2}y_\tau^2-\frac{9}{4}g_1^2-\frac{9}{4}g_2^2\right]. \tag{B.3}$$

Here, $t \equiv \ln Q/\Lambda$, where Q is the renormalization scale and Λ is a cutoff scale.

The RGEs in the MSSM are exhibited in what follows. For the gauge coupling constants,

$$\frac{d}{dt}g_a = \frac{1}{16\pi^2}b_a g_a^3, \tag{B.4}$$

where $b_a = (-3, 1, 33/5)$.

The 1-loop RGEs for the Yukawa matrices are

$$\frac{d}{dt}y_u = \frac{y_u}{16\pi^2}\left[\mathrm{Tr}(3y_u y_u^\dagger)+3y_u^\dagger y_u+y_d^\dagger y_d-\frac{13}{15}g_1^2-3g_2^2-\frac{16}{3}g_3^2\right], \tag{B.5}$$

$$\frac{d}{dt}y_d = \frac{y_d}{16\pi^2}\left[\mathrm{Tr}(3y_d^\dagger y_d+y_e^\dagger y_e)+3y_d^\dagger y_d+y_u^\dagger y_u-\frac{7}{15}g_1^2-3g_2^2-\frac{16}{3}g_3^2\right], \tag{B.6}$$

$$\frac{d}{dt}y_e = \frac{y_e}{16\pi^2}\left[\mathrm{Tr}(3y_d^\dagger y_d+y_e^\dagger y_e)+3y_e^\dagger y_e-\frac{9}{5}g_1^2-3g_2^2\right]. \tag{B.7}$$

The RGEs for soft parameters are as follows. The gaugino masses obey the RGEs,

$$\frac{dM_a}{dt} = \frac{2g_a^2}{16\pi^2} b_a M_a. \tag{B.8}$$

The RGEs for the A-terms are given by

$$\begin{aligned}
\frac{d}{dt}a_u =& \frac{1}{16\pi^2}\Big[a_u\Big\{\mathrm{Tr}(3y_u y_u^\dagger) + 5y_u^\dagger y_u + y_d^\dagger y_d - \frac{16}{3}g_3^2 - 3g_2^2 - \frac{13}{15}g_1^2\Big\} \qquad \text{(B.9)}\\
&+ y_u\Big\{\mathrm{Tr}(6a_u y_u^\dagger) + 4y_u^\dagger a_u + 2y_d^\dagger a_d + 2\left(\frac{16}{3}g_3^2 M_3 + 3g_2^2 M_2 + \frac{13}{15}g_1^2 M_1\right)\Big\}\Big],\\
\frac{d}{dt}a_d =& \frac{1}{16\pi^2}\Big[a_d\Big\{\mathrm{Tr}(3y_d y_d^\dagger + y_e y_e^\dagger) + 5y_d^\dagger y_d + y_u^\dagger y_u - \frac{16}{3}g_3^2 - 3g_2^2 - \frac{7}{15}g_1^2\Big\} \qquad \text{(B.10)}\\
&+ a_d\Big\{\mathrm{Tr}(6a_d y_d^\dagger + 2a_e y_e^\dagger) + 4y_d^\dagger a_d + 2y_u^\dagger a_u + 2\left(\frac{16}{3}g_3^2 M_3 + 3g_2^2 M_2 + \frac{7}{15}g_1^2 M_1\right)\Big\}\Big],\\
\frac{d}{dt}a_e =& \frac{1}{16\pi^2}\Big[a_e\Big\{\mathrm{Tr}(3y_d y_d^\dagger + y_e y_e^\dagger) + 5y_e^\dagger y_e - 3g_2^2 - \frac{9}{5}g_1^2\Big\} \qquad \text{(B.11)}\\
&+ y_e\Big\{\mathrm{Tr}(6a_d y_d^\dagger + 2a_e y_e^\dagger) + 4y_e^\dagger a_e + 2\left(3g_2^2 M_2 + \frac{9}{5}g_1^2 M_1\right)\Big\}\Big].
\end{aligned}$$

These can be simplified by neglecting the Yukawa couplings for the first- and second-generations and factorizing the Yukawa coupling, e.g. $a_i = y_i A_i$ $(i = t, b, \tau)$,

$$\begin{aligned}
\frac{d}{dt}A_t &= \frac{1}{8\pi^2}\left[6y_t^2 A_t + y_b^2 A_b - \frac{13}{15}g_1^2 M_1 - 3g_2^2 M_2 - \frac{16}{3}g_3^2 M_3\right], \qquad \text{(B.12)}\\
\frac{d}{dt}A_b &= \frac{1}{8\pi^2}\Big[y_t^2 A_t + 6y_b^2 A_b + y_\tau A_\tau \qquad \text{(B.13)}\\
&\quad -\frac{7}{15}g_1^2 M_1 - 3g_2^2 M_2 - \frac{16}{3}g_3^2 M_3\Big],\\
\frac{d}{dt}A_\tau &= \frac{1}{8\pi^2}\left[3y_b^2 A_b + 4y_\tau A_\tau - \frac{9}{5}g_1^2 M_1 - 3g_2^2 M_2\right]. \qquad \text{(B.14)}
\end{aligned}$$

The RGEs for the soft scalar masses are

$$\begin{aligned}
\frac{d}{dt}m_Q^2 =& \frac{1}{16\pi^2}\Big[(m_Q^2 + 2m_{H_u}^2)y_u^\dagger y_u + (m_Q^2 + 2m_{H_d}^2)y_d^\dagger y_d \qquad \text{(B.15)}\\
&+ m_Q^2(y_u^\dagger y_d + y_d^\dagger y_d) + 2y_u^\dagger m_u^2 y_u + 2y_d^\dagger m_d^2 y_d + 2a_u^\dagger a_u + 2a_d^\dagger a_d\\
&- \left(\frac{32}{3}g_3^2|M_3|^2 + 6g_2^2|M_2|^2 + \frac{2}{15}g_1^2|M_1|^2 - \frac{1}{5}g_1^2 S\right)\hat{\mathbf{1}}\Big],\\
\frac{d}{dt}m_u^2 =& \frac{1}{16\pi^2}\Big[(2m_u^2 + 4m_{H_u}^2)y_u y_u^\dagger + 2m_u^2 y_u y_u^\dagger + 4y_u m_Q^2 y_u^\dagger + 4a_u a_u^\dagger \qquad \text{(B.16)}\\
&- \left(\frac{32}{3}g_3^2|M_3|^2 + \frac{32}{15}g_1^2|M_1|^2 + \frac{4}{5}g_1^2 S\right)\hat{\mathbf{1}}\Big],\\
\frac{d}{dt}m_d^2 =& \frac{1}{16\pi^2}\Big[(2m_d^2 + 4m_{H_d}^2)y_d y_d^\dagger + 2y_d y_d^\dagger m_d^2 + 4y_d m_Q^2 y_d^\dagger + 4a_d a_d^\dagger \qquad \text{(B.17)}
\end{aligned}$$

$$
\begin{aligned}
&- \left(\frac{32}{3}g_3^2|M_3|^2 + \frac{8}{15}g_1^2|M_1|^2 - \frac{2}{5}g_1^2 S\right)\hat{\mathbf{1}}\Big], \\
\frac{d}{dt}m_L^2 =& \frac{1}{16\pi^2}\Big[(m_L^2 + 2m_{H_d}^2)y_e^\dagger y_e + y_e^\dagger y_e m_L^2 + 2y_e^\dagger m_e^2 y_e + 2a_e^\dagger a_e \\
&- \left(6g_2^2|M_2|^2 + \frac{6}{5}g_1^2|M_1|^2 + \frac{3}{5}g_1^2 S\right)\hat{\mathbf{1}}\Big], \\
\frac{d}{dt}m_e^2 =& \frac{1}{16\pi^2}\Big[(2m_e^2 + 4m_{H_d}^2)y_e y_e^\dagger + 2y_e y_e^\dagger m_e^2 + 4y_e m_L^2 y_e^\dagger + 4a_e a_e^\dagger \\
&- \left(\frac{24}{5}g_1^2|M_1|^2 + \frac{6}{5}g_1^2 S\right)\hat{\mathbf{1}}\Big], \\
\frac{d}{dt}m_{H_u}^2 =& \frac{1}{16\pi^2}\Big[6\mathrm{Tr}[y_u(m_{H_u}^2 + m_Q^2)y_u^\dagger + y_u^\dagger m_u^2 y_u + a_u a_u^\dagger] \\
&- \left(6g_2^2|M_2|^2 + \frac{6}{5}g_1^2|M_1|^2 - \frac{3}{5}g_1^2 S\right)\Big], \\
\frac{d}{dt}m_{H_d}^2 =& \frac{1}{16\pi^2}\Big[\mathrm{Tr}[6y_d(m_{H_d}^2 + m_Q^2)y_d^\dagger + 6y_d^\dagger m_d^2 y_d + 2y_e(m_{H_d}^2 + m_L^2)y_e^\dagger \\
&+ 2y_e^\dagger m_e^2 y_e + 6a_d a_d^\dagger + 2a_e a_e^\dagger] - \left(6g_2^2|M_2|^2 + \frac{6}{5}g_1^2|M_1|^2 + \frac{3}{5}g_1^2 S\right)\Big],
\end{aligned}
\tag{B.18}
\tag{B.19}
\tag{B.20}
\tag{B.21}
$$

where

$$
S \equiv m_{H_u}^2 - m_{H_d}^2 + \mathrm{Tr}(m_Q^2 - m_L^2 - 2m_u^2 + m_d^2 + m_e^2). \tag{B.22}
$$

Finally, RGEs for the μ-parameter and b-parameter are

$$
\frac{d\mu}{dt} = \frac{\mu}{16\pi^2}\Big[\mathrm{Tr}(3y_u y_u^\dagger + 3y_d y_d^\dagger + y_e y_e^\dagger) - 3g_2^2 - \frac{3}{5}g_1^2\Big], \tag{B.23}
$$

and

$$
\begin{aligned}
\frac{d}{dt}b =& \frac{1}{16\pi^2}\Big[b\Big\{\mathrm{Tr}(3y_u y_u^\dagger + 3y_d y_d^\dagger + y_e y_e^\dagger) - 3g_2^2 - \frac{3}{5}g_1^2\Big\} \\
&+ \mu\Big\{\mathrm{Tr}(6a_u y_u^\dagger + 6a_d y_d^\dagger + 2a_e y_e^\dagger) + 2\left(3g_2^2 M_2 + \frac{3}{5}g_1^2 M_1\right)\Big\}\Big].
\end{aligned}
\tag{B.24}
$$

Appendix C

Muon anomalous magnetic moment with non-universal gaugino masses

One possible evidence for new physics is the anomalous magnetic moment of the muon, which is measured precisely. The observed value is [99]

$$a_\mu^{\rm obs} = 116592089(63) \times 10^{-11}, \tag{C.1}$$

and is deviated from the SM prediction [100, 101]

$$a_\mu^{\rm SM} = 116591834(49) \times 10^{-11}, \tag{C.2}$$

so that there is a discrepancy of 3.2σ. This discrepancy could be explained by sparticle contributions, although it is also possible that $a_\mu^{\rm obs}$ and/or $a_\mu^{\rm SM}$ is changed in future experiments or more precise evaluation of the SM prediction such as the QCD effects.

Let us discuss the sparticle contributions $\Delta a_\mu^{\rm SUSY}$ to the muon magnetic moment in the NUGM scenario. The dominant contributions are loop corrections mediated by the neutralino/smuon or chargino/muon sneutrino. Following Ref. [102], the sparticle corrections can be written as a sum of the following contributions

$$\Delta a_\mu^{\rm N1} = g_1^2 m_\mu^2 M_1 \mu \tan\beta \left[J_5(M_1^2, M_1^2, m_{\tilde{\mu}_L}^2, m_{\tilde{\mu}_R}^2, m_{\tilde{\mu}_R}^2) + J_5(M_1^2, M_1^2, m_{\tilde{\mu}_L}^2, m_{\tilde{\mu}_L}^2, m_{\tilde{\mu}_R}^2) \right], \tag{C.3}$$

$$\Delta a_\mu^{\rm N2} = -g_1^2 m_\mu^2 M_1 \mu \tan\beta \left[J_5(M_1^2, M_1^2, \mu^2, m_{\tilde{\mu}_R}^2, m_{\tilde{\mu}_R}^2) + J_5(M_1^2, \mu^2, \mu^2, m_{\tilde{\mu}_R}^2, m_{\tilde{\mu}_R}^2) \right], \tag{C.4}$$

$$\Delta a_\mu^{\rm N3} = \frac{1}{2} g_1^2 m_\mu^2 M_1 \mu \tan\beta \left[J_5(M_1^2, M_1^2, \mu^2, m_{\tilde{\mu}_L}^2, m_{\tilde{\mu}_L}^2) + J_5(M_1^2, \mu^2, \mu^2, m_{\tilde{\mu}_L}^2, m_{\tilde{\mu}_L}^2) \right], \tag{C.5}$$

$$\Delta a_\mu^{\rm N4} = -\frac{1}{2} g_2^2 m_\mu^2 M_2 \mu \tan\beta \left[J_5(M_2^2, M_2^2, \mu^2, m_{\tilde{\mu}_L}^2, m_{\tilde{\mu}_L}^2) + J_5(M_2^2, \mu^2, \mu^2, m_{\tilde{\mu}_L}^2, m_{\tilde{\mu}_L}^2) \right], \tag{C.6}$$

$$\begin{aligned} \Delta a_\mu^{\rm C} = {} & g_2^2 m_\mu^2 M_2 \mu \tan\beta \left[2I_4(M_2^2, M_2^2, \mu^2, m_{\tilde{\nu}}^2) - J_5(M_2^2, M_2^2, \mu^2, m_{\tilde{\nu}}^2, m_{\tilde{\nu}}^2) \right. \\ & \left. + 2I_4(M_2^2, \mu^2, \mu^2, m_{\tilde{\nu}}^2) - J_5(M_2^2, \mu^2, \mu^2, m_{\tilde{\nu}}^2, m_{\tilde{\nu}}^2) \right], \end{aligned} \tag{C.7}$$

where

$$I_N(m_1^2, m_2^2, \ldots, m_N^2) = \int \frac{d^4k}{(2\pi)^4 i} \frac{1}{(k^2 - m_1^2) \cdots (k^2 - m_N^2)}, \tag{C.8}$$

$$J_N(m_1^2, m_2^2, \ldots, m_N^2) = \int \frac{d^4k}{(2\pi)^4 i} \frac{k^2}{(k^2 - m_1^2) \cdots (k^2 - m_N^2)}. \tag{C.9}$$

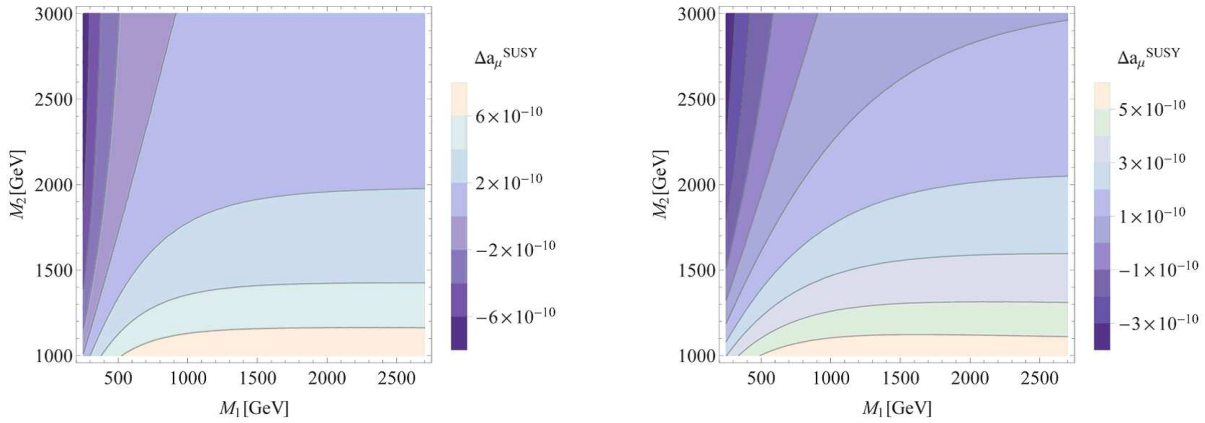

Figure C.1: Values of $\Delta a_\mu^{\rm SUSY}$ with $\tan\beta = 50$ and $\mu = 250$ (1000) GeV in the left (right) panel. The slepton masses are assumed to be $m_{\tilde{\mu}_L} = M_2 + 100$ GeV, $m_{\tilde{\mu}_R} = M_1 + 150$ GeV, $m_{\tilde{\nu}_L} = M_2 + 200$ GeV, respectively.

We can evaluate I_4 and J_5 by using the following relations iteratively

$$I_N(m_1,\ldots,m_N) = \frac{1}{m_1^2 - m_N^2}\left[I_{N-1}(m_1^2,\ldots,m_{N-1}^2) - I_{N-1}(m_2^2,\ldots,m_N^2)\right], \quad \text{(C.10)}$$

$$J_N(m_1,\ldots,m_N) = I_{N-1}(m_1^2,\ldots,m_{N-1}^2) + m_N^2 I_N(m_1^2,\ldots,m_N^2), \quad \text{(C.11)}$$

and

$$I_2(m_1,m_2) = -\frac{1}{16\pi^2}\left[\frac{m_1^2}{m_1^2 m_2^2}\log\left(\frac{m_1^2}{\Lambda^2}\right) + \frac{m_2^2}{m_2^2 m_1^2}\log\left(\frac{m_2^2}{\Lambda^2}\right)\right], \quad \text{(C.12)}$$

where Λ is a cutoff that is appeared only in I_2 due to the logarithmic divergence of corresponding diagrams. The dependence on the cutoff is canceled for $N \geq 3$, for instance,

$$I_3(m_1,m_2,m_3) = \frac{1}{16\pi^2}\frac{m_1^2 m_2^2 \log\frac{m_1^2}{m_2^2} + m_2^2 m_3^2 \log\frac{m_2^2}{m_3^2} + m_1^2 m_3^2 \log\frac{m_3^2}{m_1^2}}{(m_1^2 - m_2^2)(m_2^2 - m_3^2)(m_3^2 - m_1^2)}. \quad \text{(C.13)}$$

We can see sparticle contributions are proportional to $\tan\beta$, and larger values of $\tan\beta$ is favored to enhance the sparticle contributions.

A critical disadvantage to obtain the large discrepancy is that the wino mass M_2 is generically heavy in the NUGM scenario. Typically, its mass has to be heavier than the gluino mass which should be heavier than about 1.5 TeV. Furthermore, the heavier wino induces the heavy left-handed sleptons, including the smuon and sneutrino. Therefore, it is challenging to explain the g-2 anomaly within 1-2 σ-level which requires $\Delta a_\mu^{\rm SUSY} \simeq 2.5 \times 10^{-9}$, even though the higgsino and the bino can be $\mathcal{O}(100$ GeV).

Figure C.1 shows the sparticle contributions to the muon magnetic moment. We can see that the contribution is always smaller than 10^{-9}, and the anomaly can not be explained even if $\tan\beta = 50$.

Appendix D

Soft parameters of moduli and anomaly mediations

D.1 General formulae

In this appendix, the formulae for the soft parameters in the mixture of the moduli and anomaly mediations are shown. As derived in Ref. [34], the gravity mediated contributions can be written by derivatives of the Kähler potential, superpotential and gauge kinetic function. The soft parameters induced by the modulus and anomaly mediations in the KKLT scenario are shown in Ref. [13].

Let us start with the conformal supergravity action for matter fields given by

$$\mathcal{L}_{\rm matter} = \int d^4\theta |C|^2 \overline{Q}^{\bar{I}} e^{-K_0/3} Z_{\bar{I}J} Q^J + \left(\int d^2\theta \Big[C^3 W + f_a \, \mathcal{W}_a^2 \Big] + \text{h.c.} \right) \tag{D.1}$$

with

$$K_0 = -\sum_m \ln(\Phi_m + \overline{\Phi}_m), \tag{D.2}$$

$$Z_{\bar{I}J} = \alpha_I \delta_{\bar{I}J} \prod_m (\Phi_m + \overline{\Phi}_m)^{-n_I^m}, \tag{D.3}$$

$$W = \lambda(\Phi_m)^{IJK} Q_I Q_J Q_K, \tag{D.4}$$

$$f_a = \sum_m l_a^m \Phi_m, \tag{D.5}$$

where $\Phi_m, C, Q_I, \mathcal{W}_a$ are moduli fields, compensator, matter fields and field-strength chiral superfields in a model, respectively. The indices m, I, a run over all the moduli, matters and gauge groups, respectively. Here, the matter fields indicate the chiral superfields, e.g., the quarks, leptons and Higgses in the MSSM. In order to make the kinetic terms for the gauginos and matter fields canonically normalized, the matter fields Q^I have to be normalized by $Y^{1/2}$, where $Y_{\bar{I}J} = e^{-K_0/3} Z_{\bar{I}J}$. The soft parameters in the canonically normalized basis can be written

as

$$
\begin{aligned}
M_a &= F^A \partial_A \ln(\mathrm{Re} f_a), && \text{(D.6)}\\
m^2_{\bar{I}J} &= -F^A \bar{F}^{\bar{B}} Y^{-1/2} \left[\partial_A \partial_{\bar{B}} Y - \partial_A Y\ Y^{-1}\ \partial_{\bar{B}} Y\right] Y^{-1/2}, && \text{(D.7)}\\
a_{IJK} &= -y^{LJK}\left(Y^{-1/2} F^A \partial_A Y\ Y^{-1/2}\right)^I_L + (I \leftrightarrow J) + (I \leftrightarrow K) + y_{IJK} F^m \partial_m \ln \lambda_{IJK}, && \text{(D.8)}
\end{aligned}
$$

where $y^{IJK} = \lambda^{LMN} {Y^{-1/2}}^I_L {Y^{-1/2}}^J_M {Y^{-1/2}}^K_N$ are physical Yukawa coupling constants. The indices A, B run over the moduli fields Φ_m and the compensator C. After inserting the explicit form of the potentials and operating differentiation, the soft parameters can be written as

$$
\begin{aligned}
M_a &= \sum_m \frac{F^m}{\Phi + \overline{\Phi}_m} + \frac{b_a}{16\pi^2} g_a^2 \frac{F^C}{C}, && \text{(D.9)}\\
a^{IJK} &= y^{IJK} \sum_m \sum_{L=I,J,K} \left(\frac{1}{3} - n^m_L\right) \frac{F^m}{\Phi_m + \overline{\Phi}_m} + \sum_m y_{IJK} F^m \partial_m \ln \lambda_{IJK} \\
&\quad + \left(\frac{1}{2}\left(\gamma + \tilde{\gamma}\right)^I_L y^{LJK} + (I \leftrightarrow J, K)\right) \frac{F^C}{C}, && \text{(D.10)}\\
m^2_{\bar{I}J} &= \sum_m \left(\frac{1}{3} - n^m_I\right) \left|\frac{F^m}{\Phi_m + \overline{\Phi}_m}\right|^2 - \frac{1}{2} \sum_m \partial_{\ln m} (\gamma + \tilde{\gamma}) \left(\frac{F^m}{\Phi_m + \overline{\Phi}_m} \frac{\overline{F^C}}{\overline{C}} + \text{c.c.}\right) \\
&\quad + \frac{1}{4}\left(\dot{\gamma} + \dot{\tilde{\gamma}} + \gamma\tilde{\gamma} - \tilde{\gamma}\gamma\right) \left|\frac{F^C}{C}\right|^2, && \text{(D.11)}
\end{aligned}
$$

where

$$
\tilde{\gamma}^J_I = \left(\prod_m (\Phi_m + \overline{\Phi}_m)^{\frac{n^m_I - n^m_J}{2}}\right) \gamma^J_I, \qquad \text{(D.12)}
$$

and $\partial_{\ln m} \equiv (\Phi_m + \overline{\Phi}_m)\partial/\partial\Phi_m$ are defined. The derivatives $\dot{\tilde{\gamma}} = d\tilde{\gamma}/dt$ have to be applied only to anomalous dimensions γ, but not to the factor in the parentheses that depends on the moduli. Anomalous dimensions γ^J_I are given by

$$
\gamma^J_I = Y^{1/2} \dot{Y}^{-1/2} = \frac{1}{16\pi^2}\left[\frac{1}{2} \sum_{L,M} y^*_{ILM} y^{JLM} - 2 g_a^2 c_a(Q_I) \delta_i{}^j\right], \qquad \text{(D.13)}
$$

at 1-loop level.

If we consider the case that all of the modular weights are flavor independent and the proper Yukawa coupling constants are independent of the moduli, the formulae for the A-terms and soft masses can be simplified to

$$
\begin{aligned}
a^{IJK} &= y^{IJK} \sum_m \sum_{L=I,J,K} c^m_L \frac{F^m}{\Phi_m + \overline{\Phi}_m} + (y^{LJK}\gamma^I_L + (I \leftrightarrow J, K)) \frac{F^C}{C}, && \text{(D.14)}\\
m^2_{\bar{I}J} &= \sum_m c^m_I \left|\frac{F^m}{\Phi_m + \overline{\Phi}_m}\right|^2 \delta^J_I - \sum_m \partial_{\ln m} \gamma^J_I \left(\frac{F^m}{\Phi_m + \overline{\Phi}_m} \frac{\overline{F^C}}{\overline{C}} + \text{c.c.}\right) + \frac{1}{2} \dot{\gamma}^J_I \left|\frac{F^C}{C}\right|^2, && \text{(D.15)}
\end{aligned}
$$

where $c^m_I = 1/3 - n^m_I$.

D.2 Anomalous dimensions and their derivatives in the MSSM

The explicit forms of the anomalous dimensions and their derivatives are shown in Ref. [15], where the Yukawa couplings except for the third-generation fermions are neglected.

The anomalous dimensions for the MSSM fields $Q,\ u,\ d,\ L,\ e,\ H_u,\ H_d$ are given by,

$$16\pi^2\gamma_Q = y_u^\dagger y_u + y_d^\dagger y_d - \left(\frac{1}{30}g_1^2 + \frac{3}{2}g_2^2 + \frac{8}{3}g_3^2\right)\mathbf{1}, \tag{D.16}$$

$$16\pi^2\gamma_u = 2y_u y_u^\dagger - \left(\frac{8}{15}g_1^2 + \frac{8}{3}g_3^2\right)\mathbf{1}, \tag{D.17}$$

$$16\pi^2\gamma_d = 2y_d y_d^\dagger - \left(\frac{2}{15}g_1^2 + \frac{8}{3}g_3^2\right)\mathbf{1}, \tag{D.18}$$

$$16\pi^2\gamma_L = y_e^\dagger y_e - \left(\frac{3}{10}g_1^2 + \frac{3}{2}g_2^2\right)\mathbf{1}, \tag{D.19}$$

$$16\pi^2\gamma_e = 2y_e y_e^\dagger - \frac{6}{5}g_1^2\mathbf{1}, \tag{D.20}$$

$$16\pi^2\gamma_{H_u} = 3\mathrm{Tr}[y_u^\dagger y_u] - \frac{3}{10}g_1^2 - \frac{3}{2}g_2^2, \tag{D.21}$$

$$16\pi^2\gamma_{H_d} = 3\mathrm{Tr}[y_d^\dagger y_d + y_e^\dagger y_e] - \frac{3}{10}g_1^2 - \frac{3}{2}g_2^2, \tag{D.22}$$

where the Yukawa matrices are defined as Eq. (2.3) in Chapter 2.

The derivatives of the anomalous dimensions with respect to the renormalization scale can be written as

$$8\pi^2\dot{\gamma}_Q = y_u^\dagger b_{y_u} + y_d^\dagger b_{y_d} - \left(\frac{1}{30}b_1 g_1^4 + \frac{3}{2}b_2 g_2^4 + \frac{8}{3}b_3 g_3^4\right)\mathbf{1}, \tag{D.23}$$

$$8\pi^2\dot{\gamma}_u = 2b_{y_u} y_u^\dagger - \left(\frac{8}{15}b_1 g_1^4 + \frac{8}{3}b_3 g_3^4\right)\mathbf{1}, \tag{D.24}$$

$$8\pi^2\dot{\gamma}_d = 2b_{y_d} y_d^\dagger - \left(\frac{2}{15}b_1 g_1^4 + \frac{8}{3}b_3 g_3^4\right)\mathbf{1}, \tag{D.25}$$

$$8\pi^2\dot{\gamma}_L = y_e^\dagger b_{y_e} - \left(\frac{3}{10}b_1 g_1^4 + \frac{3}{2}b_2 g_2^4\right)\mathbf{1}, \tag{D.26}$$

$$8\pi^2\dot{\gamma}_e = 2b_{y_e} y_e^\dagger - \frac{6}{5}b_1 g_1^4\mathbf{1}, \tag{D.27}$$

$$8\pi^2\dot{\gamma}_{H_u} = 3\mathrm{Tr}[y_u^\dagger b_{y_u}] - \frac{3}{10}b_1 g_1^4 - \frac{3}{2}b_2 g_2^4, \tag{D.28}$$

$$8\pi^2\dot{\gamma}_{H_d} = 3\mathrm{Tr}[y_d^\dagger b_{y_d} + y_e^\dagger b_{y_e}] - \frac{3}{10}b_1 g_1^4 - \frac{3}{2}b_2 g_2^4, \tag{D.29}$$

where $b_a = (33/5, 1, -3)$ are the beta function coefficients for the gauge coupling constants and $b_{y_f},\ f = u, d, e$, are the beta functions for the Yukawa coupling constants times a loop factor $16\pi^2$ explicitly shown in Eq. (B.5).

The interference terms of the moduli and anomaly mediated contributions, $\theta_i \equiv (T + \overline{T})\partial\gamma_i/\partial T$, can be written as,

$$\begin{aligned}
-16\pi^2\theta_Q &= (3 - n_{H_u} - n_Q - n_u)y_u^\dagger y_u + (3 - n_{H_d} - n_Q - n_d)y_d^\dagger y_d \\
&\quad - \left(\frac{1}{30}g_1^2 + \frac{3}{2}g_2^2 + \frac{8}{3}g_3^2\right)\mathbf{1}, \qquad \text{(D.30)} \\
-16\pi^2\theta_u &= 2(3 - n_{H_u} - n_Q - n_u)y_u y_u^\dagger - \left(\frac{8}{15}g_1^2 + \frac{8}{3}g_3^2\right)\mathbf{1}, \qquad \text{(D.31)} \\
-16\pi^2\theta_d &= 2(3 - n_{H_d} - n_Q - n_d)y_d y_d^\dagger - \left(\frac{2}{15}g_1^2 + \frac{8}{3}g_3^2\right)\mathbf{1}, \qquad \text{(D.32)} \\
-16\pi^2\theta_L &= (3 - n_{H_d} - n_L - n_e)y_e^\dagger y_e - \left(\frac{3}{10}g_1^2 + \frac{3}{2}g_2^2\right)\mathbf{1}, \qquad \text{(D.33)} \\
-16\pi^2\theta_e &= 2(3 - n_{H_d} - n_L - n_e)y_e y_e^\dagger - \frac{6}{5}g_1^2\mathbf{1}, \qquad \text{(D.34)} \\
-16\pi^2\theta_{H_u} &= (3 - n_{H_u} - n_Q - n_u)\mathrm{Tr}[3y_u^\dagger y_u] - \frac{3}{10}g_1^2 - \frac{3}{2}g_2^2, \qquad \text{(D.35)} \\
-16\pi^2\theta_{H_d} &= (3 - n_{H_d} - n_Q - n_d)\mathrm{Tr}[3y_d^\dagger y_d] + (3 - n_{H_d} - n_L - n_e)\mathrm{Tr}[y_e^\dagger y_e] \qquad \text{(D.36)} \\
&\quad - \frac{3}{10}g_1^2 - \frac{3}{2}g_2^2,
\end{aligned}$$

where n_m ($m = Q, u, d, L, e, H_u, H_d$) are the modular weights for the MSSM matter fields.

We employ explicit values of the Yukawa matrices at the EW scale for the analysis in Chapter 3,

$$\begin{aligned}
y_u &= \begin{pmatrix} 0.173 \times \epsilon^5 & 0.183 \times \epsilon^{3.5} & 0.848 \times \epsilon^{2.5} \\ 0.258 \times \epsilon^4 & 0.377 \times \epsilon^{2.5} & 0.379 \times \epsilon^{1.5} \\ 0.203 \times \epsilon^{2.5} & 0.188 \times \epsilon^1 & 0.997 \times \epsilon^0 \end{pmatrix}, \qquad \text{(D.37)} \\
y_d &= \begin{pmatrix} 0.387 \times \epsilon^{3.5} & 0.672 \times \epsilon^4 & 0.681 \times \epsilon^3 \\ 0.351 \times \epsilon^{2.5} & 0.422 \times \epsilon^3 & 0.576 \times \epsilon^2 \\ 0.729 \times \epsilon^1 & 1.07 \times \epsilon^{1.5} & 0.631 \times \epsilon^{0.5} \end{pmatrix}, \qquad \text{(D.38)} \\
y_e &= \begin{pmatrix} 0.186 \times \epsilon^5 & 0.13 \times \epsilon^3 & 0.309 \times \epsilon^3 \\ 0.275 \times \epsilon^{4.5} & 0.702 \times \epsilon^{2.5} & 0.185 \times \epsilon^{2.5} \\ 0.992 \times \epsilon^{3.5} & 0.998 \times \epsilon^{1.5} & 1.04 \times \epsilon^{1.5} \end{pmatrix}, \qquad \text{(D.39)}
\end{aligned}$$

where $\epsilon = 0.225$ is the Cabbibo angle. These Yukawa matrices are motivated by the Froggatt-Nielsen mechanism [50] or the quasi-localized matter fields in 5D spacetime [103] and are consistent with the observed masses and mixings of the fermions.

Bibliography

[1] G. Aad *et al.* [ATLAS Collaboration], Phys. Lett. B **716**, 1 (2012) [arXiv:1207.7214 [hep-ex]].

[2] S. Chatrchyan *et al.* [CMS Collaboration], Phys. Lett. B **716**, 30 (2012) [arXiv:1207.7235 [hep-ex]].

[3] S. P. Martin, In *Kane, G.L. (ed.): Perspectives on supersymmetry II* 1-153 [hep-ph/9709356].

[4] D. J. H. Chung, L. L. Everett, G. L. Kane, S. F. King, J. D. Lykken and L. -T. Wang, Phys. Rept. **407**, 1 (2005) [hep-ph/0312378].

[5] G. Aad *et al.* [ATLAS and CMS Collaborations], Phys. Rev. Lett. **114** (2015) 191803 [arXiv:1503.07589 [hep-ex]].

[6] H. Abe, T. Kobayashi and Y. Omura, Phys. Rev. D **76**, 015002 (2007) [hep-ph/0703044 [HEP-PH]].

[7] H. Abe, J. Kawamura and H. Otsuka, PTEP **2013**, 013B02 (2013) [arXiv:1208.5328 [hep-ph]].

[8] A. Brignole, L. E. Ibanez, C. Munoz and C. Scheich, Z. Phys. C **74**, 157 (1997) [hep-ph/9508258].

[9] A. Brignole, L. E. Ibanez and C. Munoz, In *Kane, G.L. (ed.): Perspectives on supersymmetry II* 244-268 [hep-ph/9707209].

[10] L. Randall and R. Sundrum, Nucl. Phys. B **557** (1999) 79 [hep-th/9810155];

[11] G. F. Giudice, M. A. Luty, H. Murayama and R. Rattazzi, JHEP **9812** (1998) 027 [hep-ph/9810442].

[12] K. Choi, A. Falkowski, H. P. Nilles, M. Olechowski and S. Pokorski, JHEP **0411**, 076 (2004) [hep-th/0411066].

[13] K. Choi, A. Falkowski, H. P. Nilles and M. Olechowski, Nucl. Phys. B **718**, 113 (2005) [hep-th/0503216].

[14] K. Choi, K. S. Jeong and K. -i. Okumura, JHEP **0509**, 039 (2005) [hep-ph/0504037].

[15] K. Choi, K. S. Jeong, T. Kobayashi and K. -i. Okumura, Phys. Lett. B **633**, 355 (2006) [hep-ph/0508029]. K. Choi, K. S. Jeong, T. Kobayashi and K. -i. Okumura, Phys. Rev. D **75**, 095012 (2007) [hep-ph/0612258].

[16] R. Kitano and Y. Nomura, Phys. Lett. B **631** (2005) 58 [hep-ph/0509039].

[17] S. Kachru, R. Kallosh, A. D. Linde and S. P. Trivedi, Phys. Rev. D **68**, 046005 (2003) [hep-th/0301240].

[18] H. Abe, T. Higaki and T. Kobayashi, Phys. Rev. D **73** (2006) 046005 [hep-th/0511160].

[19] L. L. Everett, I. -W. Kim, P. Ouyang and K. M. Zurek, JHEP **0808**, 102 (2008) [arXiv:0806.2330 [hep-ph]].

[20] L. L. Everett, I. -W. Kim, P. Ouyang and K. M. Zurek, Phys. Rev. Lett. **101**, 101803 (2008) [arXiv:0804.0592 [hep-ph]].

[21] G. Jungman, M. Kamionkowski and K. Griest, Phys. Rept. **267** (1996) 195 [hep-ph/9506380].

[22] J.Kawamura, in preparation.

[23] M. S. Carena, M. Quiros and C. E. M. Wagner, Nucl. Phys. B **461** (1996) 407 [hep-ph/9508343].

[24] K. Inoue, A. Kakuto, H. Komatsu and S. Takeshita, Prog. Theor. Phys. **67**, 1889 (1982).

[25] K. Inoue, A. Kakuto, H. Komatsu and S. Takeshita, Prog. Theor. Phys. **68**, 927 (1982)

[26] N. K. Falck, Z. Phys. C **30**, 247 (1986).

[27] S. P. Martin and M. T. Vaughn, Phys. Rev. D **50** (1994) 2282 [Erratum-ibid. D **78** (2008) 039903] [hep-ph/9311340]. Y. Yamada, Phys. Rev. D **50**, 3537 (1994) [hep-ph/9401241]. I. Jack and D. R. T. Jones, Phys. Lett. B **333**, 372 (1994) [hep-ph/9405233].

[28] R. Barbieri and G. F. Giudice, Nucl. Phys. B **306** (1988) 63.

[29] R. Blumenhagen, B. Kors, D. Lust and S. Stieberger, Phys. Rept. **445**, 1 (2007) [hep-th/0610327].

[30] H. Abe and J. Kawamura, JHEP **1407** (2014) 077 [arXiv:1405.0779 [hep-ph]].

[31] R. Barbieri, S. Ferrara and C. A. Savoy, Phys. Lett. B **119**, 343 (1982).

[32] L. J. Hall, J. D. Lykken and S. Weinberg, Phys. Rev. D **27**, 2359 (1983).

[33] S. K. Soni and H. A. Weldon, Phys. Lett. B **126**, 215 (1983).

[34] V. S. Kaplunovsky and J. Louis, Phys. Lett. B **306**, 269 (1993) [hep-th/9303040].

[35] M. Dine and A. E. Nelson, Phys. Rev. D **48**, 1277 (1993) [hep-ph/9303230]. M. Dine, A. E. Nelson and Y. Shirman, Phys. Rev. D **51**, 1362 (1995) [hep-ph/9408384]. M. Dine, A. E. Nelson, Y. Nir and Y. Shirman, Phys. Rev. D **53**, 2658 (1996) [hep-ph/9507378].

[36] G. F. Giudice and R. Rattazzi, Phys. Rept. **322**, 419 (1999) [hep-ph/9801271].

[37] K. Choi, K. Y. Lee, Y. Shimizu, Y. G. Kim and K. -i. Okumura, JCAP **0612**, 017 (2006) [hep-ph/0609132].

[38] W. S. Cho, Y. G. Kim, K. Y. Lee, C. B. Park and Y. Shimizu, JHEP **0704**, 054 (2007) [hep-ph/0703163 [HEP-PH]].

[39] M. Nagai and K. Nakayama, Phys. Rev. D **76**, 123501 (2007) [arXiv:0709.3918 [hep-ph]].

[40] S. Nakamura, K. -i. Okumura and M. Yamaguchi, Phys. Rev. D **77**, 115027 (2008) [arXiv:0803.3725 [hep-ph]].

[41] K. Choi, K. S. Jeong, S. Nakamura, K. -I. Okumura and M. Yamaguchi, JHEP **0904**, 107 (2009) [arXiv:0901.0052 [hep-ph]].

[42] M. Holmes and B. D. Nelson, JCAP **0907**, 019 (2009) [arXiv:0905.0674 [hep-ph]].

[43] B. Altunkaynak, B. D. Nelson, L. L. Everett, I. -W. Kim and Y. Rao, JHEP **1005**, 054 (2010) [arXiv:1001.5261 [hep-ph]].

[44] G. F. Giudice and R. Rattazzi, Nucl. Phys. B **511**, 25 (1998) [hep-ph/9706540].

[45] A. Pomarol and R. Rattazzi, JHEP **9905**, 013 (1999) [hep-ph/9903448].

[46] R. Rattazzi, A. Strumia and J. D. Wells, Nucl. Phys. B **576**, 3 (2000) [hep-ph/9912390].

[47] M. Endo, K. Hamaguchi and F. Takahashi, Phys. Rev. Lett. **96**, 211301 (2006) [hep-ph/0602061].

[48] A. Kusenko, P. Langacker and G. Segre, Phys. Rev. D **54**, 5824 (1996) [hep-ph/9602414].

[49] K. Choi, K. S. Jeong, K. -I. Okumura and M. Yamaguchi, JHEP **1106**, 049 (2011) [arXiv:1104.3274 [hep-ph]].

[50] C. D. Froggatt and H. B. Nielsen, Nucl. Phys. B **147**, 277 (1979).

[51] H. Abe, J. Kawamura and Y. Omura, JHEP **1508**, 089 (2015) [arXiv:1505.03729 [hep-ph]].

[52] J. Kawamura and Y. Omura, Phys. Rev. D **93** (2016) no.5, 055019 [arXiv:1601.03484 [hep-ph]].

[53] B. C. Allanach, Comput. Phys. Commun. **143**, 305 (2002) [hep-ph/0104145].

[54] M. Muhlleitner, A. Djouadi and Y. Mambrini, Comput. Phys. Commun. **168**, 46 (2005) [hep-ph/0311167].

[55] M. Endo, T. Moroi and M. M. Nojiri, JHEP **1504**, 176 (2015) [arXiv:1502.03959 [hep-ph]].

[56] The ATLAS collaboration, ATLAS-CONF-2016-085, ATLAS-CONF-2016-089

[57] M. Ibe, T. Moroi and T. T. Yanagida, Phys. Lett. B **644**, 355 (2007) [hep-ph/0610277].

[58] The ATLAS collaboration, ATLAS-CONF-2015-066.

[59] The ATLAS collaboration, ATLAS-CONF-2016-077

[60] The ATLAS collaboration, ATLAS-CONF-2016-050

[61] The ATLAS collaboration, ATLAS-CONF-2016-052.

[62] J. Alwall, R. Frederix, S. Frixione, V. Hirschi, F. Maltoni, O. Mattelaer, H.-S. Shao and T. Stelzer *et al.*, JHEP **1407**, 079 (2014) [arXiv:1405.0301 [hep-ph]].

[63] T. Sjostrand, S. Mrenna and P. Z. Skands, JHEP **0605**, 026 (2006) [hep-ph/0603175].

[64] F. Caravaglios, M. L. Mangano, M. Moretti and R. Pittau, Nucl. Phys. B **539**, 215 (1999) [hep-ph/9807570].

[65] J. de Favereau *et al.* [DELPHES 3 Collaboration], JHEP **1402**, 057 (2014) [arXiv:1307.6346 [hep-ex]].

[66] M. Cacciari, G. P. Salam and G. Soyez, JHEP **0804**, 063 (2008) [arXiv:0802.1189 [hep-ph]].

[67] W. Beenakker, R. Hopker and M. Spira, hep-ph/9611232.

[68] G. Aad *et al.* [ATLAS Collaboration], Eur. Phys. J. C **75**, no. 10, 510 (2015) [arXiv:1506.08616 [hep-ex]].

[69] http://madgraph.phys.ucl.ac.be/Manual/lhco.html

[70] A. L. Read, J. Phys. G **28**, 2693 (2002).

[71] G. Cowan, K. Cranmer, E. Gross and O. Vitells, Eur. Phys. J. C **71**, 1554 (2011) Erratum: [Eur. Phys. J. C **73**, 2501 (2013)] [arXiv:1007.1727 [physics.data-an]].

[72] [ATLAS Collaboration], ATL-PHYS-PUB-2011-011, ATL-COM-PHYS-2011-818, CMS-NOTE-2011-005.

[73] The CMS collaboration, CMS-PAS-SUS-16-015 CMS-PAS-SUS-16-016

[74] The ATLAS collaboration, ATLAS-CONF-2016-078

[75] J.Kawamura, in preparation.

[76] P. A. R. Ade *et al.* [Planck Collaboration], Astron. Astrophys. **594** (2016) A13 [arXiv:1502.01589 [astro-ph.CO]].

[77] S. Mizuta and M. Yamaguchi, Phys. Lett. B **298**, 120 (1993) [hep-ph/9208251].

[78] K. Kohri, M. Yamaguchi and J. Yokoyama, Phys. Rev. D **72**, 083510 (2005) [hep-ph/0502211].

[79] U. Ellwanger, C. Hugonie and A. M. Teixeira, Phys. Rept. **496** (2010) 1 [arXiv:0910.1785 [hep-ph]].

[80] K. Rajagopal, M. S. Turner and F. Wilczek, Nucl. Phys. B **358**, 447 (1991).

[81] L. Covi, J. E. Kim and L. Roszkowski, Phys. Rev. Lett. **82**, 4180 (1999) [hep-ph/9905212]. L. Covi, H. B. Kim, J. E. Kim and L. Roszkowski, JHEP **0105**, 033 (2001) [hep-ph/0101009].

[82] N. Arkani-Hamed, A. Delgado and G. F. Giudice, Nucl. Phys. B **741**, 108 (2006) [hep-ph/0601041].

[83] C. Cheung, L. J. Hall, D. Pinner and J. T. Ruderman, JHEP **1305** (2013) 100 [arXiv:1211.4873 [hep-ph]].

[84] G. Belanger, F. Boudjema, A. Pukhov and A. Semenov, Comput. Phys. Commun. **176** (2007) 367 [hep-ph/0607059].

[85] D. S. Akerib *et al.* [LUX Collaboration], Phys. Rev. Lett. **116** (2016) no.16, 161301 [arXiv:1512.03506 [astro-ph.CO]].

[86] D. S. Akerib *et al.* [LUX Collaboration], Phys. Rev. Lett. **116** (2016) no.16, 161302 [arXiv:1602.03489 [hep-ex]].

[87] http://luxdarkmatter.org/LUX_dark_matter/Talks_files/
LUX_NewDarkMatterSearchResult_332LiveDays_IDM2016_160721.pdf

[88] E. Aprile [XENON1T Collaboration], Springer Proc. Phys. **148** (2013) 93 [arXiv:1206.6288 [astro-ph.IM]].

[89] M. Garny, A. Ibarra, M. Pato and S. Vogl, Phys. Rev. D **87** (2013) no.5, 056002 [arXiv:1211.4573 [hep-ph]].

[90] K. Jakobs, hep-ex/0107084.

[91] K. Hamaguchi and K. Ishikawa, Phys. Rev. D **93** (2016) no.5, 055009 [arXiv:1510.05378 [hep-ph]].

[92] M. Carena, G. Nardini, M. Quiros and C. E. M. Wagner, JHEP **0810**, 062 (2008) [arXiv:0806.4297 [hep-ph]].

[93] W. Siegel, Phys. Lett. **84B**, 193 (1979). D. M. Capper, D. R. T. Jones and P. van Nieuwenhuizen, Nucl. Phys. B **167**, 479 (1980).

[94] E. Bagnaschi, G. F. Giudice, P. Slavich and A. Strumia, JHEP **1409**, 092 (2014) [arXiv:1407.4081 [hep-ph]].

[95] M. E. Machacek and M. T. Vaughn, Nucl. Phys. B **222**, 83 (1983).

[96] M. E. Machacek and M. T. Vaughn, Nucl. Phys. B **236**, 221 (1984).

[97] M. E. Machacek and M. T. Vaughn, Nucl. Phys. B **249**, 70 (1985).

[98] H. E. Haber and R. Hempfling, Phys. Rev. D **48**, 4280 (1993) [hep-ph/9307201].

[99] B. L. Roberts, Chin. Phys. C **34**, 741 (2010) [arXiv:1001.2898 [hep-ex]].

[100] K. Hagiwara, R. Liao, A. D. Martin, D. Nomura and T. Teubner, J. Phys. G **38**, 085003 (2011) [arXiv:1105.3149 [hep-ph]].

[101] M. Davier, A. Hoecker, B. Malaescu and Z. Zhang, Eur. Phys. J. C **71** (2011) 1515 Erratum: [Eur. Phys. J. C **72** (2012) 1874] [arXiv:1010.4180 [hep-ph]].

[102] T. Moroi, Phys. Rev. D **53**, 6565 (1996) Erratum: [Phys. Rev. D **56**, 4424 (1997)] [hep-ph/9512396].

[103] N. Arkani-Hamed and M. Schmaltz, Phys. Rev. D **61**, 033005 (2000) [hep-ph/9903417].

早稲田大学　博士（理学）　学位申請　研究業績書

氏名　川村 淳一郎　　印

（2017 年　1 月 12 日現在）

種 類 別	題名、　発表・発行掲載誌名、　発表・発行年月、　連名者（申請者含む）
論文	（著者名はアルファベット順） H.Abe, J.Kawamura and H.Otsuka, “The Higgs boson mass in a natural MSSM with nonuniversal gaugino masses at the GUT scale’’, Progress of Theoretical and Experimental Physics 2013 (2013) 013B02.
論文	H.Abe, J.Kawamura and K.Sumita, “The Higgs boson mass and SUSY spectra in 10D SYM theory with magnetized extra dimensions’’, Nuclear Physics.B 888 (2014) 194.
○論文	H.Abe and J.Kawamura, “The 126 GeV Higgs boson mass and naturalness in (deflected) mirage mediation,’’ Journal of High Energy Physics 1407 (2014) 077
○論文	H.Abe, J.Kawamura, Y.Omura, “LHC phenomenology of natural MSSM with non-universal gaugino masses at the unification scale,’’ Journal of High Energy Physics 1508, 089 (2015).
○論文	J.Kawamura and Y.Omura, “Constraints on nonuniversal gaugino mass scenario using the latest LHC data”, Physical Review D 93, no. 5, 055019 (2016).
論文	J.Kawamura and Y.Omura, “Diphoton excess at 750 GeV and LHC constraints in models with vectorlike particles”, Physical Review D 93, no. 11, 115011 (2016).
講演（国際会議）	J.Kawamura, H.Abe and H.Otsuka, “The Higgs boson mass in a natural MSSM with nonuniversal gaugino masses at the GUT scale”, KEK-ph 2013, 高エネルギー加速器研究機構, 2013 年 3 月
講演（学会）	川村淳一郎, 安倍博之, 大塚啓, The Higgs boson mass in a natural MSSM with nonuniversal gaugino masses at the GUT scale”, 日本物理学会第 68 回年次大会, 広島大学, 2013 年 3 月
講演（研究会）	川村淳一郎, 安倍博之, 大塚啓, “natural 125 GeV higgs boson in deflected mirage mediation”, 素粒子物理学の進展 2013, 京都大学, 2013 年 8 月
講演（学会）	川村淳一郎, 安倍博之, “natural 125 GeV higgs boson in deflected mirage mediation”, 日本物理学会 2013 年秋季大会, 高知大学, 2013 年 9 月
講演（国際会議）	J.Kawamura and H.Abe, “The Higgs boson mass and naturalness in (deflected) mirage mediation”, KEK-ph 2013 FALL, 高エネルギー加速器研究機構, 2013 年 9 月
講演（シンポジウム）	川村淳一郎, 安倍博之, “超対称性の破れの伝達機構に基づくヒッグス質量と小さな階層性問題の解析”, 卓越した大学院拠点形成支援事業平成 25 年度シンポジウム, 早稲田大学, 2013 年 12 月

早稲田大学　博士（理学）　学位申請　研究業績書

種 類 別	題名、　発表・発行掲載誌名、　発表・発行年月、　連名者（申請者含む）
講演 （学会）	川村淳一郎，安倍博之，“The NMSSM Higgs boson mass in the deflected mirage mediation”，日本物理学会第 69 回年次大会，東海大学，2014 年 3 月
講演 （国際会議）	J.Kawamura and H.Abe，“The 126 GeV Higgs boson mass and naturalness in (deflected) mirage mediation”，SUSY2014，Manchester University，2014 年 7 月
講演 （研究会）	川村淳一郎，安倍博之，角田慶吾，“The Higgs boson mass and SUSY spectra in 10D SYM theory with magnetized extra dimensions”，素粒子物理学の進展 2014，京都大学，2014 年 7 月
講演 （国際会議）	J.Kawamura and H.Abe，“The 126 GeV Higgs boson mass and naturalness in (deflected) mirage mediation”，富士吉田，Summer Institute 2014，2014 年 8 月
講演 （研究会）	川村淳一郎，安倍博之，“The 126 GeV Higgs boson mass and naturalness in (deflected) mirage mediation”，Workshop on geometry, extra dimensions and string phenomenology in Miyazaki，宮崎県，2014 年 11 月
講演 （セミナー）	川村淳一郎，“The 126 GeV Higgs boson mass and naturalness in (deflected) mirage mediation”，E 研ランチセミナー，名古屋大学，2015 年 1 月
講演 （学会）	川村淳一郎，安倍博之，大村雄司，“natural MSSM with nonuniversal gaugino masses at the LHC”，日本物理学会第 70 回年次大会，早稲田大学，2015 年 3 月
講演 （セミナー）	J.Kawamura，“LHC phenomenology of natural MSSM with non-universal gaugino masses at the unification scale”，北海道大学，2015 年 8 月
講演 （セミナー）	J.Kawamura，“LHC phenomenology of natural MSSM with non-universal gaugino masses at the unification scale”，高エネルギー加速器研究機構，2015 年 9 月
講演 （研究会）	川村淳一郎，安倍博之，大村雄司，“LHC phenomenology of natural MSSM with non-universal gaugino masses at the unification scale”,素粒子物理学の進展 2015，2015 年 9 月
講演 （学会）	川村淳一郎，安倍博之，大村雄司，“non-universal gaugino mass シナリオの LHC 実験による検証”，日本物理学会 2015 年秋季大会，大阪市立大学，2015 年 9 月
講演 （国際会議）	J.Kawamura and Y.Omura，“current bounds on non-universal gaugino masses scenario at the LHC”，KEK-ph 2016，高エネルギー加速器研究機構，2016 年 2 月
講演 （国際会議）	J.Kawamura and Y.Omura，“Constraints on non-universal gaugino mass scenario using the latest LHC data”，SUSY2016，Melbourne University，2016 年 7 月
講演 （国際会議）	J.Kawamura and Y.Omura，“Constraints on non-universal gaugino mass scenario using the latest LHC data”，PASCOS2016，ICISE，2016 年 7 月

早稲田大学　博士（理学）　学位申請　研究業績書

種 類 別	題名、　発表・発行掲載誌名、　発表・発行年月、　連名者（申請者含む）
講演 （国際会議）	J.Kawamura and Y.Omura, “Constraints on non-universal gaugino mass scenario using the latest LHC data”, HU-IBS2016, Hokkaido University, 2016年8月
講演 （学会）	川村淳一郎, 大村雄司, “bino-higgsino dark matter in Non-Universal Gaugino Masses scenario”, 日本物理学会2016年秋季大会, 宮崎大学, 2016年9月